1-1-2017

An Enhanced Nerve Conduit Combined With Exercise To Improve Functional Recovery After Peripheral Nerve Injury

Tonya Jo Whitehead
Wayne State University,

AN ENHANCED NERVE CONDUIT COMBINED WITH EXERCISE TO IMPROVE FUNCTIONAL RECOVERY AFTER PERIPHERAL NERVE INJURY

by

TONYA JO WHITEHEAD

DISSERTATION

Submitted to the Graduate School

of Wayne State University,

Detroit, Michigan

in partial fulfillment of the requirements

for the degree of

DOCTOR OF PHILOSOPHY

2017

MAJOR: BIOMEDICAL ENGINEERING

Approved By:

Advisor: Harini G Sundararaghavan, Ph.D.	Date
John M. Cavanaugh, M.D., P.E.	Date
Mai T. Lam, Ph.D.	Date
Howard W.T. Matthew, Ph.D.	Date

DEDICATION

For every little girl that was told

she couldn't be a scientist…

ACKNOWLEDGEMENTS

I first would like to thank Dr. Sundararaghavan for selecting me to be her first doctoral trainee. I certainly wouldn't have gotten this far without her patient guidance and gentle prodding. Your encouragement and belief in my ability has sustained me on this long journey. It was a memorable experience learning how to navigate Wayne State with you. It has been a pleasure to work with you and learning from you. I am honored to now be able to count you among my friends.

To the rest of my committee, Dr. John Cavanaugh, Dr. Mai Lam, and Dr. Howard Matthew, thank you for your guidance and suggestions as I built this research plan. Thank you for the use of your equipment and lab space, those resources were critical to my success. But most of all, thank you for interjecting a bit of humor along the way. I look forward to continuing to learn from you as a colleague.

Dr. Chen, Dr. Peduzzi-Nelson, and Dr. Mazhari, thank you for working closely with me on the animal study and lending so much of your time. I could not have done this without the benefit your experience and assistance.

To my parents, who have always believed in me much more than I believed in myself. Thank you for teaching me from the very beginning to love learning and seek out knowledge. Mom, you were my first real science teacher, a female role model in STEM before I knew how important that is to young women. Dad, you taught me to love engineering, from working on cars and tractors, to wiring barns, to writing computer programs, you always told me I could be whatever I wanted to. Did you ever think that it would lead me here? You both instilled in me a love of teaching, which has also become a large part of my life. Thank you for your continued support, I promise I will come home to visit more now!

To my best friends Bob and Joanna, even though I don't get to see you as much as I would like, thank you for always supporting me and being their whenever I needed you. Joanna, thank you most of all, for being willing to help edit. I really can't thank you enough!

For the other PhDs in my lab thank you for sharing this crazy ride with me. Melissa, even though we started off a bit rough, you have become one of my best friends. I can't believe that we don't get to sit

in the office together every day any more. I am glad that I've gotten to know you and I know that we will remain close. I look forward to having more adventures and stories to tell. Beth, we were friends even before working in the lab together and I know we will remain friends long after. You are an amazingly strong person, your passion is inspiring, and I know you will achieve unbelievable things. Lizzy, I'm glad that I was able to spend countless hours with you in surgery rooms. You were a huge help to this project and it gave me a chance to get to know you. I love your sense of humor and never give up attitude. I look forward to seeing you accomplish all of your goals.

To all of the undergrads that have helped with this project. There are too many of you to name, but know that I will always appreciate the many hours you put in supporting this project. I hope someday I can repay you.

To the entire staff at the Office for Teaching and Learning, thank you for your continual support and encouragement. I am so thrilled that you accepted me and I'm excited to take the next steps of my career with you.

Finally, to all of my friends and family, thank you all for your support and continual love. Each one of you had a part in me getting here. I cherish each and every one of you.

TABLE OF CONTENTS

LIST OF TABLES

LIST OF FIGURES

LIST OF ABBREVIATIONS

aFGF	Acidic Fibroblast Growth Factor
ANOVA	Analysis of Variance
BBB	Basso, Beattie and Bresnahan
BDNF	Brain Derived Neurotrophic Factor
bFGF	Basic Fibroblast Growth Factor
BMP-2	Bone Morphogenetic Protein-2
BSA	Bovine Serum Albumin
CNS	Central Nervous System
CNTF	Ciliary Neurotrophic Factor
DAB	3,3′-Diaminobenzidine
DAPI	4',6-diamidino-2-phenylindole
DCM	Dichloromethane
DMEM	Dulbecco's Modified Eagle's Medium
DRG	Dorsal Root Ganglia
ECM	Extracellular Matrix
EGF	Epidermal Growth Factor
ELISA	Enzyme-linked Immunosorbent Assay
ESEM	Environmental Scanning Electron Microscope
EtOH	Ethanol
FBS	Fetal Bovine Serum
FDA	Food and Drug Administration
FGF-1	Fibroblast Growth Factor-1
FGF-2	Fibroblast Growth Factor-2
GDNF	Glial Cell Line-derived Growth Factor

GF	Growth Factor
GGF	Glial Growth Factor
H&E	Hematoxylin and Eosin
HA	Hyaluronic Acid
HD	Hyaluronidase
HFP	Hexafluoropropylene
HRP	Horseradish Peroxidase
IGF-1	Insulin-like Growth Factor 1
IGF-2	Insulin-like Growth Factor 2
LIF	Leukemia Inhibitory Factor
MeHA	Methacrylated Hyaluronic Acid
MS	Microspheres
NGC	Nerve Growth Conduits
NGF	Nerve Growth Factor
NGS	Normal Goat Serum
NT-3	Neurotrophic Factor 3
NT-4/5	Neurotrophic Factor 4/5
OsO_4	Osmium Tetroxide
PBS	Phosphate Buffered Saline
PCL	Polycaprolactone
PDGF	Platelet Derived Growth Factor
PEO	Polyethylene Oxide
PLGA	Poly-Lactic-co-Glycolic Acid
PNI	Peripheral Nerve Injury
PNS	Peripheral Nervous System

PT	Physical Therapy
PVA	Polyvinyl Alcohol
SC	Schwann Cells
SC	Sub-cutaneous
SCI	spinal cord injury
SEM	Scanning Electron Microscope
SFI	Sciatic Function Index
SSI	Static Sciatic Index
TGF-β	Transforming Growth Factor - β
TNF-α	Tumor Necrosis Factor
VEGF	Vascular Endothelial Growth Factor

CHAPTER 1: INTRODUCTION AND BACKGROUND

Problem Summary

Peripheral nerve injuries (PNI) are estimated to affect 20 million people in the United States making it a critical clinical issue [29]. This damage can lead to loss of function and sensation in the injured limb as well as debilitating pain [30]. Nerve injuries are often described by size; short gaps are those that can be repaired with direct end-to-end suturing, while critical size defects (>5mm) cannot be sutured and require an implant to bridge this gap, though they show some spontaneous growth [31]. The gold standard treatment for these injuries is an autologous nerve graft, typically harvested from sural nerves [31]. Unfortunately, this procedure leads to donor site morbidity and requires the patient to have multiple surgeries, and frequently resulting incomplete recovery. As an alternative, implants from cadavers (allografts) or other species (xenografts) have been attempted [32], however, to prevent rejection, these require immunosuppressants which can cause additional complications [33].

As another approach, several models of nerve growth conduits (NGC) have been developed and approved for use by the FDA [7, 19, 34]. These are primarily empty tubes used to connect damaged nerve ends to direct them toward each other, a process initiated by growth factor release for the severed nerve ends and supporting glial cells. Several researchers are seeking to improve on these NGCs by adding features designed to promote neurite growth as well as influence attachment and growth direction. This is done by filling the hollow NGC with features including controlled growth factor release and a scaffold for cellular attachment and migration [35-38].

The goal of the work presented in this thesis is to enhance these simple NGCs using a combination of mechanical cues (compliant material), topographical cues (aligned fibers), and chemical cues (growth factor releasing microspheres) and test the improved NGC in combination with physical therapy.

Structure of the Nervous System

The nervous system gathers, transmits, processes, and stores information [39]. It is broken down into two main sections: the central nervous system (CNS) and the peripheral nervous system (PNS). The

central nervous system consists of the brain and spinal cord, while the peripheral nerves emerge from the CNS forming a network throughout the body similar to the vascular system [40, 41]. For this study, we are primarily interested in repair of damage to the PNS.

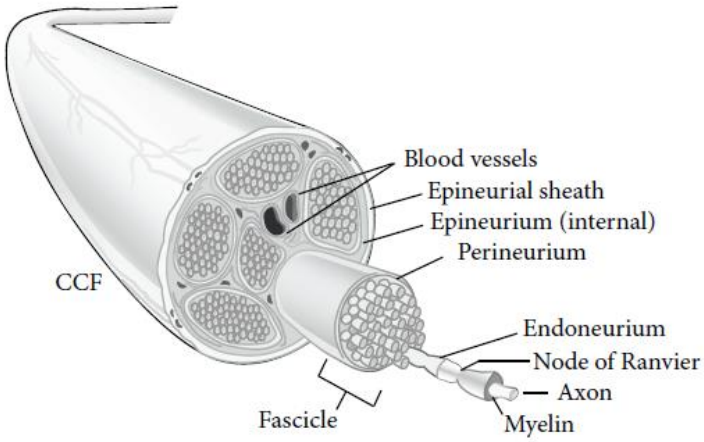

Figure 1-1: Peripheral Nerve Anatomy: From the outside in you see the Epineurial sheath surrounding the entire nerve, including blood vessels. The inner nerve fiber bundles are surrounded by the perineurium, the individual fibers are surrounded by the endoneurium and myelin. Reprinted from International Review of Neurobiology, Vol 87, Maria Siemionow, Grzegorz Brzezicki, "Chapter 8: Current techniques and concepts in peripheral nerve repair", pages 141-172, Copyright (2009), with permission from Elsevier. [21]

A nerve can be described as the discrete organ of the PNS since it consists of neural components, connective tissue, a nutritive blood supply, and is surrounded by connective tissue [42]. Peripheral nerves consist of three distinct sheaths; from inner to outer they are: endoneurium, perineurium and epineurium [21]. The epineurium surrounds the entire nerve bundle and interacts with the other connective tissues in the body. It also is a supportive and protective connective tissue and carries the main supply channels of the interneural vascular system [43]. The perineurium is the middle connective tissue sheath that surrounds the nerve fibers and is made up of compact cellular layers [42]. It is a dense, mechanically strong, and metabolically active sheath that surrounds each fascicle [44]. The perineurium surrounds the individual Schwann Cells (SC) and nerve fibers. The endoneurium is a loose, soft connective tissue that embeds and protects the fascicles, cushioning them during the movements of the extremities. Most of the cell population in the endoneurium consists of SCs and endothelial cells, while fibroblasts make up only 4% [45].

Individual peripheral nerve fibers can be classified in many ways: one way is by the type of signal they transmit, which leads to three broad categories: sensory, motor and interneurons [46-48]. Sensory nerves originate from the sensory ganglia, while motor neurons originate from the somatic and autonomic motor neurons in the CNS [43]. Somatic motor neurons, connect to skeletal muscle fibers to provide direct motor function [49]. Each motor neuron terminates at several nerve fibers creating a motor unit [50]. Contrastingly, autonomic fibers, which control involuntary functions, create synapses in ganglion with secondary autonomic neurons which connect to the visceral nervous system [46, 49]. Another classification of nerves is efferent, going from the CNS to other organs and tissues or afferent, coming from the organs and tissues and sending information to the brain [48]. Interneurons work between the motor and sensory neurons to create a complex signaling network that provides a feedback loop [48].

Table 1-1: Nerve fiber types and properties: Size and myelination effect nerve conduction speed [13]

Fiber Class	Myelin	Diameter (μm)	Conduction Velocity (m/s)	Spinal Cord Tract	Location	Function
Aα	+	6–22	30–120	Ipsilateral dorsal column	Efferent to muscles	Motor
Aβ	+	6–22	30–120	Contralateral spinothalamic tract	Afferent from skin and joints	Tactile, proprioception
Aγ	+	3–8	15–35	Ipsilateral dorsal column	Efferent to muscle spindles	Muscle tone
Aδ	+	1–4	5–30	Contralateral spinothalamic tract	Afferent sensory nerves	Pain, cold, temperature, touch
B	+	1–3	3–15	Preganglionic	Preganglionic sympathetic	Various autonomic functions
sC	–	0.3–1.3	0.7–1.3	—	Postganglionic sympathetic	Various autonomic functions
dC	–	0.4–1.2	0.1–2.0	Contralateral spinothalamic tract	Afferent sensory nerves	Various autonomic functions Pain, warm, temperature, touch

Reprinted from Hand Clinics, Vol 29, Ron M.G. Menorca, Theron S. Fussell, John C. Elfar, "Nerve Physiology Mechanisms of Injury and Recovery", Pages 317-330, Copyright (2013), with permission from Elsevier

The nerve fibers within a nerve can be either myelinated (Type A and B) or not (Type C) [13, 51]. SCs, the ensheathing glial cells of the PNS, are critical for normal nerve function and for nerve repair. They constitute 90% of the nucleated cells within the peripheral nerves. There are two types of SCs: myelinating,

which wrap large single nerve fibers, and ensheathing, which wrap groups of smaller nerve fibers. The ensheathing SC's cytoplasmic process segregates and surrounds axons [52]. In the PNS, myelinated nerve fibers consist of a single axon that is enveloped by a SC and is usually larger than 1.5 μm in diameter [43]. The flat glial process of the SC wraps tightly around the nerve fiber several times creating a multilayer (myelin) sheath. Along the length of the axon, multiple SCs cover the myelinated nerve, the spaces between them are called the nodes of Ranvier [40]. This myelin structure allows for faster transmission of action potentials along the fiber by capturing the ions within the nerve fiber between the nodes [52]. A summary of nerve types, sizes, and conductions speeds are shown in Table 1-1.

Different types of nerve fibers can be found in the same nerve bundle, this is referred to as a mixed nerve [53]. One example of a mixed nerve is the sciatic nerve: the largest single nerve in the body, it runs from the lower back to the legs in humans and other animals. As a mixed nerve, it contains many different sizes and types of nerve fibers. Studies conducted by Swett et al. showed that the sciatic nerve in one strain of rats contained 2005 ± 89 individual motor neuron fibers [54] and 10,500 ± 2000 sensory neuron fibers [55]. When considering nerve repair systems, it is important to consider the mixture of nerves types.

Peripheral Nerve Injury

PNI affects 2.8% of patients with trauma, presenting a critical clinical issue [56]. That comes to over 200,000 patients annually in the United States [57] and over one million worldwide [30]. These injuries often happen during traumatic accidents and are caused by mechanical, thermal, chemical or ischemic damage [19]. Combat veterans have an especially high occurrence of peripheral nerve injury [58]

The bulk of our current knowledge of the aftermath of nerve injury began to accumulate with Augustus Waller in 1850 [43, 52]. While performing tests on frogs, Waller observed the disorganization of the axon and myelin sheaths distal to nerve injury. This breakdown became known Wallerian Degradation.

After nerve injury, the nerve fibers are exposed to extracellular components leading to both morphological and metabolic changes occurring not only at the site of the injury, but also along the axon proximal and distal to the injury, in the nerve cell body, and at the distal end where the axon innervates

either muscle or sensory receptors [52, 53]. On the proximal side, metabolically, the neurons switch from a “signaling mode” to a “growing mode”[59] with protein synthesis switching from neurotransmitter-related to axonal growth-related [60]. Growth mode includes up-regulations of neuropeptides, cytoskeletal proteins, and growth associated proteins [40]. Morphologically, the proximal side of the nerve degenerates for some distance from the injury, and then almost immediately begins to sprout new nerve fibers [61]. These fibers are guided by SC along the remaining endoneurium.

We see Wallerian Degradation occur distal to the injury. Briefly, this process involves the degradation of myelin and the attraction of macrophages which along with the SCs, phagocytose the damaged nerve material increasing the nerve gap [40]. Distal axon degradation is the beginning of the breakdown after PNI, however this doesn’t happen immediately. After 24-48 hours, the axons bead and swell leading to sudden granular disintegration of the cytoskeleton. Soon after PNI, SC in the distal stump begin to dedifferentiate. Within 48 hours these SCs stop producing myelin proteins, switch to neurotrophins and begin proliferating. These SCs play an early role in clearing myelin debris which can act as a barrier to axon growth [43]. Calcium influx activates calpain, a protease essential for cytoskeletal and axonal degradation. Disruption of the endoneurium leads to the inflammatory response which peaks 4-7 days after injury [52].

Schwann cells promote axon regeneration by secreting extracellular matrix (ECM) molecules and trophic factors [62]. Following nerve injury SC upregulate several neurotrophins and glial growth factor [30]. Along with growth promoting factors SCs secrete cytokines and chemokines that recruit immune cells to take over debris removal and growth factor production. Following the breakdown of the axon the empty endoneurium shrinks and retracts increasing the nerve gap [16]. This is followed by the formation of fibrin cables, which the SCs align on, forming bands of Bungner [30]. Axons extending from the proximal stump then grow along this SC bridge. At the outset, an excess number of axons attempt to bridge the nerve gap. As some reach appropriate targets in the distal stump they will enlarge and myelinate, while those that do not find a target will be pruned [51]. However, when gaps are large the bands of Bungner are unable to form, without direction, the regenerating axons never find their targets [19]. These cases require further

support that mimics the support provided the by the bands of Bungner. See Figure 1-2 for a visual depiction of Wallerian Degradation.

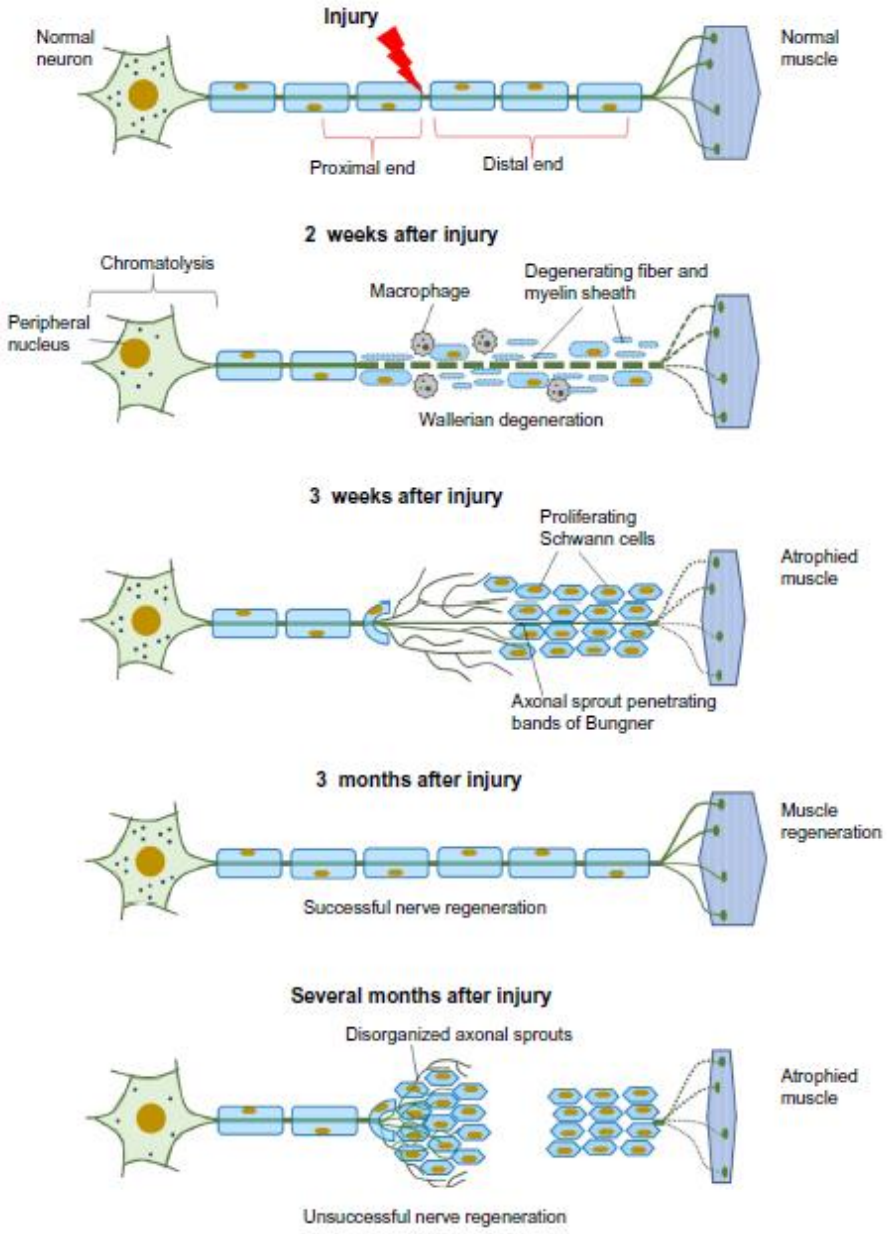

Figure 1-2: Wallerian Degradation Following nerve transection injury, the axon distal to the injury breaks down. Macrophages and Schwann Cells are attracted to the site to clear the cellular and membrane debris. The Schwann Cells then produce fibrous Bands of Bungner for the axons to follow and reconnect to their target. If the gap is too large, however, the axon will not find its target without additional support. This figure has been reproduced freely under a Creative Commons Attribution license. © 2014 Arslantunali et al. Originally published by Dove Medical Press Limited [19]

The effects of nerve injury are not limited to the damaged nerve: changes also occur distally at the nerve targets as well as proximally at synapses both in the CNS and ganglia. When motor neurons are injured and degrade, the associated skeletal muscle becomes denervated, losing neurotransmitter, neurotrophic factor and other signals [63]. The lack of stimulation results in loss of function and progressive muscle atrophy. Muscle fibers undergo molecular and cellular changes like gene expression and can lose up to 80% of their mass [63].

On the proximal side dorsal root ganglia (DRGs), which contain the cell bodies of the afferent spinal sensory system, lose trophic support from the periphery. This leads to adaptive changes including cell and organelle size increase, dendrite retraction, movement of the cell nucleus and a shift to synthesizing materials for axon repair and growth [64]. Reorganization of projections in the CNS also take place: in some cases they are positive, compensating for the missing input, but they may result in neuropathic pain, hyperreflexia, dystonia or phantom limb awareness [64]. Repairing peripheral nerves remains a challenge for the medical and engineering community, despite more than a century of research since Waller.

Current Clinical Nerve Repair Strategies

A rating system for nerve injuries was introduced by Seddon in 1942 [65] and further expanded by Sunderland in 1951 [19, 66]. These are summarized in Figure 1-3. As injury classification increases, more layers of tissue are injured or disrupted. The likelihood of recovery without intervention also decreases with increased grade. For this study, we most interested in Sunderland's fifth degree injury which corresponds to neurotmesis, where the entire nerve trunk is transected completely and there is a scar formation. As a result, neuroma and Wallerian degeneration occur at the proximal and distal ends, respectively. In such severe injuries, surgical repair is required [19].

When complete disruption occurs, injuries are further divided into three categories based on size and the likelihood of recovery: short, long, and critical [30]. Short gaps are those that can be repaired with direct end-to-end suturing. Long gaps cannot be sutured and require some sort of bridging, but still show spontaneous recovery. Critical injuries are those that require more support than a simple bridge, these are

considered over 3 cm in humans and 1 cm in rats [30]. In non-critical injuries, functional repair is seen in 6-16 wks.

Surgical Repairs and Transplantations

For injuries that are short enough that they will not produce tension, direct end-to-end or end-to-side surgical connection is the gold standard and has been for over 50 years [43, 61]. However, the practice has existed for much longer: end-to-side nerve repair was first reported by Letievant in 1873 along with other surgical strategies [43]. In the past 50 years microsurgery has gone from a highly specialized procedure only performed at select centers to a common clinical strategy for the repair of peripheral nerve injury [53]. However, despite impressive technical advancements in nerve reconstruction, complete recovery and normalization of nerve function almost never occurs and the clinical outcome is often poor [45, 67-69].

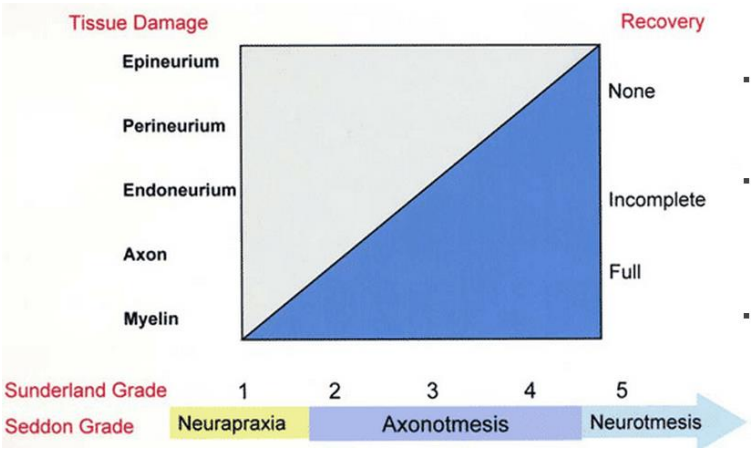

Figure 1-3: Peripheral Nerve Injury Classification: Seddon described three levels of peripheral nerve injury in 1942, which was expanded by Sunderland in 1952. Reprinted from Neurosurgical Focus, Vol 16, M. G. Burnett and E. L. Zager, "Pathophysiology of Peripheral Nerve Injury: A Brief Review", Pages 1-7, Copyright (2004), with permission from PNS Publishing group. [16]

For gaps that are too long for direct end to end connection, autologous grafts (autografts) are the gold standard. These grafts are often taken from sensory nerves elsewhere in the body, and are generally limited to about 5mm repairs due to a lack of donor nerves in the patient [30]. Autograft results in morbidity and often pain at the donor locations. In addition, there is often a size mismatch which can lead to constriction of the regenerating nerve and impede recovery [30]. The first reports of the use of autografts

were made by Philipeaux and Vulpaiin in 1870 [43]. For even larger gaps, the use of allografts, grafts from another individual, or xenografts, grafts from a cadaver, are required. Allografts were first reported by Albert around 1880 [43].

Another strategy used to overcome the lack of autografts is to use other autologous material. One example of this is the vein graft which has shown some positive results when used on sensory nerves with noncritical defects, but these do not possess the mechanical strength to bridge critical gaps [34]. To help improve their mechanical strength, vein grafts have been filled with muscle fibers. The improvements seen with this model are attributed to the topographical cue provided by the aligned fibers and the addition of ECM protein that allow for cell adhesion [70].

Manufactured Nerve Conduits

Nerve conduits have been used to reduce some of the complications involved with autografts and allografts in long nerve injuries. A nerve conduit is essentially a tube into which the distal and proximal end of an injured nerve are inserted. Throughout literature the terms “nerve guide,” “nerve guide conduit,” “nerve growth conduit,” “nerve scaffold,” “nerve tube,” and “tubilization” are used nearly interchangeably [71]. For this description nerve growth conduit (NGC) will be used exclusively. The first recorded attempt to bridge a nerve gap with a tube was made in 1880 by Gluck using decalcified bone [43].

The history of NGC can be divided into three categories: non-absorbable, resorbable, and biomimetic. The earliest materials were non-absorbable. These include polyethylene, polyvinyl, rubber, tantalum metal cuffs, and in clinical practice, Gore-Tex [53]. Early results were not particularly promising; however, silicon conduits did lead to positive results in the clinical setting. The main downfall of non-absorbable materials is the immune response to foreign material, which can lead to fibrosis [53].

The second type of nerve conduits are resorbable tubes. Numerous types have been tested and, as of 2014, eight had made it all the way through the FDA approval process into clinical use [19, 31, 34]. Clinical results as well as animal studies of most of these conduits have shown problems with biocompatibility, swelling and degradation rate [34]. The one that seems to show the best results in humans is Nuerotube, which is made from woven polyglycolic acid and is reported to be degraded in 6-12 months.

A 2000 study by Weber et al. showed that that this conduit performed better on short gaps than end to end repair and better than autografts in long gaps [72]. However, the use of hollow NGCs is currently limited to a critical nerve gap of approximately 4 cm [73].

The third and still developing generation of nerve conduits are biomimetic, meaning that they strive to mimic the extracellular matrix where the nerves grow naturally. This not only encompasses the material used for the conduit itself but also involves adding a 3D structure and molecular support to the conduit [53]. These allow the creation of a controlled microenvironment for the regeneration of nerve fibers and have shown some clinical success [74]. According to a 2012 review by Angius et al., more than 70 different materials have been used for nerve conduits. The most commonly used naturally derived materials are collagen and chitosan, while the most common synthetic material is silicone, all of which have shown promise in various studies [71]. Overall, nerve conduits limit myofibroblast infiltration, reduce scaring and neuroma formation, reduce collateral sprouting, and help concentrate neurotrophins [30].

Tissue Engineering Aspects of Nerve Conduits

Engineers are trained to learn as much as they can about a problem and then use the tools they have to design, build and test those approaches to see how they impact the system [75]. Tissue Engineers have been doing this for peripheral nerve injuries for decades. Research shows that cells are highly responsive to cues in the surrounding environment, especially during periods of growth and development. A fundamental strategy in tissue engineering-based treatment approaches is to artificially recreate the environmental cues to influence cell behavior [39]. Several authors have reviewed these strategies in recent years including Arslantunali et al. [19] in 2014, Muheremu and Ao in 2015 [76], Safa and Buncke in 2016 [77], Gaudin et al. [78] and Rbia and Shin in 2017 [79].

Physical Characteristics

The first aspect of a nerve conduit that needs to be considered is the physical demands that it must withstand. Being implanted *in vivo* means that it will experience stress and strain due to movement of the body. Additionally, it must be able to endure the temperature and chemical makeup of the body. According

to Nectow et. al. the factors to be considered in the mechanical design of nerve conduits are tensile strength, suturability, physical fit, degradation profile and swelling [34]. Tensile strength of the implant should be similar to that of the native tissue, for nerves that is an ultimate stress of ~11.7MPa [80]. Sundararaghavan et al. showed that neurites show growth preference toward soft substrates when presented with a gradient of stiffness [81]. Layering multiple materials is one potential solution to satisfying these conflicting mechanical requirements

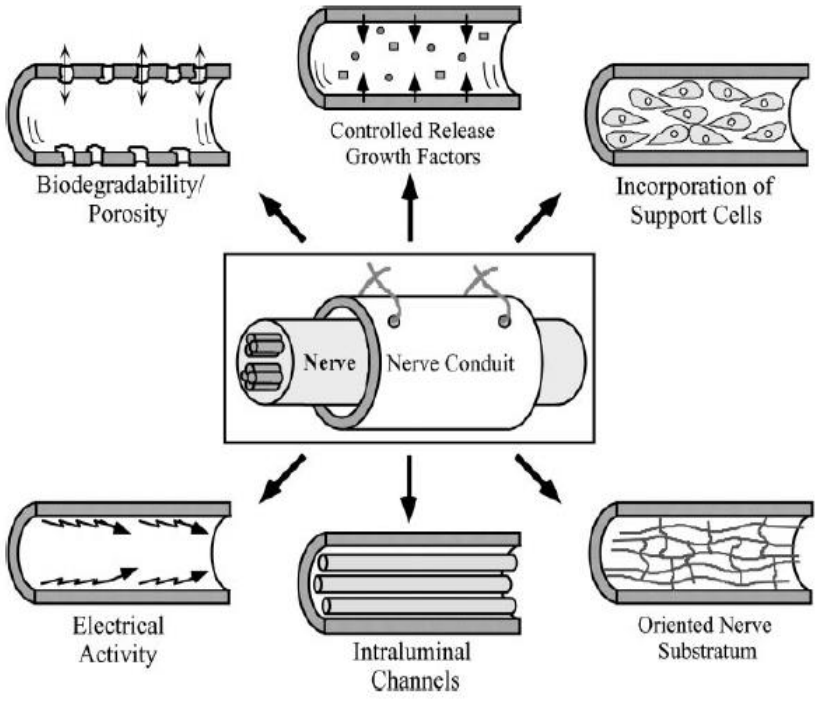

Figure 1-4: Nerve Conduit Characteristics: Several different characteristics have been added to help improve the functionality of nerve conduits [18].

To prevent long-term immune response, many conduits are made from materials that breakdown once implanted. To be most effective, absorbable materials should be completely degraded by the time the nerve is repaired [34]. The conduit must not constrict the growing axon, either by collapsing or swelling, because this will impede nerve growth [18, 19, 47]. Additionally, the conduit needs to be porous or otherwise permeable to allow the free passage of nutrients and metabolites into the conduit to support neural and supporting cell survival and to allow the removal of waste produced by the cells [18, 47, 61, 82]. Most of these characteristics are achieved through the choice of material in the conduit. For this work, we are

focused on adding to existing conduits that meet these requirements. Therefore, our goal is to enhance the conduit without compromising any of the existing features.

Physical features of the nerve conduit can also be used to provide signals directly to the cells. Micron scale features act at the cellular level, while nanoscale features act at the subcellular level [83]. Most notable on a subcellular level for nerve regeneration is signaling to the growth cone, which is the leading segment of the regenerating neurites. Due to the sensitivity of neural cells to nanoscale cues, attention must be given to nanoscale topography in the process of tissue engineering design [39]. Few choices of biomaterials are truly smooth at the nanoscale, so most implanted materials present nanoscale cues, whether intended or not [84]. Nanoscale surface roughness has been shown to improve cellular adhesion to substrates [85]. Topographical cues are physical features of the substrate that influence individual cells. The use of this form of signal comes from knowledge about the major role that aligned ECM plays in guiding neural cell migration and differentiation [39]. The basement membrane on which axons originally grow is a three-dimensional meshwork with pores and fibers with dimensions ranging from tens to hundreds of nanometers [86]. Numerous in vitro studies have successfully shown that topographical cues significantly influence neurite outgrowth and alignment, synaptic connections, and cellular differentiation [87, 88].

Cell culture experiments on topographically patterned substrates have explored the effects of grooves, pits, ridges, steps and waves [39]. Neurite extension can be directly guided along grooves or ridged surfaces in a manner resembling fasciculation, the naturally occurring process in which axons grow along pre-existing axons [89]. Aligned nanofibers are thought to mimic fibrous extracellular matrix proteins such as collagen and fibrinogen, which have similar dimensions and alignment [90]. The aligned nanofibers mimic the bands of Bungner and can be used to promote directed nerve regeneration by guiding glial migration and axonal growth [91, 92]. A study by Jiang et al. looked at the effect of the size of aligned nanofibers on neurite regeneration [93]. The group produced three different conduits: a control that was a pressed film of polycaprolactone (PCL) formed into a nerve guide, a conduit with aligned “micro-sized” fibers, and one with aligned “nano-sized” fibers. The two fibrous scaffolds had similar porosities, but with

pore sizes of 1.33 and 0.28 μm respectively. The conduits were implanted to repair a rat sciatic nerve injury and compared to an autograft control. At the end of three months both fibrous scaffolds showed better axon myelination, a measure of axon maturity, than the film conduit. However, the nanofiber conduit was statistically better than both the microfiber and film conduits. The nanofiber conduits also seemed to improve functional recovery with significantly higher compound muscle action potential amplitudes, a measure of muscle reinnervation [93]. It follows then that the physical surface the regenerating axons encounter should be a nano-scale fibrous network.

Molecular Characteristics

In addition to mimicking the physical characteristics of the natural environment, nerve conduits should also model the molecular environment. The ECM and intracellular space surrounding cells is filled with different molecules and we see a change in these molecular signals in response to axonal injury. Neural cells respond to many of these specific biochemical cues [30]. Surface-bound adhesion molecules are found on cell membranes and within ECM that provide binding sites able to mediate cellular attachment and growth [39]. The most common of these in neural tissue engineering are laminin and fibronectin [30, 39]. Laminin is commonly used for nerve regeneration due to its positive influence on neurite outgrowth and growth cone chemotaxis [34, 38]. Adhesive proteins and peptides are often absorbed or conjugated to the nerve conduit material or are applied as a coating. Nerve conduits containing these molecular signals mirror what happens in the injury environment. For example, after peripheral nerve injury, aligned Schwann cells secrete laminin, creating a substrate that is not only topographically oriented, but also rich in growth-promoting adhesion molecules [39].

Another molecule group in the neural development and regeneration environment are neurotrophic factors. They have been found to influence neural development, survival, outgrowth, and branching [18, 57, 94-97]. Neurotrophic factors offer outgrowth and survival cues to the nerve that are often essential for full regeneration of critical defects [34]. Neurtrophins, a closely related group of neutrophic factors, made up of nerve growth factor (NGF), brain derived neurotrophic factor (BDNF), neurotrophin-3 (NT-3) and neurotrophin-4/5 (NT-4/5), have been heavily used in nerve regeneration studies [18, 34, 44, 95, 98-101].

Other growth factors such as ciliary neurotrophic factor (CNTF), acidic fibroblast growth factor (aFGF), basic fibroblast growth factor (bFGF), glial cell line-derived growth factor (GDNF) and vascular endothelial growth factor (VEGF) have all also been looked at for peripheral nerve regeneration [47, 59, 99, 102-104]. Table 1-2 provides a summary of the neural responses to neurotrophic factors. Chen et al. performed a study to test the synergistic effects of different types of neurotrophic factors. The study used eight groups: NGF alone, CNTF alone, GDNF alone, NGF+CNTF, CNTF+GDNF, NGF+GDNF, NGF+CNTF+GDNF, plus a control group [105]. After 12 weeks, the results showed that NGF and GDNF acted significantly on the survival of sensory neurons and motor neurons, respectively. CNTF was a dominant factor promoting cell body development, and GDNF had the most powerful effect on neurite outgrowth and elongation of sensory neurons and motor neurons [105]. Combined administration of the three factors resulted in optimal functional recovery following sciatic nerve injury in rats [105]. This study will examine NGF in vitro with sensory neurons and GDNF in vivo for motor and sensory neurons.

Table 1-2: Neurotrophic factors: Neurotrophic factors have been shown to promote axonal growth and survival. [18]

Neural response promoted	Neurotrophic factors
Motor neuron survival	BDNF, NT-3, NT-4/5, CNTF, GDNF
Motor neuron outgrowth	BDNF, NT-3, NT-4/5, CNTF, GDNF
Sensory neuron survival	NGF, NT-4/5, GDNF
Sensory neuron outgrowth	NGF, BDNF, NT-3
Spinal cord regeneration	NGF, NT-3, CNTF, FGFs
Peripheral nerve regeneration	NGF, NT-3, NT-4/5, CNTF, GDNF, FGFs
Sensory nerve growth across the PNS-CNS transition zone	NGF, NT-3, GDNF, FGFs

Abbreviations: Brain-derived neurotrophic factor (BDNF), neurotrophin-3 (NT-3), neurotrophin-4/5 (NT-4/5), ciliary neurotrophic factor (CNTF), glial cell line-derived growth factor (GDNF), nerve growth factor (NGF), acidic and basic fibroblast growth factors (FGFs).

Due to the weeks to months that it takes for injured neurons to bridge gaps and reach their targets, it is important to be able to provide these growth factors over an extended period of time. Direct drug injections can be invasive, and injected drugs tend to diffuse away from the target site, whereas

biomaterials-based delivery systems can be used to non-invasively deliver drugs in a controlled and fine-tuned manner [39].

Biomaterial delivery systems fall into two major categories: affinity based release, or reservoir based systems [106]. Affinity based system use non-covalent bonds to adhere proteins and peptides to the nerve conduit [107, 108]. The affect of various affinity levels in these delivery systems were tested by Wood et al.; they secured NGF into a fibrin matrix inside a nerve conduit using three different binding peptides known to have different affinities. While they didn't see an increase in the total number of nerve fibers over free NGF, they did see an increase in the size and myelination of the fiber, both signs of fiber maturity. Size and myelination increased further with the higher binding affinity. While they did not reach the level of the graft control, this study does show that affinity based systems can improve nerve growth conduits [109].

Reservoir based systems come in many forms and involve containing the protein within a material or matrix. Examples of this include micro and nanospheres, hydrogels, and nanofibers or combinations of these [106]. Agarwal et al. recently reported the development of a NGC that included concentric cylinders with space between for NGF. The inner cylinder included a single small hole for the neurotrophic factor to diffuse out of. They showed that animals using the conduit diffusing NGF had significantly higher muscle mass and muscle reinnervation at 180 days [101]. In another study, Wang et al. reported the use of microspheres made from poly-lactic-co-glycolic acid (PLGA) to encapsulate NGF and place it into a chitin nerve conduit. The results were compared to groups that received the conduit alone, the conduit with an NGF solution or a conduit containing empty microspheres. After three months of implantation the NGF microsphere group showed significantly more nerve fibers, myelin sheath thickness and axonal area. The empty microsphere group was not significantly different than the saline or NGF solution groups indicating that the presence of the microspheres was not inhibitory to nerve fiber growth [110].

Cellular Support

Several groups have also incorporated cells into nerve conduits. By implanting Schwann cells it is thought you can speed the process of debris clearing and developing the bands of Bungner speeding and

increasing axonal growth [111]. SCs have also been shown to excrete neurotrophins to support nerve regeneration [112]. Alternatively, stem cells have been incorporated into conduits. The mechanism of stem cell support is not completely understood. Some studies show that the cells differentiate into neural support cells [113, 114]. Other studies have used vectors to modify various cell types, including Schwann cells and fibroblasts, to up-regulate growth factors and incorporated the cells into nerve conduits [62].

Physical Therapy & Exercise

As mentioned earlier, after nerve transection the muscle targets of motor neurons are left deinnervated leading to mechanical and biochemical changes. The benefits of physical therapy after nerve injury are widely accepted and routinely used in during rehabilitation following nerve injury in the clinical setting [115]. Exercise is known to reduce or prevent muscle atrophy and is thought to drive cortical remodeling [116]. However, a review of the published literature on exercise in animal models shows highly contradictory results, including some inhibition of reinnervation and muscle function return. This is at least in part due to a wide variety in the types of injuries, and the mode, intensity, duration and onset of exercise regimes [57, 116]. As an example, just looking at one type of injury, sciatic nerve crush, you can quickly find a study which used wheel running (a voluntary activity) for both three and seven days [117], another that used 25 minutes of swimming per day for 7 weeks [118] and a third that uses a treadmill for one hour per day for 14 days [119].

Studies out of the English group however, have started to compare different modalities side by side to better understand how exercise affects peripheral nerve regeneration [57]. Findings showed that moderate exercise for two weeks resulted in longer axon regeneration than was seen in electrically stimulated or untrained animals in a fibular nerve transection and repair [120]. They also found an interesting gender difference between types of treadmill training. Female rats showed increased axon length with interval training but not with continuous training, while the opposite was true for males [121]. Another study showed that the time of the start of exercise after nerve repair changed the Hoffmann reflex (H reflex), but didn't show any difference in the direct muscle response to electrical stimulus (M wave) [122]. The Navarro

group also looked at electrical stimulation and exercise and found that together they show a faster return of direct muscle response than either treatment separately [123]. In another study from that group active exercise (treadmill running), where the animal must initiate movement, and passive exercise (motorized bike), where the limbs are moved for the animal, were compared for animals with a sciatic nerve injury and repair [115]. Both methods showed improvement in M wave amplitude over controls, but did not show significant difference between the active and passive regimes. A possible explanation for the benefit of exercise in peripheral nerve regeneration is that neuronal factors known to promote neuronal survival are upregulated by increased levels of physical activity. Some of these include NT-3 and NT-4/5, GDNF, BDNF, and insulin-like growth factor 1 (IGF-1) and IGF-2 [124].

Preclinical Model: Rat Sciatic Nerve Axonotomy

A great deal can be determined about biomaterials and treatments using in vitro testing. However, to date no comprehensive system that mimics the complexity of the natural environment of the nervous system has been developed. Therefore, a critical step in the validation of any system of peripheral nerve repair is *in vivo* testing. A systematic review by Angius et al. compiled a list of animal models that were used over 60 years from 1950-2010 for *in vivo* study of nerve regeneration [71]. They found that eight different species and 17 different nerves have been used. In nearly 75% of the studies rats and sciatic nerves where used [71]. This indicates a strong prevalence of this model, and provides a large set of data to compare results with.

Savastano et. al. summarized the use of the rat sciatic nerve model for several types of injury, which was used at least as far back as 1906 [125]. Briefly, an incision is made in the inner thigh and the muscle is separated to expose the sciatic nerve. What is done at this point depends on the type of injury that you are trying to replicate. To model neurapraxia, an ameroid ring can be placed around the nerve which will swell and compress the nerve. For an axonotmesis the nerve is crushed with a tool such as forceps. For neurotmesis the nerve is cut with a scalpel or scissors. Depending on the treatment being tested, it may then

be sutured back together, have a segment removed and replaced with a conduit or have a section removed, inverted and replaced (a common model of autograft) [125].

Part of the appeal of the sciatic nerve is its ease of accessibility. It is also a mixed nerve containing both sensory and somatic and autonomic motor neurons. Rats show strong neural regenerative capacity. Beyond simple functional recovery and pain testing, the use of transgenic animals and viral vectors allows researchers to dig deeply into the biochemical pathways that govern many aspects of neural injury [125].

Significance & Innovation

Despite decades of research, regeneration and reinnervation after peripheral nerve transection remains a challenge. The primary standards of measure for nerve repair are functional recovery, the regeneration of the nerve, reinnervation of the muscle, and elongation of axons after therapy [126]. Researchers have tried to accomplish these goals using several methods with limited success. Bellamkonda et al. suggest that holistic approaches, which seek to provide combinations of cues to influence multiple aspects of healing and regeneration, offer great therapeutic potential in the treatment of neural injury and disease [39]. Two of the most promising therapeutic models are delivery of growth factors to the site and exercise regimens to maintain muscle tone and promote nerve activity [18, 64, 127-130]. These treatments have been studied individually numerous times. To our knowledge, a system that incorporates mechanically tuned and topographically specific substrate with direct neurotrophin delivery has not been created or characterized previously. Nor has that type of system been combined with physical therapy in the form of exercise.

Research has shown that cells respond to several factors in their environment including mechanical, topographical, and chemical signals. Peripheral neurons are known to prefer a soft substrate, be directed by aligned fibers, and respond to neurotrophic factor [18, 34, 47]. Combining these signals into an NGC is hypothesized to produce a synergistic effect resulting in enhanced, directed, and accelerated neurite growth and thus more robust and faster functional recovery.

Udina et al. reviewed the current status of exercise therapy in peripheral nerve regeneration [116]. The published literature shows wide variance in types of injury tested, type of exercise used, duration of exercise, and session time of the exercise. The diversity of studies makes comparison between protocols difficult. However, all but one of the studies on sciatic nerve injuries showed that the exercise (swimming, biking or treadmill running) used was beneficial to regeneration, reinnervation, or axonal elongation [57, 116].

One recent study tested a collagen nerve conduit with and without Schwann cells in combination with exercise [131], while another did the same with mesenchymal stem cells [132]. This proposed study will fill an existing gap in literature determining if there is a synergistic effect of combining a NGC containing extended release of growth factors with physical therapy. After developing and characterizing an internal structure addition for NGCs combining topographical, mechanical, and chemical cues the system will be tested in a rat sciatic nerve injury model in combinations with exercise to model physical therapy.

Expanding the complexity of the nerve growth conduit system and adding exercise to the treatment protocol is a significant step toward a highly effective nerve repair strategy. Each step that is taken lends hope to thousands of people that live with the debilitating reality of nerve injury; the effects of which include loss of muscle control or function, spasticity, and pain. Return of nerve function to these individuals would greatly improve their quality of life.

Hypothesis and Specific Aims

I hypothesize that combining a nerve growth conduit that includes chemical, mechanical, and topographical cues, similar to the native ECM, with physical activity will lead to a synergic effect, resulting in increased axonal growth and functional recovery for peripheral nerve injury patients.

Specifically, aligned electrospun fiber, providing a topographical signal, made from cross-linked Methacrylated Hyaluronic Acid (MeHA), providing a mechanical cue, will be combined with microspheres for extended release of growth factors, providing a chemical cue, to encourage cell growth. This cellular

level support will further be combined with treadmill running, an active exercise regimen, encouraging use of the developing neurons to improve functional nerve reconnections and prevent muscle atrophy.

To test this hypothesis two specific aims have been developed:

1. Create, characterize, and test a NGC scaffolding based inner structure that incorporates multiple cell growth signaling modalities; specifically, topographical (aligned fibers), mechanical (soft substrate), and chemical (growth factors release).

2. Test the effect of the developed inner structure with a nerve growth conduit system in a rat sciatic nerve model with and without the incorporation of an exercise regimen. Evaluating functional recovery and nerve regeneration through behavioral analysis, electrical signal transduction, and histological analysis.

CHAPTER 2: COMBINING GROWTH FACTOR RELEASING MICROSPHERES WITHIN ALIGNED NANOFIBERS ENHANCES NEURITE OUTGROWTH

Portions of this chapter are contained in the publication: T.J. Whitehead, C.O.C. Avila, and H.G. Sundararaghavan, *Combining Growth Factor Releasing Microspheres within Aligned Nanofibers Enhances Neurite Outgrowth*. Journal of Biomedical Materials Research Part A, 2017 Sept 6.

Tonya Whitehead was responsible for experimental design. She conducted experiments including microsphere preparation, scaffold preparation, SEM and ESEM imaging, cell culture, and NGF ELISA. She compiled and analyzed data, and assisted with manuscript preparation.

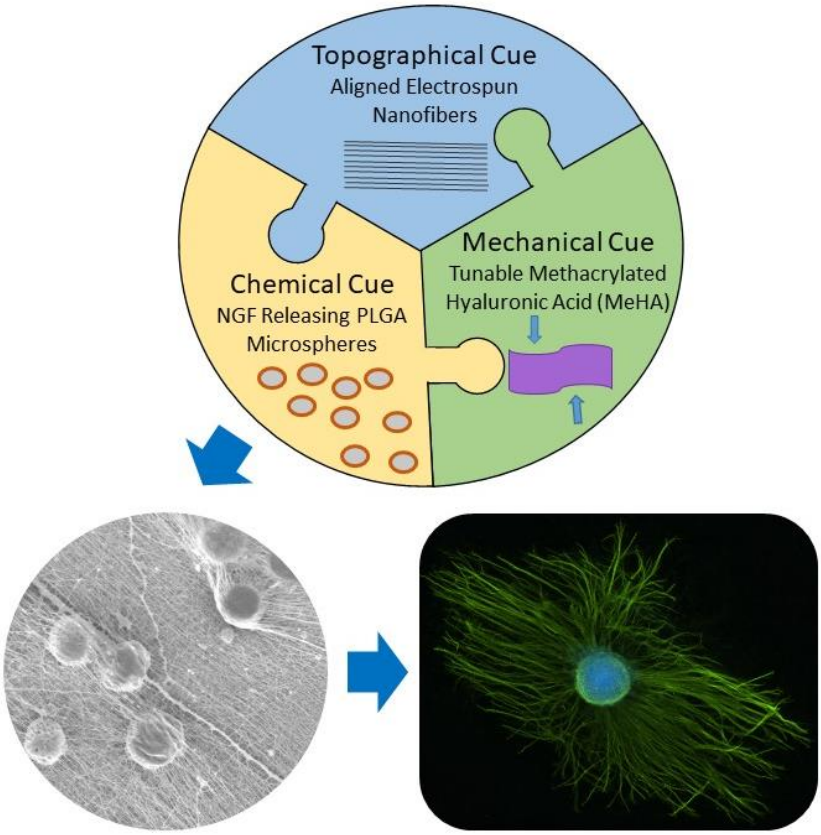

Figure 2-1: Graphical Abstract. The goal of this project is to enhance the simple, hollow tube, nerve growth conduits (NCGs) currently available by using a combination of mechanical (soft substrate), topographical (aligned nanofibers) and chemical cues (growth factor releasing microspheres) to stimulate nerve regeneration. We begin by testing the material properties and chemical release; followed by in vitro testing of the system with dorsal root ganglia explants. Results show that the combination enhances and directs outgrowth for up to four weeks.

Introduction

Peripheral nerve injuries are estimated to affect 20 million people in the United States making it a critical clinical issue [133]. This damage can lead to loss of function and sensation in the injured limb as well as debilitating pain. Short gaps can be repaired with direct end-to-end suturing. Critical size defects (>5mm) cannot be sutured and require an implant to bridge this gap, though they show some spontaneous growth [30]. The gold standard treatment for these injuries is an autologous nerve graft, typically harvested from sural nerves [30]. Unfortunately, this procedure leads to donor site morbidity and requires the patient to have multiple surgeries, and still often results in incomplete recovery. Alternatively, processed xenografts and nerve growth conduits (NGC) have been developed and approved for use by the Food and Drug Administration [19]. NGCs are primarily hollow tubes used to connect damaged nerve ends to direct them toward each other, a process initiated by growth factor release for the severed nerve ends. Several studies have shown that neuronal cells respond to biomaterial cues including mechanical, topographical, and chemical signals [38, 134]. Previously investigated modifications to NGCs were designed to promote neurite growth as well as influence attachment and growth direction by filling the hollow NGC with features including controlled growth factor release and scaffold-based cues for cellular attachment and migration [7, 35, 37, 135], however, few studies combine multiple cues.

The goal of this project is to develop an internal structure that can be added to commercially available NGCs using a combination of chemical cues (growth factor releasing microspheres), mechanical cues (compliant substrate), and topographical cues (aligned fibers). Peripheral neurons are known to prefer a compliant substrate, be directed by aligned fibers, and respond to nerve growth factor (NGF) [82, 136]. We include a low-modification methacrylated hyaluronic acid as our compliant substrate and electrospin this material into aligned nanofibers. Controlled release of growth factors is included by immobilizing NGF releasing poly-lactic-co-glycolic acid (PLGA) microspheres within the fibrous network. We hypothesize that combining these signals into the NGC will result in increased neurite growth and thus better functional recovery. This manuscript describes the in vitro testing of the additional cues.

Materials and Methods

Microsphere Production

Protein was encapsulated in PLGA (Lactel, Birmingham, AL) using a Water-Oil-Water double emulsion technique. The 200µL inner water phase contained various concentrations of NGF from 0µg/mL to 100µg/mL in 1% bovine serum albumin (BSA) in phosphate buffered saline (PBS) and 4µL of 2% polyvinyl alcohol (PVA). This was dispersed in the oil phase of 300mg of three different ratios (50:50, 65:35, 72:25) of PLGA dissolved in 3mL of dichloromethane (DCM) using a wand sonicator for 10 seconds. The resulting emulsion was dispersed in the outer water phase consisting of 0.5% PVA using a vortex mixer and mixed on a stir plate for a minimum of 1 hour to allow the DCM to evaporate and the PLGA to stabilize. The microspheres were then removed from solution by centrifugation (2000 RPM for 10 minutes), rinsed three times, lyophilized and stored at -20 °C.

Microsphere Characterization

Microsphere encapsulation was quantified using BSA as a model protein and measured using a Comassie Blue Assay (Thermo Scientific). All remaining solutions and supernatants from the microsphere production process were retained and then tested for protein content following the manufacture instructions for the assay. Percent encapsulation was calculated as: (Initial Protein – Measure Protein)/Initial Protein. Microsphere size was calculated by taking brightfield images of the microspheres using a Nikon Eclipse inverted microscope. The dry microspheres were spread on a petri dish in a 3.3% polyethylene oxide (PEO) solution to prevent movement during imaging. A custom Matlab script was used to find the diameter of all microspheres in five images from three different samples.

Scaffold Fabrication

Hyaluronic Acid (ECM Science, Detroit MI) (HA) was methacrylated as previously described by Burdick et al. [137]. Briefly, HA was dissolved in water and methacrylic anhydride (Sigma) was added dropwise on ice while maintaining a basic pH using NaOH. Methacrylated HA (MeHA) was created at approximately 15% methacrylation, confirmed through nuclear magnetic resonance spectroscopy (NMR).

A solution of 2% MeHA, 3% 900kD PEO, and 0.05% Irgacure 2959 crosslinker (all w/v) was electrospun onto a spinning mandrel as described previously [5]. For scaffolds containing microspheres, 30mg of microspheres were added per milliliter of electrospinning solution. A positive charge of 22 kV (without microspheres) or 24kV (with microspheres) was applied across a 15cm gap between the end of the needle and the rotating collection mandrel. For scaffolds with aligned fibers, the mandrel was rotated at 10 m/s, for random fibers the mandrel rotated at 0.5 m/s. The scaffolds were crosslinked under 10mW/cm^2 365nm light for 30 minutes then rinsed in DI water for at least 24 hours to remove PEO, prior to use for cell seeding, imaging, or mechanical testing. For cell testing, they were also coated with Fibronectin (Sigma) at 5µg/cm2. Scaffolds of four types were fabricated: aligned fibers with microspheres (Aligned+MS), aligned fibers without microspheres (Aligned-MS), random fibers with microspheres (Random+MS) and random fibers without microspheres (Random-MS).

Scaffold Characterization

Mechanical Properties: Mechanical tests were performed in both dry and hydrated conditions for all four scaffold types described above. Fifteen scaffolds were cut into 1cm x 8cm rectangular strips, where the length (8cm) of the strips was parallel to the direction of rotation of the mandrel during electrospinning, and rinsed for PEO removal. Samples were frozen at -18°C before rapid freezing in liquid nitrogen; samples were then lyophilized. For dry mechanical testing, the scaffold samples were clamped in an Instron 5943 using 120 grit sandpaper on the grips, to prevent slipping, and stretched at a strain rate of 1%/min until fracture. For hydrated mechanical testing, the scaffold samples were immersed in phosphate buffered saline (PBS) for 24 hours prior to testing and tested as described above while submerged in a PBS bath at 37°C. Immediately prior to testing the gage length, width, and thickness of each sample were recorded. The resulting stress-strain curves were recorded using BlueHill software and analyzed in Matlab. The slope of the linear portion of the curve was reported as Young's modulus. The ultimate stress was the maximum stress recorded for each curve. Samples that were damaged in processing or broke at the clamps were excluded, however all groups had $n > 5$.

Alignment: Alignment was calculated for both the dry and hydrated condition of all four scaffolds. For dry conditions samples (n=3) were rinsed and lyophilized. Samples were gold coated before images of each sample were taken using a JOEL JSM - 6510LV Scanning Electron Microscope (SEM) on high vacuum at 25kV. For hydrated conditions, samples (n=3) were rinsed and lyophilized, then rehydrated with PBS for 24hrs prior to imaging. Samples were imaged in an SEI Quanta 450FEG in environmental SEM (ESEM) with vacuum at 1 Torr and 10 kV beam. Alignment was determined by the OrientationJ, a plugin for ImageJ (NIH v1.46), which evaluates each image to find color boundaries and determine the angle that most lines in the image are oriented. It then produces a coherence percentage indicating the percent of the fibers oriented in the primary direction of the image.

Porosity: Circular samples (n>3), 25mm in diameter and 0.5mm thick, of each scaffold were measured for porosity using the Archimedes' Principle [138]. Dry samples were rinsed and lyophilized as described above, hydrated samples were soaked in PBS for 24 hours and patted dry prior to testing. A density bottle filled with ethanol (density d) was weighed (W1). A scaffold sample of weight WS was immersed in the density bottle. The density bottle was again filled with ethanol and weighed (W2). The scaffold was then immediately removed and the density bottle weighed (W3) again. The following parameters of a scaffold were calculated [138]: the volume of the scaffold pores (Vp , $Vp=(W2-W3-Ws)/d$), the volume of the scaffold skeleton (Vs, $Vs=(W1-W2+Ws)/d$), the density (ρ, $\rho=Ws/VS$), and the porosity (ε, $\varepsilon=(Vp/(Vp+Vs))$.

Degradation: Rinsed aligned scaffolds with microspheres (Aligned+MS) and without microspheres (Aligned-MS) were cut into circular samples 25mm in diameter and approximately 0.5mm. Each sample was weighed and measured prior to testing. Individual samples were placed in 5mL of PBS or 10U hyaluronidase in PBS and stored at 37°C [137]. Three times a week for 4 weeks all samples had the PBS or hyaluronidase solutions replaced. Removed solutions were stored at -20° for testing for uronic acid content. Each week 3 samples of each scaffold type were removed from their solution, washed in DI water 3 times, and dried under vacuum. The dry sample weight and measurements were recorded and compared with the initial dry weight to determine the fractional mass remaining [35, 139].

Additionally, the solution removed from the degradation bottle was tested for uronic acid, the byproduct of hyaluronic acid breakdown, using a carbazole colormetric test. Unknown samples and controls were mixed with sulfuric acid and tetraborate decahydrate over ice then heated for 10 minutes to 100°C. They were then cooled on ice and had a 0.125% carbazole solution added. After again heating to 100°C for 15 minutes the samples were read at 530 nm on a plate spectrophotometer. The amount of hyaluronic acid that had broken down was interpolated from the uronic acid found in the unknown sample by comparison to the uronic acid from the know samples [137].

DRG Growth Analysis

Scaffolds were attached to 12 mm methacrylated coverslips, rinsed and seeded with freshly harvested dorsal root ganglia (DRGs) from 9-11 day old chicken embryos. Cells were grown in cell culture media: Dulbecco's Modified Eagle's Medium (DMEM) supplemented with 10% Fetal Bovine Serum (FBS), 1% Glutamate, and 1% Penicillin Streptomycin. Scaffolds not containing microspheres were supplemented with 50 ng/mL NGF in the media. After 5 days, the cells were fixed in 4% Paraformaldehyde and stained with a neurofilament antibody, an AlexaFlour 488 secondary antibody and 4',6-diamidino-2-phenylindole (DAPI). Images of the cells were taken using a Nikon Eclipse inverted fluorescence microscope and analyzed using a custom Matlab script to measure growth ratio and aspect ratio. Growth ratio is the number of pixels that stain positive for neurofilament divided by the number of pixels that stain positive for DAPI. For aspect ratio, the Matlab script creates an oval that represents the shape of the illuminated pixels, the reported aspect ratio is the length of the long axis of this oval divided by the short axis of the oval.

Encapsulated NGF Optimization: To determine the optimal concentration of NGF for future experiments, 65:35 PLGA microspheres were created with 0µg/mL (n=7), 25 µg/mL (n=3), 50 µg/mL (n=7), 75 µg/mL(n=8) and 100 µg/mL (n=6) encapsulated NGF. These microspheres were electrospun into scaffolds and seeded with DRGs and analyzed as described above.

Aligned vs Random: Samples of Aligned + MS (n=20), Aligned – MS (n=13), Random + MS (n=12) and Random – MS (n=19) were fabricated on methacrylated glass coverslips. The microspheres

were made of 65:35 PLGA and contained 100 μg/mL of NGF. Samples containing microspheres received media with no NGF, while samples without microspheres received culture media containing 50ng/mL NGF. DRGs were seeded and analyzed as described above.

Protein Release and Bioactivity Testing

NGF released from the microspheres was tested by enzyme-linked immunosorbent assay (ELISA). Three 300 mg samples of microspheres, both with and without NGF, were incubated at 37°C in 5mL cell culture media. After 2 days, 1 week, and weekly thereafter for 7 weeks, the media was removed and replaced with fresh media. The conditioned media was then tested for NGF by ELISA following manufacturer's instructions. Additionally, the conditioned media was used to grow DRGs on tissue culture plastic to test NGF bioactivity as described below.

Extended NGF Release: Freshly harvested DRGs from 9-11 day old chick embryos were placed directly on tissue culture plastic and grown with the conditioned media, described above, from day 2 through week 4. Each of the three samples, for each condition, for each time point were placed on DRGs from three separate chicks. DRGs that did not attach, attached near the edge of the well limiting the growth or were damaged in the staining process were not used in the final analysis. The images were analyzed with the custom Matlab scripts described above. The major axis of the oval generated for the neurofilament channel was used as the growth distance for each image.

Statistical Analysis

Sample means were compared using a one-way analysis of variance (ANOVA) test and Fisher's LSD post hoc analysis with statistical significance indicated at $p \leq 0.05$, unless otherwise noted.

Results

Microsphere Characterization and Electrospinning

In this study, microsphere size was 18.7 ± 5.1μm and 85% of the presented protein was incorporated into the microspheres. The size of the microspheres can be adjusted by changing the amount of time spent sonicating the initial emulsion. Longer sonication results in smaller microspheres. There were no significant

differences in size among the three ratios of PLGA tested. Figure 2-2 shows a histogram of the microsphere sizes. Early studies of PLGA microspheres containing NGF reported encapsulation efficiency as high as 95%. More recent studies have shown rates of 64% and 74% in similar applications [140-142].

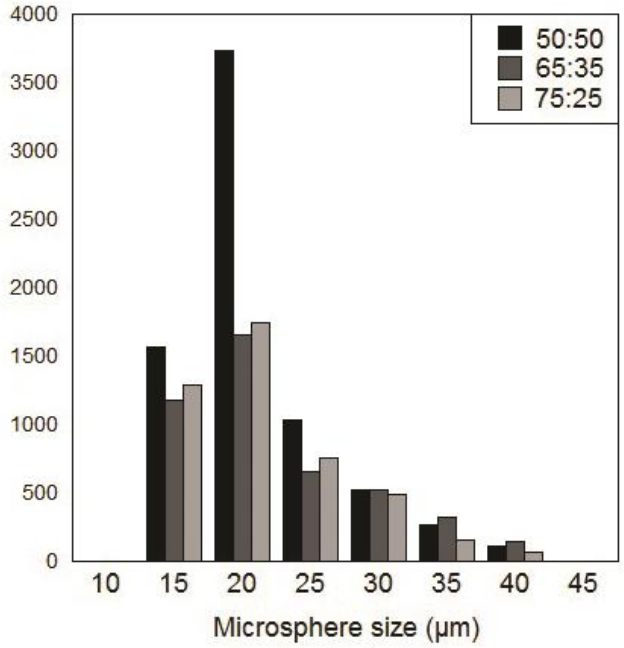

Figure 2-2: PLGA Microsphere Size. Histogram of PLGA microspheres sizes in bins of 5 µm from three ratios of Lactic:Glycolic Acid (50:50, 65:35, 75:25). Microspheres range in size from 10 µm – 45 µm, with a average of 18.7 µm. There was no significant difference in the three groups.

Scaffolds of four types were fabricated for testing: aligned fibers with microspheres (Aligned + MS), aligned fibers without microspheres (Aligned - MS), random fibers with microspheres (Random + MS) and random fibers without microspheres (Random - MS). Sample images of each condition are shown in Figure 2-3. Microspheres were seen throughout the electrospun scaffolds, making a 3-dimensional fibrous network. In characterizing these scaffolds, we evaluated how the microspheres affect alignment, porosity, mechanical properties and neurite extension.

Scaffold Characterization

The addition of microspheres to the scaffolds or hydration did not significantly change the alignment percentages in either the random or aligned conditions (Table 2-1). Corresponding aligned and random conditions were significantly different with $p \leq 0.001$.

Table 2-1: Scaffold alignment and porosity

		Aligned + MS	Aligned - MS	Random + MS	Random - MS
Dry	Alignment (%)	56.17±2.80# n = 3	59.99±12.52# n = 3	18.70±10.73 n = 3	19.42±7.56 n = 3
	Porosity (%)	71.92 ±2.91 n = 15	71.17 ±5.36 n = 12	83.23 ±2.82 n = 5	67.03 ±8.94¥ n = 8
Hydrated	Alignment (%)	64.43±12.31# n = 3	72.25±16.32*# n = 3	18.52±12.58 n = 3	24.02±10.62 n = 3
	Porosity (%)	45.02 ±6.91* n = 8	50.78 ±4.15* n = 10	34.31 ±12.53* n = 5	54.58 ±8.22¥ n = 6

* Indicates $p<0.05$ compared to dry in the same condition, # Indicates $p<0.05$ compared with random scaffolds in the same condition, ¥ Indicated $p<0.05$ compared with scaffolds with microspheres.

Porosity was calculated for all conditions using fluid displacement of three-dimensional samples for both dry and hydrated conditions (Table 2-1). The fibers swelled from hydration, going from dry conditions to hydrated conditions, the porosity of the samples decreased. Aligned + MS and Aligned - MS decrease in porosity 26.09% and 20.39% (respectively) after hydration. Random + MS had the largest decrease at 48.92%, while Random – MS had the smallest at 12.45%. All conditions, except Random-MS were significantly different comparing dry to hydrated measurements with $p \leq 0.001$. The addition of

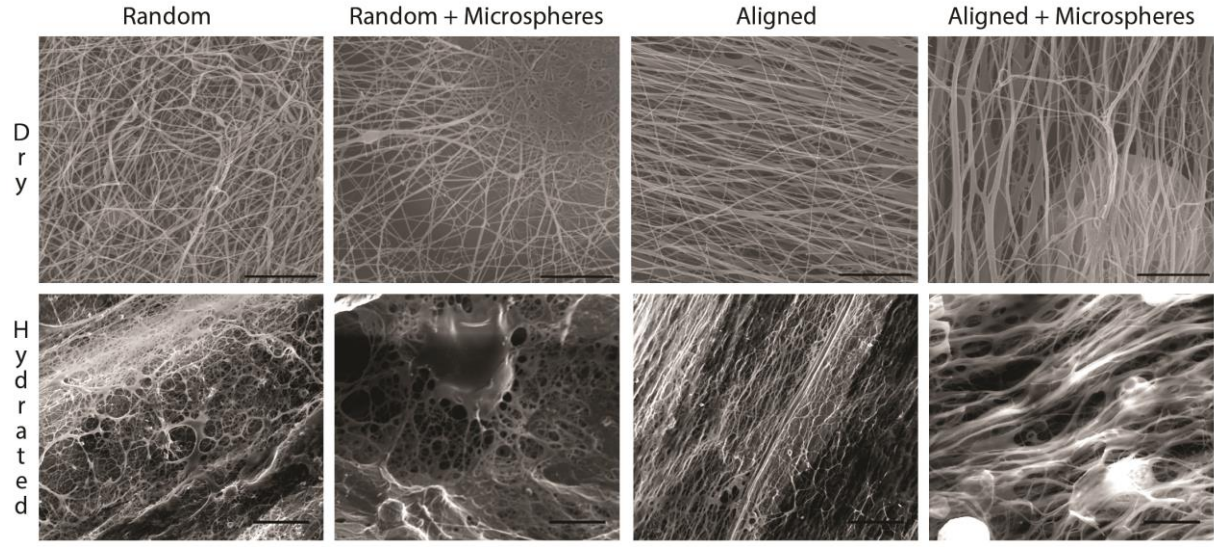

Figure 2-3: SEM/ESEM Scaffold Images. Top panel shows dry electrospun MeHA scaffolds with aligned and random fibers with and without PLGA microspheres using traditional SEM. (scale bar=10 μm). Bottom panel shows scaffolds in a hydrated state using ESEM. (scale bar=50μm)

microspheres to the aligned conditions did not significantly change the porosity, however, the addition did significantly change the porosity of the random samples with $p \leq 0.001$. The porosity measurements for the dry conditions are similar to the 50-90% porosity reported by others in literature [143].

Bulk mechanical testing was also done on all scaffolds types both dry and hydrated (Table 2-2). Our mechanical testing machine is equipped with a water bath allowing us to not only test the scaffold when hydrated, but also submerged in PBS at 37°C. The hydrated conditions had moduli starting near the 0.50 MPa (Random + MS) and increasing to 2.86 MPa (Aligned + MS). As expected, after hydration, all conditions had a significant decrease in both Young's Modulus, from 10.48-88.99 MPa for dry conditions down to 0.43-2.86 MPa for hydrated conditions, and ultimate strength, from 0.71-3.75 MPa for dry conditions down to 0.035-0.37 MPa for hydrated conditions ($p \leq 0.05$).

Table 2-2: Mechanical Testing

		Aligned + MS	Aligned - MS	Random + MS	Random - MS
Dry	Modulus (MPa)	36.84 ±10.75$^{\#}$	88.99 ±19.90$^{\#¥}$	19.26 ±10.91	10.48 ±2.09
	Ultimate Stress (MPa)	1.72 ±0.77$^{\#}$	3.75 ±1.03$^{\#¥}$	0.71 ±0.29	0.79 ±0.20
	n	6	5	9	8
Hydrated	Modulus (MPa)	2.86 ±0.90*	0.95 ±0.09*	0.43±0.02*	0.76 ±0.09
	Ultimate Stress (MPa)	0.31 ±0.13*	0.37 ±0.03*	0.035 ±0.009*	0.068 ±0.008*
	n	6	7	13	6

* Indicates $p<0.05$ compared to dry in the same condition, # Indicates $p<0.05$ compared with random scaffolds in the same condition, ¥ Indicated $p<0.05$ compared with scaffolds with microspheres.

Degradation testing was done to confirm that the materials will break down to make room for the regenerating neurites. Samples of a fixed diameter were cut from Aligned + MS and Aligned - MS scaffolds. Three samples were placed in PBS and three in Hyaluronidase (HD). After 3 weeks, all conditions had lost at least half of their mass. The high rate of mass loss for samples containing microspheres is likely due to the breakdown of PLGA into lactic and glycolic acid. The amount of HA that was broken down during that time was also measured for five samples of each condition. As expected, more uronic acid, a byproduct of HA degradation, was released from scaffolds in the hyaluronidase than in pure PBS as seen in Figure 2-4.

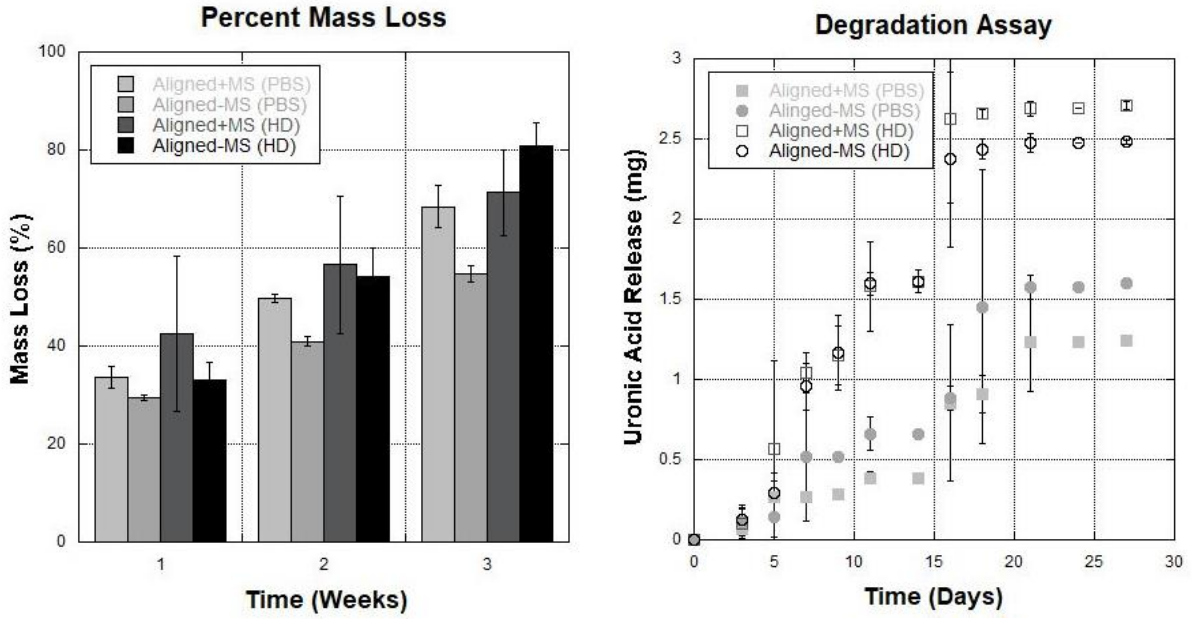

Figure 2-4: Degradation. A) Mass lost by Aligned+MS and Aligned-MS samples over 3 weeks in either PBS or hyaluronidase (HD). Samples with microspheres degraded faster likely due to the breakdown of the PLGA. B) Uronic acid released from Aligned+MS and Aligned-MS samples over 4 weeks. Samples in hyaluronidase (HD) released uronic acid, a byproduct of the breakdown of HA faster than those in PBS.

NGF Encapsulation

As the concentration of NGF increased, the total amount of neurite outgrowth also increased. This correlation indicates that the NGF remained bioactive following production and that we could successfully increase the concentration of NGF within the microspheres. The quantification of neurite outgrowth area normalized to the DRG body area can be seen in Figure 2-5c. The 100 µg/mL condition was significantly different from the 0, 25, and 50 µg/mL conditions ($p \leq 0.05$). For the remaining NGF tests, the 100 µg/mL concentration was used because this conditioned showed the longest neurite outgrowth.

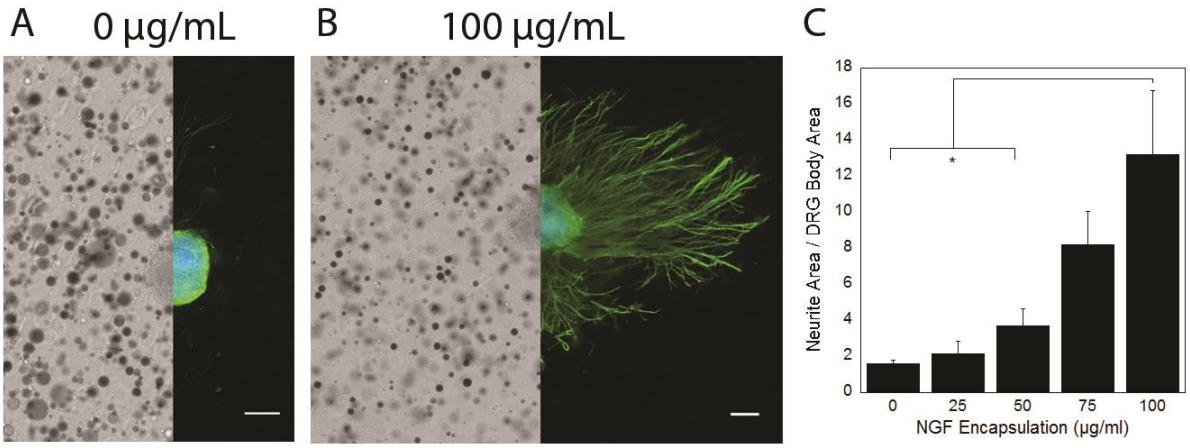

Figure 2-5: NGF Encapsulation Test. Brightfield image of scaffolds with microspheres split with fluorescent images of DRGs with neurites stained for neurofilament antibody with FITC secondary (green) and nuclei stained with DAPI (blue). (A) DRGs grown on scaffolds with empty microspheres. DRGs show little outgrowth without NGF. (B) DRGs grown on scaffolds with microspheres filled with 100 µg/ml NGF show robust outgrowth. (Scale bar= 250 µm). (C) Total neurite area / DRG body area for DRGs grown on scaffolds with 0-100 µg/ml. DRG growth is significantly longer for 100 ng/ml compared to 0, 25 and 50 µg/ml conditions ($p<0.01$). Error bars represent standard error.

Aligned Fibers Enhanced and Directed Growth

All four scaffold types were seeded with DRGs to test neurite outgrowth. For scaffolds without microspheres, NGF was added to the media as a positive control. Sample images can be seen in Figure 2-6. The difference in DRG body size is due to anatomical differences in embryos that the DRGs were harvested from, additionally DRGs vary in size in different areas of the spinal cord [144].

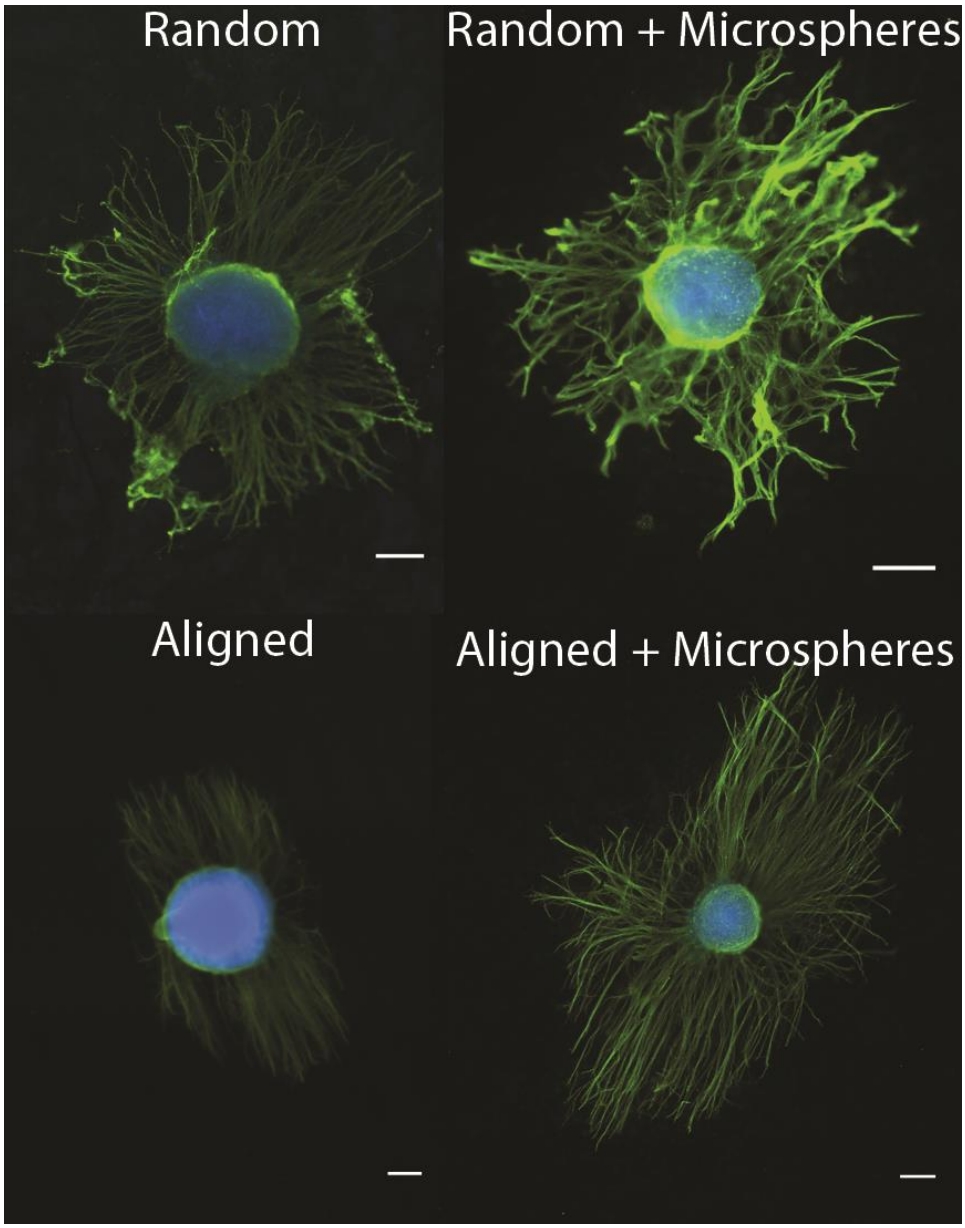

Figure 2-6: Sample Images of DRGs. DRGs were cultured for 5 days on aligned and random scaffolds with and without microspheres. Samples without microspheres were supplemented with 50ng/ml in the media. Neurite growth is robust in all conditions. Aligned fibers direct neurite outgrowth. (scale bar= 250 µm)

The DRG images on the bottom row show neurites growing along the aligned fibers primarily in one direction, while on the top row the neurites are growing in all directions from the neurite body on the random fibers. This is quantified in Figure 2-7b, where the aspect ratio for neurite growth on aligned fibers is significantly higher for both the microspheres and media NGF conditions when compared to the corresponding random fiber conditions ($p \leq 0.05$). This indicates that the aligned fibers influence the direction of neurite growth. The quantification of growth ratio can be seen in Figure 2-7a. Since all the cells were provided with NGF it was expected that all of them would show some growth. The question was whether the encapsulated NGF would perform similarly to the fresh NGF in media. Analysis showed no significant differences in neurite growth among the four conditions indicating that NGF survived the production process. However, further testing was required to determine how long the NGF would remain functional during release.

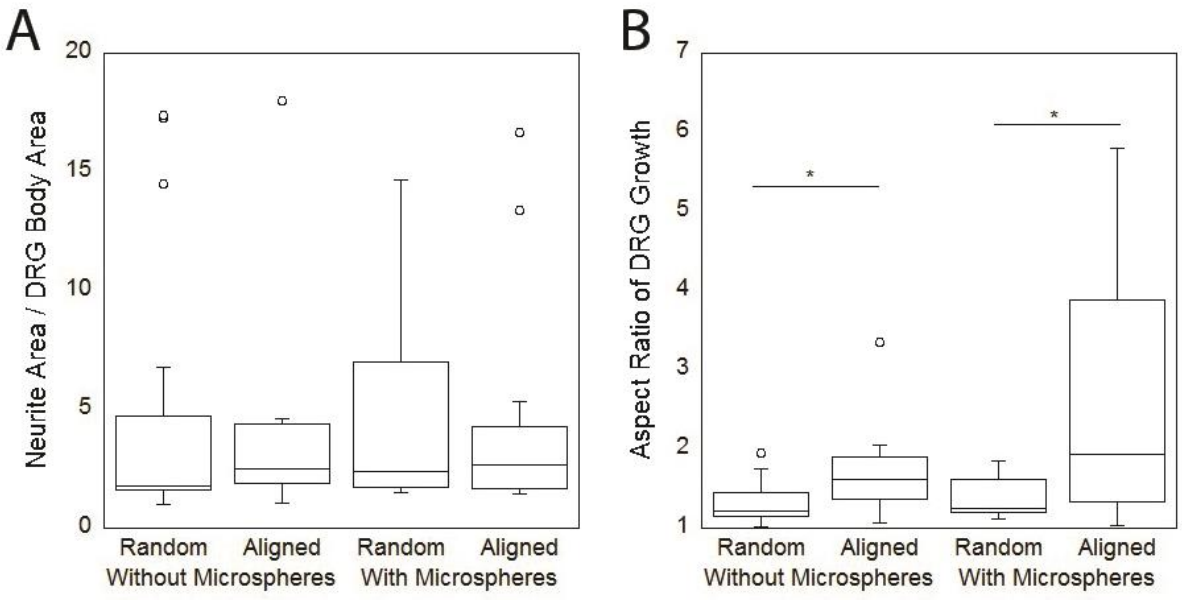

Figure 2-7: Neurite Outgrowth Quantification. (A) Neurite area, measured through neurofilament staining, divided by DRG body area shows no significant differences for all four conditions. Indicating that the NGF released from the microspheres stimulated growth similar to the fresh NGF in media (B) Aspect ratio measurements of DRG growth shows alignment significantly increased the aspect ratio of DRG growth indicating directed outgrowth ($p<0.05$).

NGF Release

An ELISA was used to quantify the temporal release of NGF from the microspheres for all three L:G ratios. The release curve obtained is shown in Figure 2-8. As expected the 75:25 PLGA had the smallest initial burst and slowest overall release providing a supply of NGF for nearly 4 weeks. For this reason, 75:25 PLGA was used in the final test of NGF long term viability.

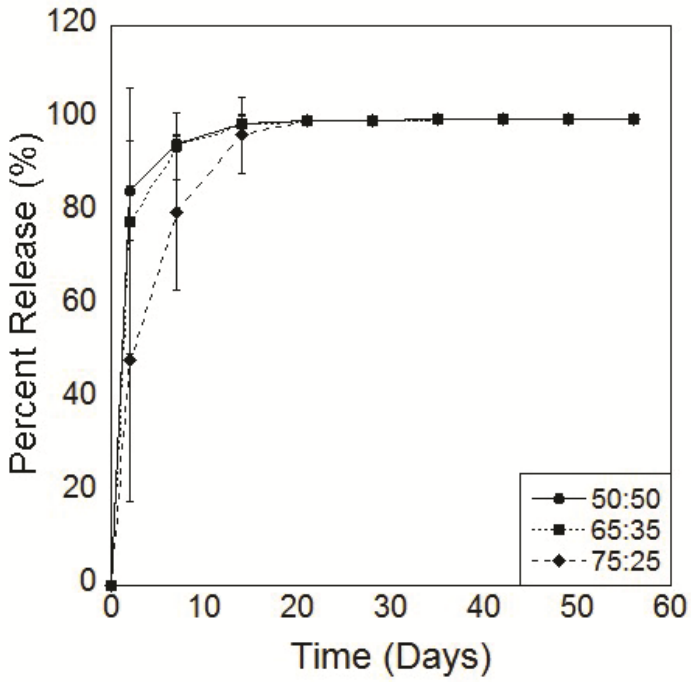

Figure 2-8: NGF ELISA. NGF release measured through ELISA for the three L:G ratios of PLGA microspheres. 75:25 showed the slowest release of NGF. Error bars represent standard error.

Extended Release from Microspheres: In this experiment, the only NGF provided to the test cells came from microspheres (conditioned media) that were encapsulated for days-weeks. DRG growth was compared to cells grown with media containing fresh NGF (positive control) and with no NGF in the media. The resulting growth ratios can be seen in Figure 2-9. Due to batch to batch variation in the DRGs all samples for a given week were normalized to the positive control. At the 2, 7, and 14-day time points the NGF released from the microspheres performed at or above the level of the NGF in the media. At 21 and 28 days, the growth was to closer to the negative control condition (no NGF), indicating that the NGF had

less effect at these points. This decrease could be attributed to a reduction in the amount of NGF released at the later time points as seen in Figure 2-8.

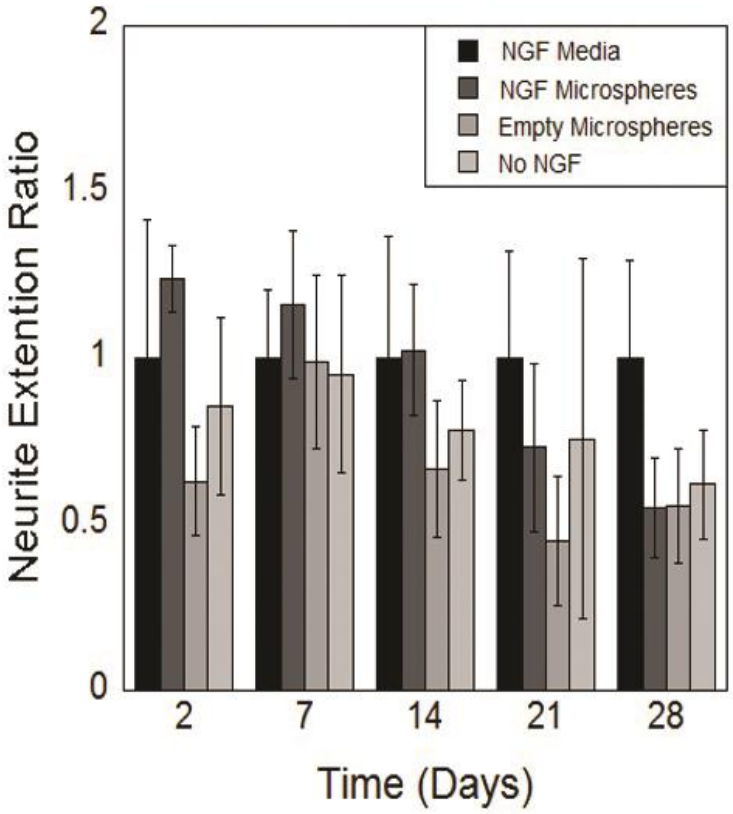

Figure 2-9: NGF Extended Release Bioactivity. Neurite outgrowth for DRGs grown for 5 days in conditioned media by microsphere breakdown releasing NGF into the media. All conditions are normalized to the NGF Media condition for that time point. Data shows that NGF released from microspheres up to 14 days performs as well or better then 50ng/mL of fresh NGF in the media. Error bars represent standard error.

Discussion

This study focuses on using hyaluronic acid (HA), a naturally occurring, nonimmunogenic biopolymer as the base biomaterial. HA is a glycosaminoglycan composed of repeating disaccharide units of D-glucuronic acid and N-acetylglucosamine, which is naturally increased in the extracellular matrix in the nervous system during embryonic development [145] and responsible for maintaining tissue homeostasis in the adult body [146]. HA has also been repeatedly shown to promote regeneration of peripheral nerves [110, 147, 148]. Additionally, HA is easily modified with methacrylates, which can be crosslinked to tailor the stiffness of the substrate [137]. The mechanical properties of the growth substrate

has been shown to affect growth and migration in all cell types and nerves specifically have been shown to prefer compliant substrates [81]. When presented with a gradient of stiffness to grow on, significantly more neurites grew down the gradient, toward the more compliant material, than up the gradient toward the stiffer material [81]. For reference, rabbit tibial nerves have been shown to have a Young's modulus of 0.50 MPa [80]. In this study, we were able to fabricate a fibrous HA scaffold in the range of natural nervous tissue, with mechanics ranging from 0.5 – 2.86 MPa when hydrated (Table 2-2).

The hydrated state of biomaterials is rarely quantified in literature despite it being the final state of the material during both in vivo and in vitro experiments. Electrospun MeHA quickly absorbs water in the presence of PBS and swells forming a fibrous hydrogel. We used ESEM to visualize the hydrated fibers. We found that the topographical cues of our material remain in the hydrated state, with scaffolds continuing to have an aligned topography; regenerating neurons have been shown to follow topographical cues [93]. The porosity of the scaffold did decrease when hydrated, however, this result was not surprising due to the hydrophilic nature of HA.

Cells throughout the body express growth factors and other chemical cues that can signal cells to migrate, proliferate and/or differentiate. Several neurotrophins, such as NGF and brain-derived neurotrophic factor (BDNF) have been identified to enhance and accelerate neurite growth [149, 150]. For this experiment NGF was selected because it has repeatedly been shown to enhance the growth of dorsal root ganglia (DRG), the cell type used for in vitro testing [151, 152]. Unfortunately, growth factors have short half-lives and, for regeneration potential, growth factors need to be delivered for several weeks to months. Many systems have attempted to add controlled release to electrospun fibrous networks with varying levels of success. These methods include blend electrospinning, emulsion electrospinning, core shell electrospinning and protein conjugation [153]. Each of these methods, however, have drawbacks. Blend electrospinning is subject to undesired distribution of factors in homogeneous aggregates. Emulsion electrospinning uses toxic and/or flammable organic solvents that could hinder in vivo use of the products [154]. Core-shell electrospinning or co-axial electrospinning has a complex design which requires precise control of all spinning parameters [155] and may not be feasible for large scaffolds.

The system tested here protects the protein using a biodegradable microsphere made of PLGA that is trapped within the electrospun aligned fibrous network. PLGA was selected as the microsphere material because its breakdown can be chemically controlled by the ratio of lactic and glycolic acid. PLGA is also an FDA approved polymer that has been extensively tested as a drug delivery system for NGF for more than two decades [156]. Micro-sized spheres were selected, rather than nano-sized, to ensure that they would contain enough protein to allow for sustained release and be too large to enter cells through endocytosis [157]. The microspheres also had to be small enough to fit through the electrospinning needle and be carried with the polymer to the collection site during electrospinning, while still being large enough to be captured in the scaffold to prevent them from moving away from the site of injury. Over time the microsphere shell is broken down, by hydrolysis, releasing the encapsulated protein to encourage nerve growth.

Microspheres have previously been tested as a controlled delivery method both by direct injection into the injury site and by inserting into NGCs [158, 159]. Loose microspheres in the conduit resulted in unpredictable final locations of the microspheres and therefore unpredictable results [140]. When immobilized along the walls of a NGC, they provided a source of chemical cues but lacked the additional benefit of topographical and mechanical cues [160]. Having the microspheres immobilized throughout the scaffold creates a more uniform signal and integrating with aligned fibers allows us to combine chemical and topographical cues. This system also allows for patterning of microspheres within the conduit to create gradients to further direct cell growth and has the potential for including several chemical cues with tailored release profiles. Together, this scaffold has mechanical, topographical and chemical cues to encourage nerve regeneration.

This system can easily be translated into a NGC for in vivo testing or clinical use. Through electrospinning, we fabricate a sheet of material that can be removed from the mandrel, cut to the size needed and inserted into existing NCGs prior to implantation. As an alternative, we have developed a stepwise electrospinning process to create the entire NCG. The outer shell is electrospun first, then the

internal components are electrospun on top. Finally, the material is cut to the appropriate size and rolled into a conduit.

Based on the results described above, we have successfully fabricated a fibrous material, incorporated with PLGA microspheres, which can enhance and direct neurite growth (Figure 2-6 & 2-7). Our material characterization shows that scaffold fibers remain aligned and have sufficient porosity in the hydrated state to support nerve growth. Bulk mechanical testing of this material showed that scaffold properties are comparable to nerve mechanics in the hydrated state. Finally, we show that the growth factor remains bioactive for more than 3 weeks (Figure 2-8 & 2-9).

Conclusions

This study has presented an original system for production of scaffolds that provide long term delivery of protein. The combination of aligned fibers to provide a topographical cue, compliant substrate to provide a mechanically preferred environment, and protein released from microspheres to chemically direct the cells is a significant step toward mimicking the natural environment in vivo. The grouping of different modes of cell signaling shows an additive effect, improving the end result. The described scaffold system will next be incorporated into a NGC and tested in vivo using a rat sciatic nerve injury model. While the tests performed here supported the use of this system in peripheral nerve repair, changes to the electrospinning material and proteins incorporated could allow a similar system to be used in other tissue engineering environments.

CHAPTER 3: A NERVE GROWTH CONDUIT WITH MECHANICAL, TOPOGRAPHICAL, AND CHEMICAL CUES IN A RAT SCIATIC NERVE MODEL WITH PHYSICAL THERAPY

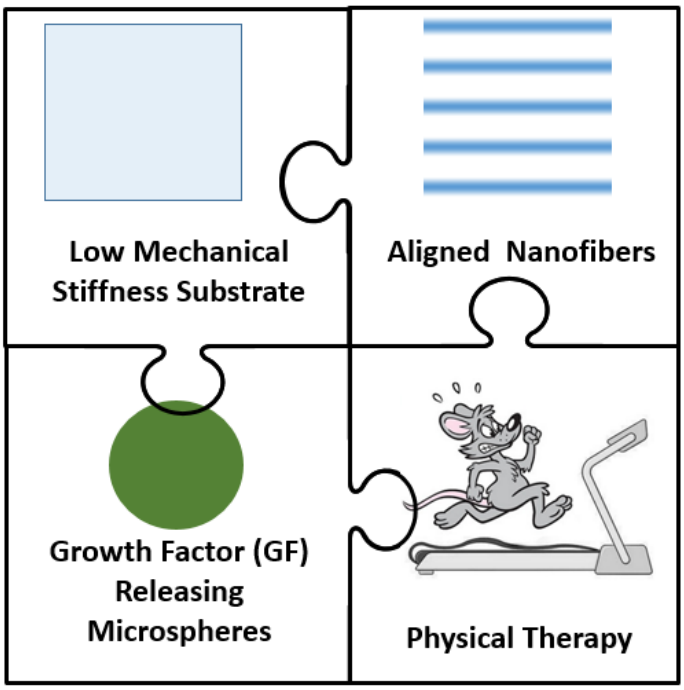

Figure 3-1: Graphical Abstract. This study aims to move a step closer to solving the puzzle of large gap peripheral nerve repair. It tests a novel nerve growth conduit containing mechanical, topographical, and chemical cues in a rat sciatic nerve transection model. Physical therapy in the form of treadmill running is added as and additional cue to reduce muscle atrophy in support of functional recovery.

Introduction

On average each year, in the United States, there are 500,000 reported peripheral nerve injury cases [14]. These nerve injuries are divided into two broad categories: primary repair, which can be corrected without any additional material or tissue, and gap repair, which requires the use of additional support. Gap repairs can be further subdivided in to small and large gaps. Of cases that involve surgical repair 34.2% are large gap repairs [14]. Large gap injuries are most often repaired with an autograft, despite the fact that nerve growth conduits (NGC) were first approved by the FDA in 1995 (Figure 3-2) [14, 31]. Autografts provide a way to connect the ends of the damaged nerve in a complete nerve-specific microenvironment which includes extra cellular matrix (ECM), for the injured nerves to grow on, which is mechanically similar to the damaged nerve, and contains appropriate growth factors and supporting Schwann cells [77]. Unfortunately, autografts require the patient to have additional surgeries and which often results in donor

site morbidity, which can result in pain or loss of function. Additionally, the harvested nerves often do not match the size of the injured nerve which can reduce effectiveness.

These complications create the need for an alternative method. Currently, the most commonly used

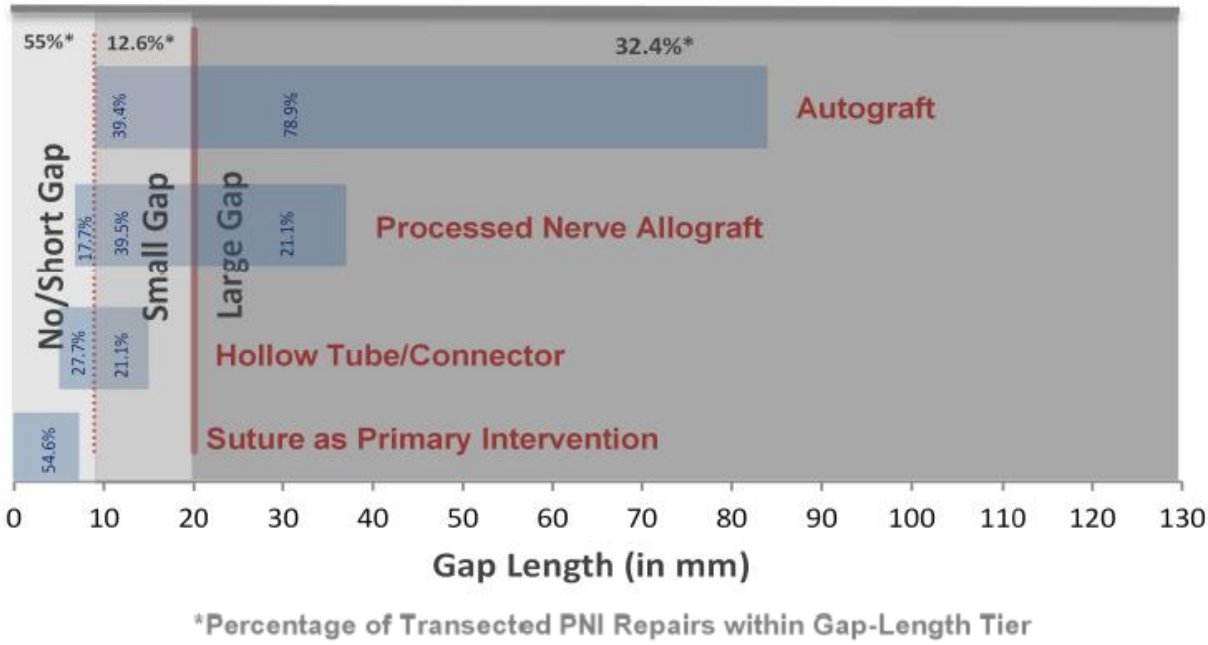

Figure 3-2: Frequency of Methods of PNI Repair by Injury Size. PNI can be broken down into three categories: No Gap, Small Gap, and Large Gap. The frequency of each repair strategy used for each gap size is described. Hollow tube connectors, also known as nerve growth conduits, are used primarily in small gap repairs. As the gap size increases the use of processed nerve allograft and autografts become more common. This figure was originally published in the Analysis of the Peripheral Nerve Repair Market in the United States, 2012 by Magellan Medical Technology Consultants, Inc. and was reproduced freely as part of the public domain.[14]

alternative clinical treatment is a processed allograft [14]. These grafts provide the same support structure found in autograft, but without the supporting Schwann cells [77]. Similar to autographs, allografts may suffer from a size mismatch with the injured nerve. This project aims to create a manufacturable system that can mimic the microenvironment that exists naturally in an autograft.

A large body of research exists exploring tissue engineering concepts to enhance the simple hollow tube nerve conduit model currently available to surgeons. One strategy is to add chemical cues to the scaffold in the form of growth factors [142, 161, 162]. Santos et al. described the production of microsphere incorporating various neurotrophins (NGF, BDNF and GDNF). The results of putting microspheres in the center of a nerve conduit were compared with delivering the growth factor to the conduit in solution. The use of locally-delivered microspheres significantly increased the number of regenerating axons. Another

modification is to provide topographical cues within the scaffold through the use of nanofibers [163-166]. Creating aligned fibers helps to guide the axon toward its target. Additionally, nerve cells are known to prefer soft substrates; this can be taken advantage of by carefully selecting the material used as a substrate. As these cumulative modifications are made, the fundamental needs of the conduit must also be considered. Many review articles have also discussed the need for the conduits to be porous to allow the passage of nutrients, providing electrical stimulation, and including support cells [18, 19, 77, 101, 167]. It is also noted that combining signals could increase the productivity of the conduit [18, 19, 39].

This study incorporated several of the modifications mentioned above into a single nerve growth conduit, which is one step closer to simulating the nerve-specific micro environment that make autografts the gold standard of repair. We combined a resorbable outer conduit, with a nerve-specific internal structure. The inner structure consisted of methacrylated hyaluronic acid (MeHA), an ECM protein with mechanical properties comparable to those of nerve tissue. The MeHA was electrospun into aligned nanofibers, which provide a topographical signal to direct the regenerating axons toward their target at the other end of the conduit. Chemical cues, specifically glial-cell derived neurotrophic factor (GDNF), are delivered through microspheres, which act as a reservoir, releasing the proteins as the microsphere shell breaks down.

Other factors outside the immediate micro environment of nerve regeneration can affect the outcomes following peripheral nerve injury. During chronic denervation, muscles will atrophy from lack of use. Physical therapy, both active and passive, can help to reduce this muscle loss, which leads slow and incomplete functional recovery [115]. Additionally, exercise leads to the upregulation of some neurotrophic factors which can support nerve regeneration [168]. To see if these benefits have an additional effect on recovery, physical therapy in the form of treadmill running, an active exercise, was added to the treatment protocol for some groups.

Materials and Methods

Animal Study Design

A power analysis was conducted based on results seen by Jin et al.. for Compound Muscle Action Potential (CMAP) [147] and Xu et al for functional testing [169] using alpha = .05 and Power = .80. Functional tests indicated the need for four animals per groups, while CMAP indicated the need for eight. Nine animals per group was selected for this study to ensure significance in all testing and to allow for the possibility of loss of animals prior to CMAP recording.

Forty-five female Lewis rats weighing ~135g were purchased from Envigo. The animals were divided randomly into five testing groups: 1) conduit with MeHA aligned fibers (Fibers); 2) conduit with MeHA aligned fibers with physical therapy (Fibers + PT); 3) conduit with MeHA aligned fibers and GDNF microspheres (Fibers + GF); 4) conduits with MeHA aligned fibers, GDNF microspheres, and physical therapy (Fibers + GF + PT); 5) Autologous graft control (Autograft). A summary of the groups can be seen in Table 3-1. All work with animals was approved by the Wayne State University Institutional Animal Care and Use Committee.

Table 3-1: Group Descriptions

Group	Surgical Treatment	Growth Factor	Physical Therapy	n
Auto	Autograft	None	None	9
Fibers Only	Conduit with MeHA Fibers	None	None	9
Fibers + PT	Conduit with MeHA Fibers	None	Treadmill	9
Fibers + GF	Conduit with MeHA Fibers	GDNF	None	9
Fibers + GF + PT	Conduit with MeHA Fibers	GDNF	Treadmill	9

Microsphere Production

GDNF was encapsulated in poly-lactic-co-glycolic acid (PLGA - Lactel, Birmingham, AL) using a Water-Oil-Water double emulsion technique. The 200µL inner water phase contained 100µg/mL GDNF in sterile water and 4µL of 2% polyvinyl alcohol (PVA). This was dispersed in the oil phase of 300mg of 75:25 PLGA dissolved in 3mL of dichloromethane (DCM) using a wand sonicator for 10 seconds. The resulting emulsion was dispersed in the outer water phase consisting of 0.5% PVA using a vortex mixer for 60 seconds then placed on a stir plate for a minimum of 1 hour to allow the DCM to evaporate and the

PLGA to stabilize. The microspheres were then removed from solution by centrifugation (2000 RPM for 10 minutes), rinsed three times, lyophilized and stored at -20 °C until use [5, 170].

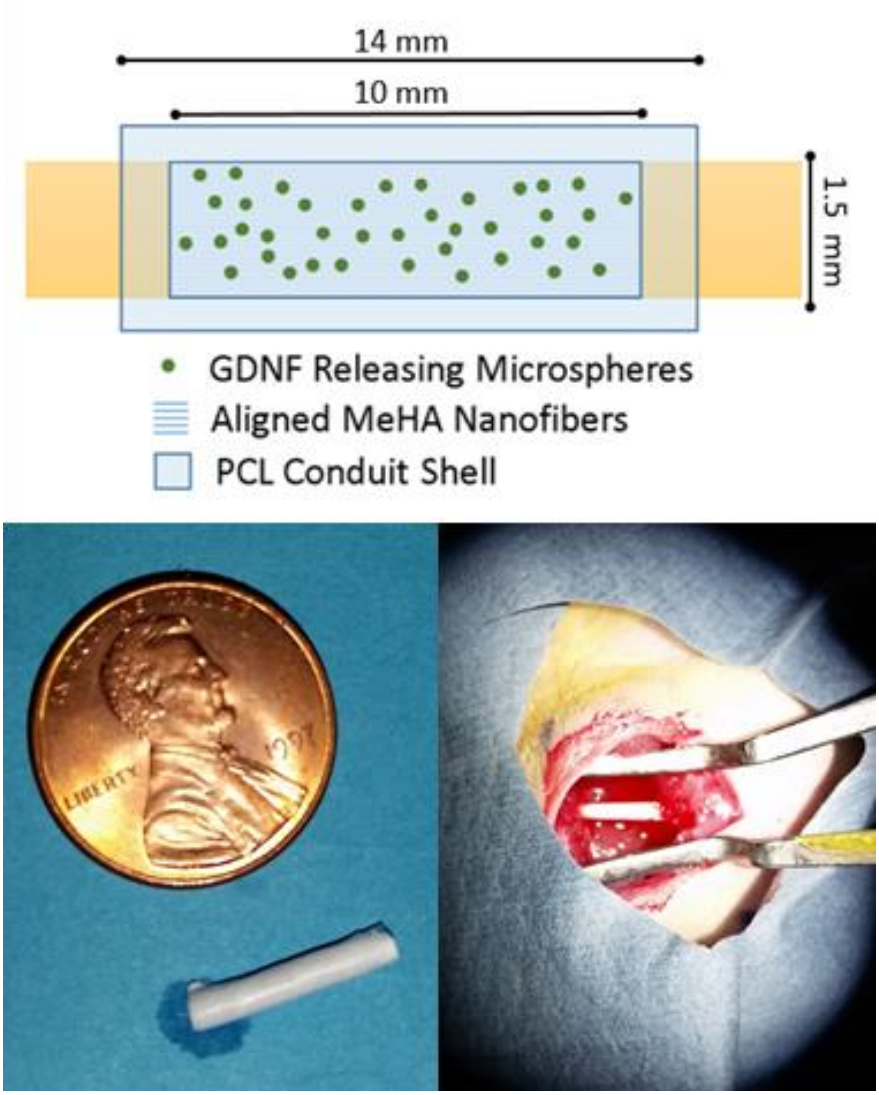

Figure 3-3: Conduit Schematic and Macro Images. A) The conduit consists of aligned fibers for topographical and mechanical cues containing microspheres that release growth factors to provide a chemical cue. B) The finished conduit. C) A conduit immediately following implantation to repair a 8mm nerve gap.

Conduit Production

For the outer layer of the conduits, 6% w/v 80 kDa polycaprolactone (PCL) was dissolved in hexafluoropropylene (HFP) and electrospun at 13kV with a flow rate of 1mL/hr onto a mandrel spinning at 10m/s to create aligned fibers to a thickness of ~250µm. The sheet was then removed and cut into 14mm x 10mm pieces. These pieces were later rolled so that the fibers were oriented around the circumference of

the conduit. To add the inner layer, which consisted of methacrylated Hyaluronic Acid (MeHA) fibers or MeHA fibers with MS depending on the test group, the PCL pieces were placed back on the collection mandrel so that their fibers were parallel to the axis of the mandrel. Custom made masks, with voids the length and circumference of inner surface of the conduit were placed over the PCL, so that the MeHA only deposited on the PCL in the area that would become the inner surface of the PCL conduit. MeHA, with and without microspheres, was electrospun as previously described [170]. Briefly, a solution of 2% MeHA, 3% polyethylene oxide PEO, and 0.5% Irgacure 2959 photoinitiator was spun at 22kV, for fibers only, or 24kV for fibers with MS, at a flow rate of 1.2mL/hr onto a mandrel spinning at 10m/s to create aligned fibers to a thickness of 250μm. The individual pieces were removed and the custom masks were carefully cut off. The MeHA fibers were thus perpendicular to the PCL fibers. The unrolled conduits were crosslinked for 30 minutes under 10mW/cm^2 365nm light. They were then rolled, and the edge was sealed with tissue adhesive, N-butyl-2-cyanoacrylate [161]. The resulting conduits were 14mm long, with 10 mm of fibers on the inner surface, and an inner diameter of 1.3mm. Conduits were sterilized through low temperature ethylene oxide exposure over two days and sealed in sterile containers. Containers were opened 24 hours prior to implantation surgery in a sterile environment to add sterile phosphate buffered saline (PBS) which dissolved the PEO carrier in the inner layer.

Implantation Surgery

The rats were given sub-cutaneous (SC) injection of sustained release Buprenex (0.5 mg/kg) for pre-emptive analgesia at least 30 minutes before surgery. Rats were then anesthetized using 5% isoflurane in oxygen at 1 liter/minute and maintained under anesthesia with 1.5-2.5% isoflurane. Ointment was applied to the eyes to prevent drying. The surgical site was shaved and cleaned. The animal was then placed on a water circulating heating pad covered and draped with sterile towels so that only the surgical region is exposed. Following aseptic procedures, a dorsal lateral skin incision was made on the left hind limb between the lateral aspect of the knee joint and greater trochanter of the femur bone to expose muscles and fascia. The skin was separated from the superficial fascia exposing the muscle. A gap was then created in the thigh muscle (biceps femoris) to expose the sciatic nerve.

For the autograft group, a 10 mm segment was removed from the sciatic nerve, reversed, and immediately sutured back in place with four to six epineural sutures of monofilament polyamide (8-10/0 Ethilon). For treatment groups an 8 mm section of the nerve will be removed, the remaining ends were inserted 2 mm into the nerve conduit (described above) so that they reached the inner scaffolding. The conduits were sutured in place with two sutures per end of monofilament polyamide. The muscle fascia was closed with 3-0 absorbable sutures, then the skin incision was closed with stainless steel wound clips. The rats were then removed from isoflurane and a thin layer of metronidazole in New Skin as described by Zhang et al. [171] was applied to the toes of the left foot to prevent autophagia. They also received SC injections of carprofen (5mg/kg) and lactated ringers (3% of body weight (g)) immediately following surgery. Rats were kept on the water circulating heating pad until alert. Oral Gabapentin (100mg/kg) was then administered.

Post-Surgical Care

Following surgery, SC carprofen was administered for two days, oral Gabapentin was administered for five days, and Metronidazole and New Skin topical was applied every four days throughout the study. Animals were monitored twice daily for dehydration and skin lesion for 2 weeks, then once daily for the duration of the study. They were kept on soft bedding to reduce the likelihood of pressure sores developing on the injured limb from altered stance. Additional enrichments were provided for the animals post-surgery to further deter them from autophagia or chewing at the incision site. Weekly, each animal received a novel chew, each day of the week they received a different foraging treat in addition to their standard feed. Wound clips were removed 10-12 days following surgery.

Testing Acclimation and Exercise Treatment

At least five times prior to surgery all animals were taken to the testing and exercise room for acclimation. They were placed in testing equipment, without any test being run and allowed to explore for at least 5 minutes to become comfortable with the environment. Prior to surgery, all animals were also given at least five training sessions with the treadmill prior to surgery, lasting 10 minutes each.

After surgery all animals were taken to the exercise room 5 days a week. Animals in exercise groups were placed on the treadmills for two 30 min sessions, with a 10 min break between where they were returned to their cage [115]. The treadmill speed was 5m/min. Animals in non-exercise groups were placed on non-running treadmills for the same durations.

Behavior and Functional Testing

One week prior to implantation surgery (baseline) and weekly starting one week following surgery all animals underwent the following behavioral and functional tests. Researchers performing tests were blinded to the treatment the animals received.

Static Sciatic Index: Rats were placed in individual plexiglass containers with a video camera underneath. After the animals were allowed to acclimate for 5 minutes, the rat's stance was recorded for 2 minutes. Individual frames were extracted from the video and given codes to blind researchers. The following parameters were measured from the images at each time point: Print Length (PL) from the tip of the third toe to the heel; Toe Spread (TS) the distance between the tip of the first and fifth toes; and Intermediate Toe Spread (ITS) the distance between the tips of the second and forth toes. Measurements were taken of both the experimental (O) side and contralateral side (N). The following ratios were then calculated:

Toe spread factor (TSF) = (OTS – NTS) / NTS

Intermediate toe spread factor (ITSF) = (OITS – NITS) / NITS

Print length factor (PLF) = (OPL – NPL) / NPL

The static sciatic index (SSI) was then calculated using the following equation:

SSI = (108.44 x TSF) + (31.85 x ITSF) – 5.49 [172, 173]

Ladder Walking (Footfall): A ladder was constructed as described by Bolton et al. [174]. The ladder was 1 meter long by 5 cm wide with thin smooth metal bars with spaces between the bars varying in width between 1.5 and 4 cm. The ladder was mounted ~4 feet above the ground to prevent animals jumping off. Figure 3-4A shows the ladder used for testing. Animals were allowed to walk back and forth across the

ladder at their own pace. The number of footfalls were recorded for each hind limb on three passes across the ladder. The total number of misses for the experimental side for each time point is presented.

Von Frey filament test (mechanoreceptor test): The von Frey filament mechanoreceptor test was carried out as described by Schaeffer et al. [175]. A single tester performed all hindpaw withdrawal testing and was blinded to the surgical procedure used on the sciatic nerve. For each session, following 5 min of acclimation in an acrylic box placed on a wire mesh platform, rats were stimulated on the plantar surface of each hindpaw using von Frey filaments ranging from 0.4 to 60 grams (Figure 3-4B). Each filament was applied for a period of 1-2 seconds and repeated three times at 4-5 second intervals. The threshold for paw withdrawal was recorded as the filament that produced a paw withdrawal three consecutive times. Values were reported as ratios of experimental side force required for response to contralateral side force required for response.

Figure 3-4: Ladder Walk and von Frey Testing Equipment. A) Ladder walk setup: Subjects walked across the ladder three times while the number of times they missed a rung was recorded. B) Von Frey testing setup: Subjects were placed in a acrylic box with a mesh bottom. After a minimum of 5 minutes acclimation increasing strengths of fibers were applied to the animals hind foot until they withdrew their paw.

Electrophysiological Recording and Tissue Harvest

Two months following implantation surgery animals were anesthetized using 5% isoflurane in oxygen at 1 liter/minute and maintained under anesthesia with 1.5-2.5% isoflurane. Ointment was applied to the eyes to prevent drying. The animal was placed on a heating pad then bilaterally the surgical site was shaved and cleaned. A dorsal lateral skin incision was made on each hind limb between the lateral aspect of the knee joint and greater trochanter of the femur bone to expose muscles and fascia. The skin was separated from the superficial fascia, exposing the muscle. A gap was then created in the thigh muscle (biceps femoris) to expose the sciatic nerve. The proximal aspect of the gastrocnemius muscle was identified at the posterior part of the knee joint. The bony protuberance at the distal end of the gastrocnemius was cut to detach the muscle from the foot. For stimulation, a custom-made hook electrode was placed under the sciatic nerve above the implanted conduit. Recording electrodes were made of stainless steel wire insulated by Teflon coating except for a bare tip of about 2 mm. A pair of recording electrodes were implanted via a 22- gauge needle into the midbelly regions of the gastrocnemius muscle with insertion direction proximally from the posterior part of the knee joint distally into the muscle. A ground electrode was placed on the tail of the rat. Prior to stimulation, a force transducer was attached to the detached distal end of the gastrocnemius muscle to record muscle contractile force produced by the electrical stimulation. Electrode and transducer placement can be seen in Figure 3-5. To evoke CMAPs, increasing electric stimulations of 0.1 – 15 V were administered for 0.3ms to the sciatic nerve at the firing rate of 1 Hz. Each voltage step was induced at minimum 10 times before moving to the next voltage. Neural activity EMG and force transducer output were recorded using a Biopac MP36 Data Acquisition Unit. The recordings were then repeated on the contralateral side.

Following recording, a 15 mm section of both sciatic nerves was removed, photographed, and fixed and stored in 4% paraformaldehyde until preparation histological and immunohistochemistry analysis. The gastrocnemius muscle was also collected bilaterally, weighed, then fixed and stored in 4% paraformaldehyde. The animals were sacrificed with an intraperitoneal overdose of sodium pentobarbital.

Electrophysiological Recording Analysis

A custom Matlab script was used to analyze the CMAP and muscle contractile data. First, the stimulation channel was normalized to a mean value of zero volts between stimulation spikes. The exact location of the stimulations was identified and used to designate processing blocks in the CMAP and muscle force channels. For muscle contractile force, the maximum voltage recoded following each stimulation was identified and averaged over all stimulations for each input voltage. Finally, the lowest voltage to result in a muscle contraction and which voltage resulted in the strongest contraction was determined for each leg of each animal.

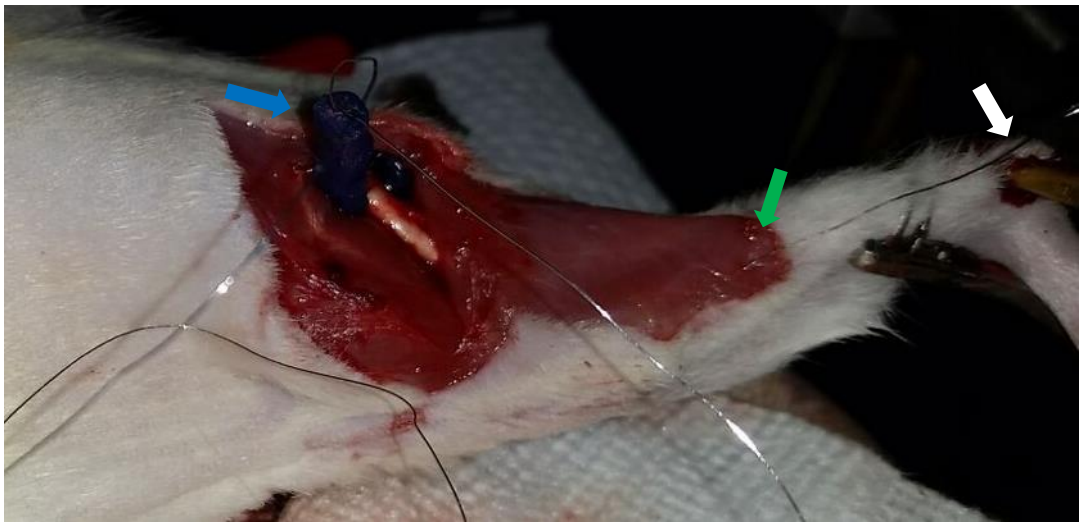

Figure 3-5: Electrode and Force Transducer Placement. A blue custom hook electrode was placed around the nerve proximal to the injury site (blue arrow). The recording electrodes are imbedded into the gastrocnemius muscle (green arrow) to record CMAP signals. A force transducer was also attached to the distal end of the gastrocnemius muscle to record muscle contractile forces (white arrow).

For CMAP recordings, signals were filtered individually in the 900 ms following the stimulation. The filtered data was used to determine the time when the signal returned to neutral after stimulation. The latency from stimulation to peak of action potential, the area under the positive portion of the curve, the overall amplitude, and the overall duration of the action potential were calculated for each animal at each stimulation voltage (Figure 3-6). Averages of all factors were determined over all stimulations for each input voltage. Additionally, the minimum voltage required to stimulate a response and the voltage that elicited the strongest response were determined for each leg of each animal.

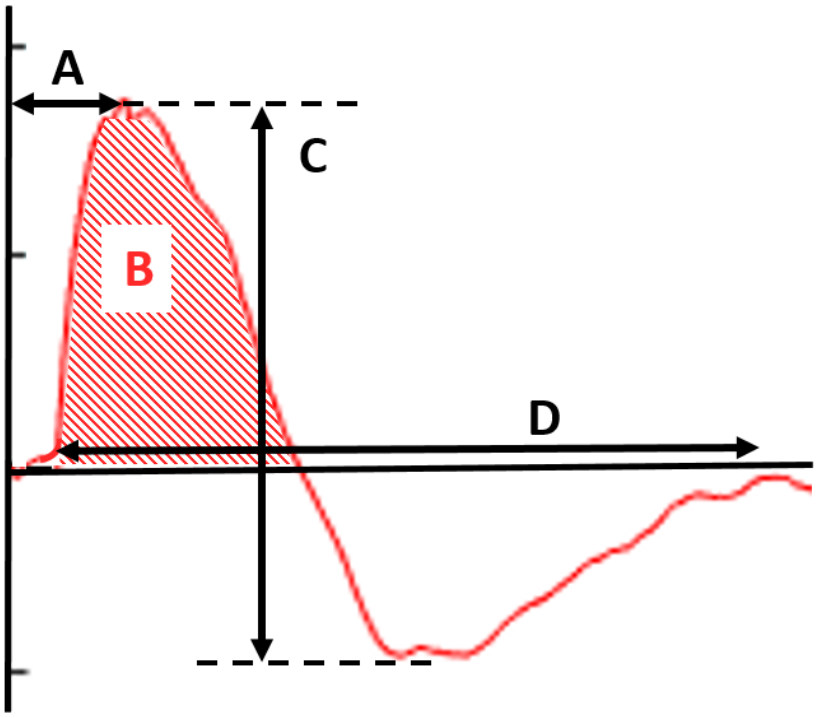

Figure 3-6: CMAP Calculations. Several measurements were taken from each stimulation applied to the nerve. A) The latency, which was measured as the distance from the stimulation pulse to the peak of the action potential response. B) The area under the action potential curve. C) The amplitude of the action potential, measured from the highest to lowest points. D) The duration, measured from the onset of the action potential until the signal stabilizes again.

Histology and Immunohistochemistry

Several histological and immunohistochemistry preparations were undertaken to examine tissue health, nerve regeneration, myelination, and support cell presence.

Hematoxylin and Eosin (H&E): Harvested nerve segments were dehydrated through increasing ethanol (EtOH) and xylene passages, then embedded in paraffin. The nerve tissue was sectioned longitudinally at 7µm thickness. Paraffin was removed from the tissue sections through multiple submersions in xylene. The tissue was then rehydrated through a decreasing EtOH gradient and deionized water. The tissue sections were stained with hematoxylin for 1 min, then dipped in eosin Y. The stained samples were rinsed with tap water, dehydrated through an increasing EtOH gradient and xylene, then mounted using DPX.

Anti-Neurofilament Light: Longitudinal sections of nerve were prepared as described under H&E. Following rehydration slices were incubated in 1% hydrogen peroxide (H_2O_2) for 1 hour; they were then rinsed with phosphate buffered saline (PBS). A solution of primary antibody for light chain neurofilament (Millipore ab9568) with 1% bovine serum albumin (BSA) and 2% normal goat serum (NGS) diluted in PBS was placed on the slides for 48 hrs at 4ºC. Control slices received a solution with only 1% BSA. After rinsing with PBS the primary antibody was bound with secondary antibody containing horseradish peroxidase (HRP) (Abcam ab6721) for 1.5 hours. Samples were rinsed with PBS then allowed to react with 3,3′-Diaminobenzidine (DAB) for 5 minutes. Once color developed they were rinsed and mounted and imaged as described above.

Anti-Neurofilament Intermediate and S100: Longitudinal sections of nerve were prepared as described under H&E. Following rehydration slices were rinsed in wash solution (1% BSA, 0.5% Triton-X) three times. They were then incubated for 1 hour in 10% NGS for blocking. A solution of primary antibody for intermediate chain neurofilament (Sigma N5389) and S100 (Sigma S2644) was placed on the slides overnight at 4ºC. Control slices received a solution with only PBS. After rinsing with PBS the primary antibody for neurofilament was bound with secondary antibody with an Alexa flour 488 tag (green) and S100 was bound with CF 568 (red) for 1 hour. Finally, DAPI was added for 5 minutes to stain cell nuclei blue. After rinsing with PBS slices were imaged with a Nikon Eclipse inverted microscope.

Osmium Tetroxide (OsO_4): The harvested nerves were first rinsed with PBS for 10 minutes. The nerve sample was cut into 3 equal pieces, keeping track of the position and proximal end of each piece. They were then placed in a 2% solution of OsO_4 for 2 hours, followed by dehydration with 3 rinses of each step of an extended EtOH and xylene gradient as described by Di Scipio et al. [176]. The 3 pieces of each nerve sample were then embedded in the same paraffin block so that the proximal end of each piece was oriented in the same direction. They were then sliced transversely and rehydrated, stained with H&E, and mounted as described above.

Statistical Tests

One-way ANOVA with Fisher's LSD post hoc testing was used to compare groups at each time point. Significance is reported as $p < 0.05$. Error bars represent standard error unless otherwise noted.

Results

Conduit

Two different types of conduits were produced. Each had an overall length of 14 mm to allow the injured nerve to be inserted 2 mm. The outer shell was made of PCL. The inner diameter of the PCL layer was 1.3 mm which is slightly larger than the injured nerves to prevent the regenerating nerve from being pinched. The first conduit type contained an inner structure of only aligned MeHA fibers. The second conduit type contained an inner structure consisting of aligned MeHA fibers with GDNF microspheres captured within the fibrous structure. A cross-section of those conduits prior to hydration and rinsing can be seen in Figure 3-7. Conduits were also produced without the GDNF microspheres as a negative control. Conduits were implanted into Lewis rats that underwent the following testing.

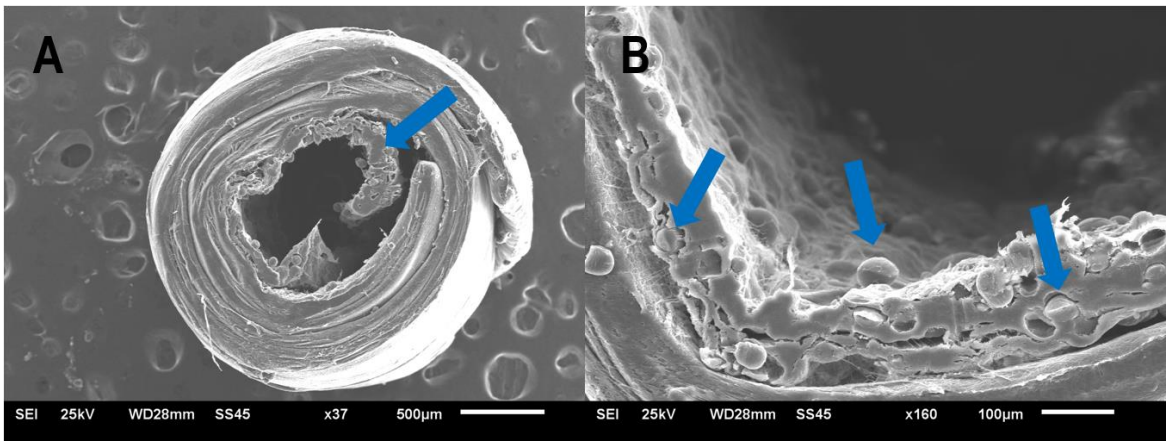

Figure 3-7: Conduit SEM. A) Shows a cross section of the center of a completed conduit. The inner MeHA and MS layer is indicated with a blue arrow. B) A higher magnification of the MeHA inner structure shows that MSs are found throughout the depth of the internal fibers. Three at different depths are indicated with blue arrows.

Ladder Walking

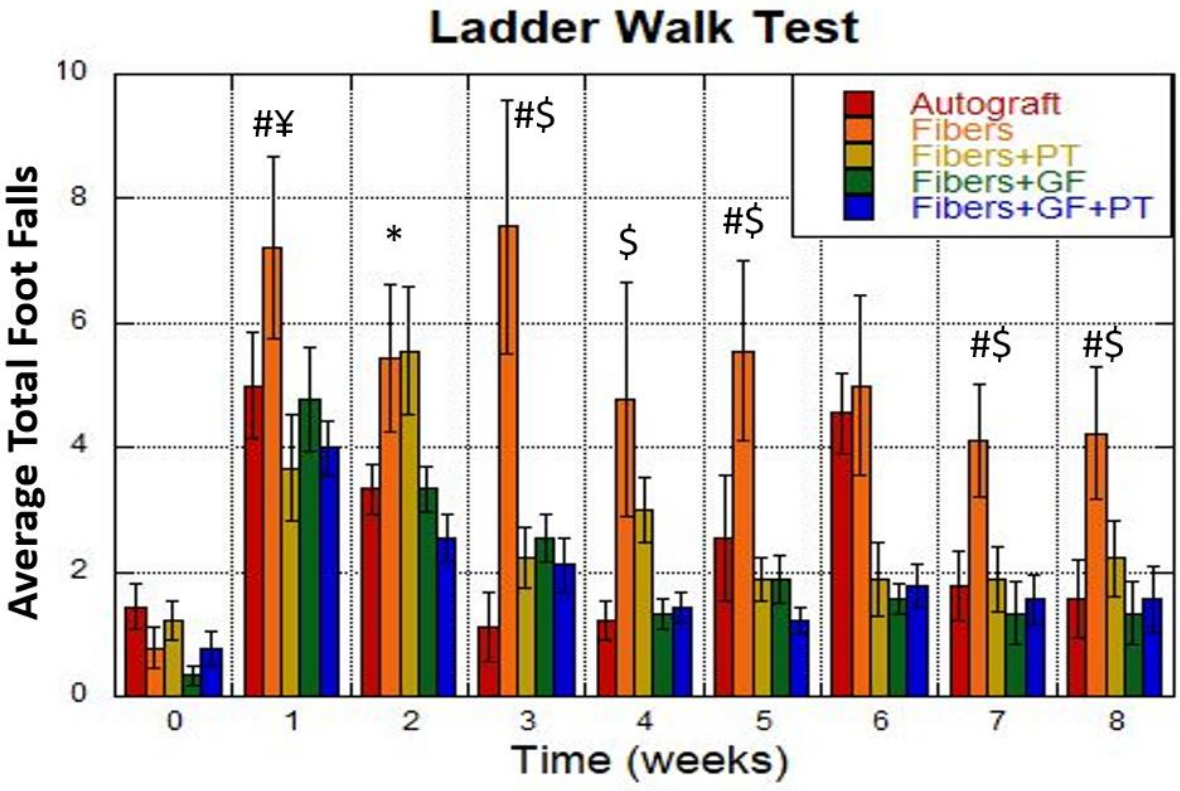

Figure 3-8: Footfall Test. Prior to surgery (0) and weekly after surgery animals (n=9) walked across a horizontal ladder and the number of times they missed a rung was recorded. Lower scores indicated better gross motor skills in the injured leg. All groups showed improvement over the duration of the study, with autograft improving fastest followed by GF groups. Statistical significance ($p < 0.05$): # Fibers + PT differ from Fibers; $ Fibers + GF differ from Fibers; * Fibers + GF + PT differ from Fibers + PT; ¥ Fibers + GF + PT differ from Fibers + GF. This indicates that both the PT and GF have some effect on the functional recovery.

Prior to surgery and weekly following surgery all subjects were allowed to walk across a ladder. Observers recorded the number of times each animal missed a rung over three passes (Figure 3-8). At 1 week Fibers was significantly different from Fibers + PT and Fibers + GF was different from Fibers + GF + PT, indicating the physical therapy is having some effect. At week 2 Fibers + PT was significantly different than all groups except Fibers. During several weeks both Fibers + GF and Fibers + PT were significantly different from the Fibers group. This indicates that both the physical therapy and the GDNF were both having a positive effect. Autograft group animals returned to counts similar to baseline within 3 weeks. In week 4 the groups with GDNF were near the autograft group. By week 5 the Fibers + PT group

also had a low number of misses. Fibers were significantly different from all other groups for weeks 3, 5, and 8.

von Frey Fibers

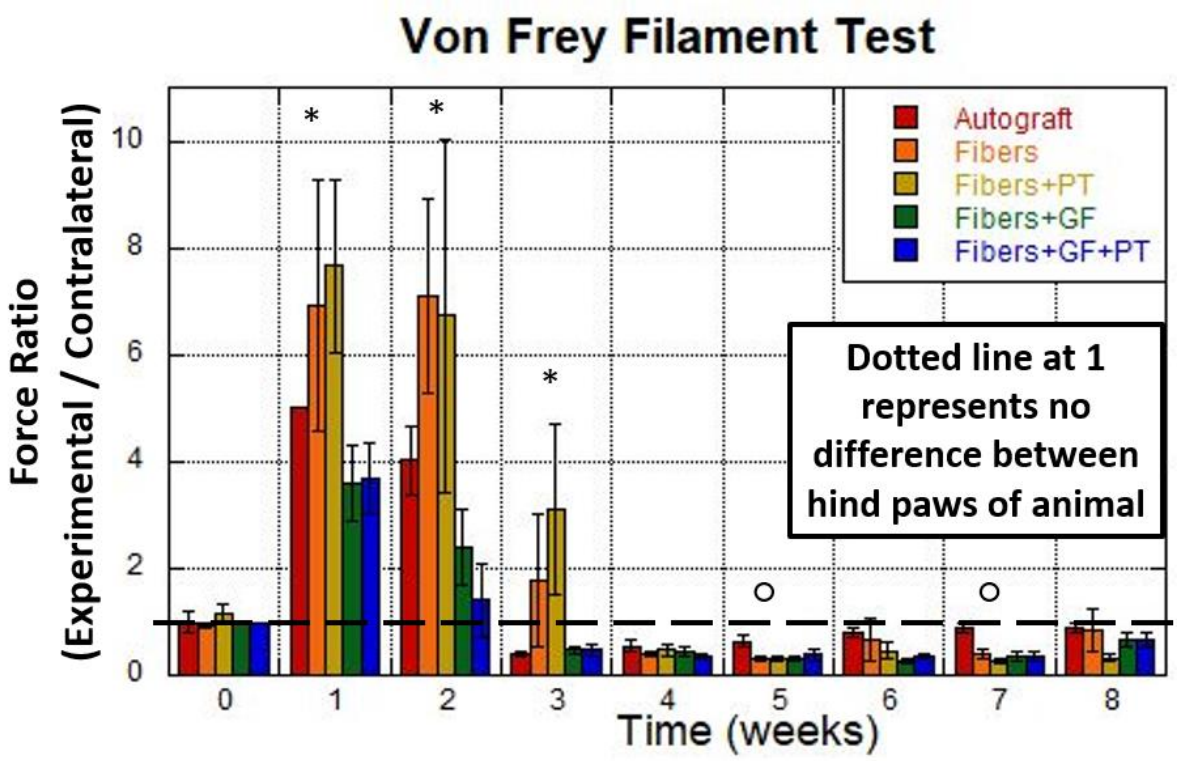

Figure 3-9: von Frey Mechanoreceptor Test. Calibrated fibers are used to test the pain threshold of animals pre- and post-surgery. Following surgery all groups lost sensory response in their injured leg. At 3 weeks autograph and GF groups showed a hypersensitivity, with the fibers groups following at 4 weeks. Statistical significance ($p < 0.05$): * Fibers + GF + PT differ from Fibers + PT; ○ Autograft different from all other groups.

In addition to gross motor function provided by motor neurons, functional recovery requires the regeneration of sensory neurons. One type of sensory neuron is a mechanosensory nerve, which responds to physical touch and registers the sensation of pain. Von Frey fibers can be used to provide a precise mechanical pressure stimulation. The animals were tested prior to surgery and weekly following surgery. The results show the ratio between the experimental leg and contralateral leg. Prior to surgery all groups responded to the same force on both hind limbs. Immediately following surgery, all groups required higher stimulus force to elicit a response on the experimental side. At week 1-3 Fibers + GF + PT was significantly different than Fibers + PT. Autographs and GF groups fell below 1 at week 3 indicating hypersensitivity, which can indicate new nerve growth. It is unlikely, however, the nerves in the sciatic reconnected; the

response more likely suggests compensation from the sural nerve [177]. At week 5 & 7 Autograft is significantly different from all other groups, having nearly returned to its pre-surgery values. It is unclear if change is due to the regeneration of the sciatic nerve or continued growth of the sural nerve, additional information from other tests is needed.

Static Sciatic Index

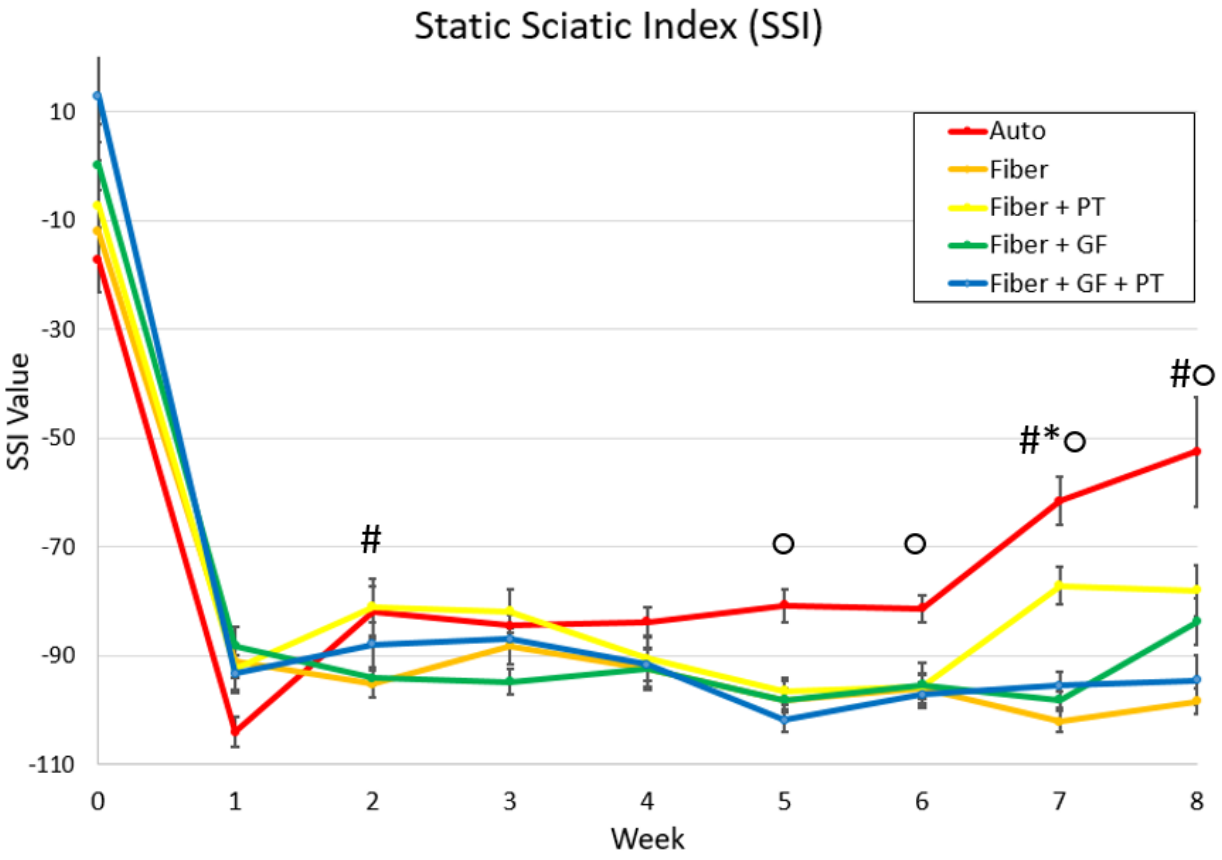

Figure 3-10: Static Sciatic Index (SSI). The sciatic index is a quantification of the severity of impairment in the sciatic nerve based on the animal's ability to spread it toes. A value of 0 indicates no impairment, with -100 being complete impairment. Autograft animals show consistent improvement through the 8 weeks of the study. Fiber + PT has some improvement in week 7 and 8. All other groups show minimal change following week 1. Statistical significance ($p < 0.05$): # Fibers + PT differ from Fibers; * Fibers + GF + PT differ from Fibers + PT; ○ Autograft different from all other groups.

One of the main results of sciatic nerve transection in rats is the loss of functional control of the muscles that govern the movement of the toes. Animals with no injury will spread their toes wide to give the best support, while those with injuries will keep their toes tightly together. Following surgery all groups showed complete impairment, as expected. Over the course of 8 weeks the autograft group recovered the

most. At week 2 Autograft and Fibers + PT were both significantly different than Fibers and Fibers + GF. In week 3 Autograft and Fibers + PT were both significantly different than Fibers + GF. Interestingly, the PT groups showed slightly higher performance during the weeks that they were using the treadmills. However, this is only significantly different for the groups without GF at week 2. After week 5 Autograft is significantly different than all other groups. After week 6 Fibers + PT are also significantly different than the other groups.

Gastrocnemius Muscle Mass

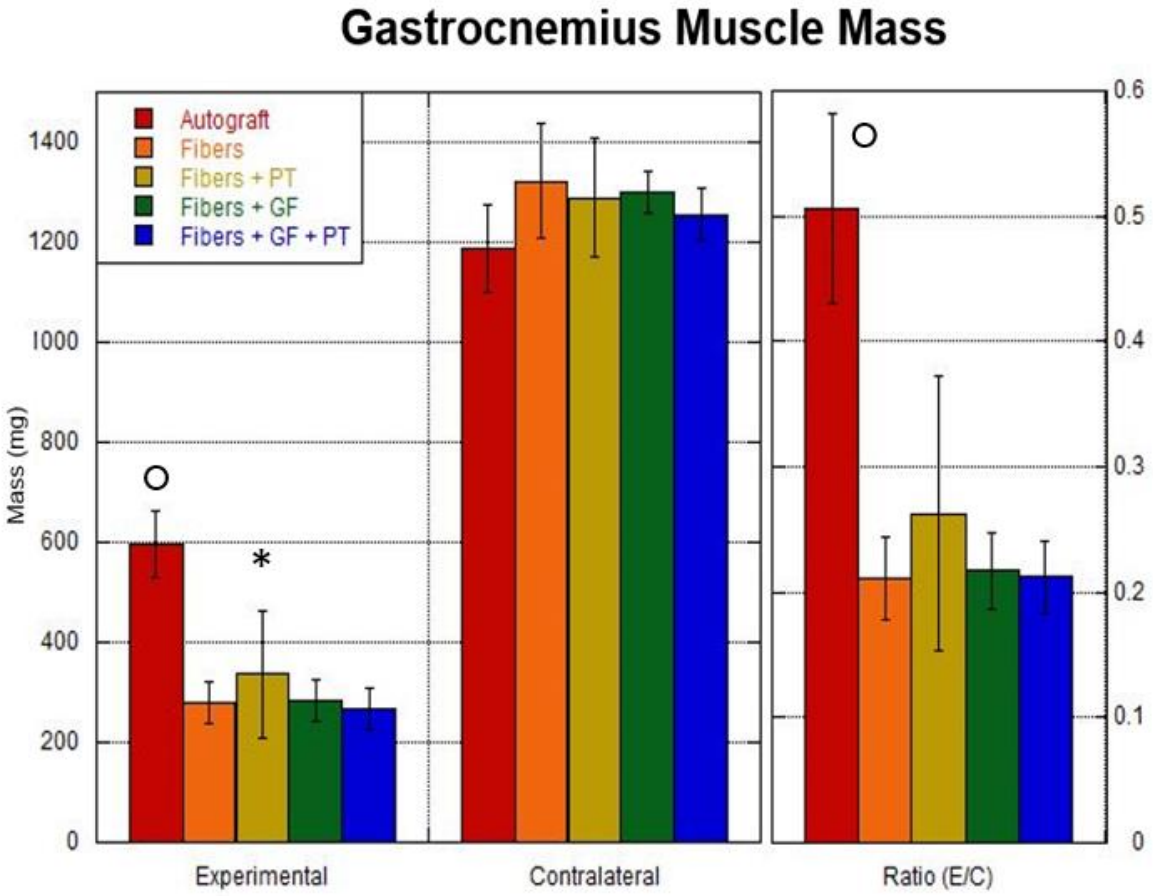

Figure 3-11: Gastrocnemius Muscle Mass. Muscle mass can indicate the amount of muscle atrophy that occurred due to injury. At the end of this study the Autograft group had 50% less muscle mass on the injured side, while the other groups had 75-80% less. Statistical significance ($p < 0.05$): ○ Autograft different from all other groups; * Fibers + GF + PT differ from Fibers + PT ($p = 0.05$)

One way to quantify the muscle atrophy is by mass. At the end of the study the gastrocnemius muscle was harvested bilaterally and weighed. All experimental groups show a 70-80% muscle loss, while the autograft group only showed a 50% loss. Interestingly, Fiber + PT was significantly different from the

Fibers + GF + PT group. Autograft was significantly different from all other groups. Because weights are only available at the end of the study, it is difficult to determine if the autograft group experienced similar muscle atrophy to the other groups earlier in the study. However, it is likely that they did and subsequently recovered some muscle mass as the muscle was reinnervated. Muscle fiber and neuromuscular junction analysis is needed to confirm this.

Muscle Contractile Force

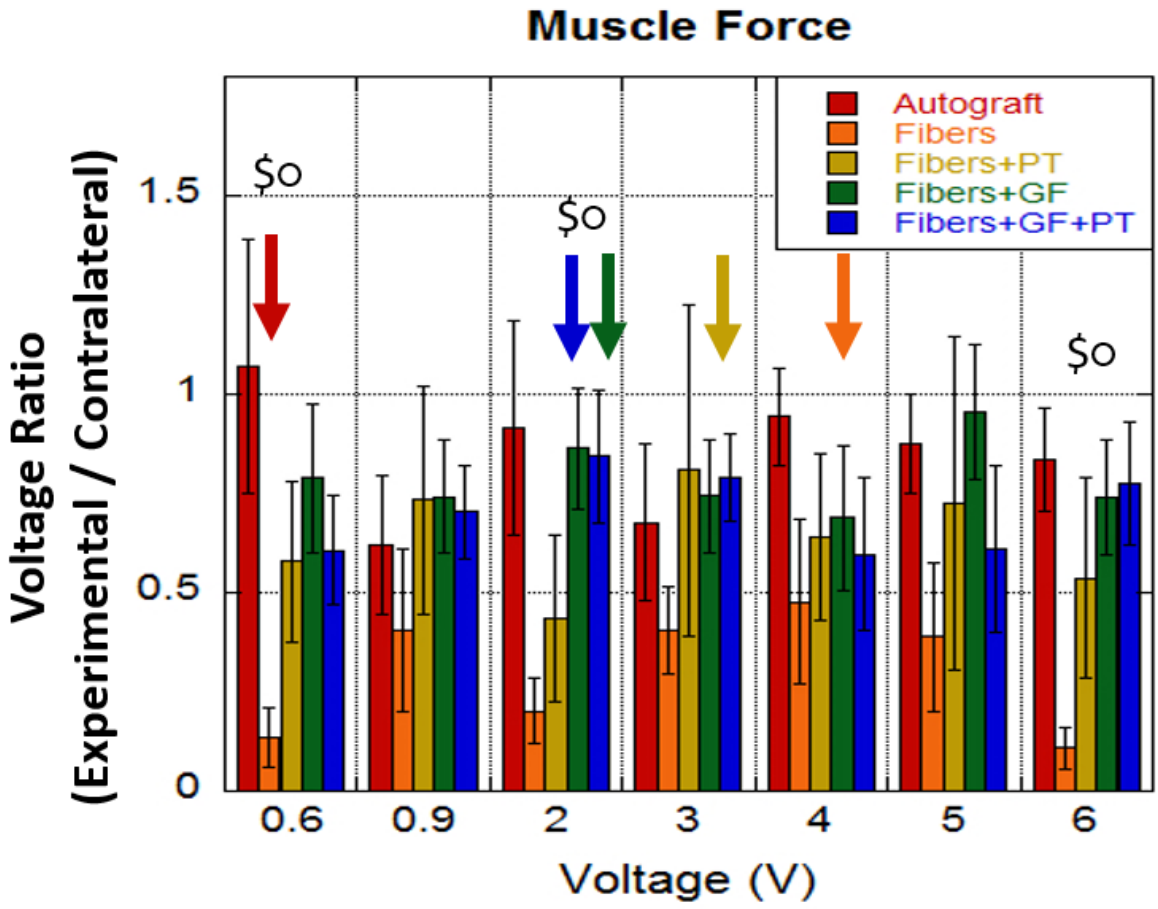

Figure 3-12: Muscle Contractile Force. At the end of the study, a force transducer was used during electrical stimulation to measure the amount of force produced by the gastrocnemius muscle. The figure shows the ratio of the experimental side muscle to the contralateral side at various stimulation voltages. Low values indicate poor muscle strength on the injured side. Arrows indicate the voltage where that group has a peak in force ratio. Statistical significance ($p < 0.05$): * Fibers different from Auto, Fibers + GF, and Fibers + PT ; # Fibers different from Autograft.

The strength of muscle contraction is related to the number of muscle fibers that activate during the contraction. Muscles begin to atrophy when they lose neural stimulation, therefore muscle atrophy is a

common side effect of peripheral nerve injury. Contractile strength can give an indication of how much the muscle has atrophied and the number of active neural muscular junctions that exist. As nerve connections to the muscle are restored the contractile force should also increase. For the spectrum of voltage ranges used the Autograft group show the strongest response, while the Fibers group showed the weakest. Interestingly, we see a peak in force for both GF groups at a higher voltage than we do for the groups that do not have growth factors. The experimental side was weaker than the contralateral side at all voltage levels. Fibers alone are significantly different than Fibers + PT, Fibers + GF + PT and Autograft at 0.6, 2, and 6 Volts.

Compound Muscle Action Potential

Compound Muscle Action Potential (CMAP) can provide us with information about the effectiveness of the nerve signaling and the amount of muscle fiber that is innervated. Each muscle fiber has axons that connect to multiple different muscle fibers. Collectively, the nerve and muscles it innervates are referred to as a motor unit [50, 178]. The amount of force produced by a muscle depends on the number of motor units activated. The combination of action potentials that are signaling to motor units is the CMAP.

A voltage sweep was used in this study to show the differences in motor unit activation. Since CMAP is an additive signal from multiple motor units or muscle fibers, a larger CMAP value indicates an increase in muscle fiber activity [179]. Several measurements were made from the recorded EMG signals. First, the area under the positive portion of the curve was measured. This gives an indication of the number of fibers that were firing. Next, the amplitude of the curve was calculated. Muscle fibers that are firing in sync, which is the normal response, create a taller and narrower impulse; a wider curve indicates fibers firing out of sync. To further describe the specific shape of the response, duration of the initial peak and the overall wave were calculated. The amplitude divided by the duration of the stimulated peak, referred to here as shape factor, can be compared to the normal condition. Finally, the latency of the peak was calculated. This indicates the amount of time from the stimulus to the action potential being created in the muscle. Selected voltages for each of the above parameters are shown in Figures 3-13 through 3-17 on the following pages.

Table 3-2: Voltage Which Produces Strongest Response

Parameter	Control	Auto	Fibers	Fibers+PT	Fibers+GF	Fibers+GF+PT
Area	.9	4	6	5	7	3
Amplitude	.9	4	7	5	8	5
Duration	.9	4	7	5	.9	.1
Latency	.9	.2	.2	.8	1	2

In addition to the parameters calculated at each stimulation voltage, the voltage that elicited the strongest response was calculated for each group. For comparison the average minimum and average peak voltages from all the animal's contralateral recordings is used as the control value. These values are summarized in Table 3-2.

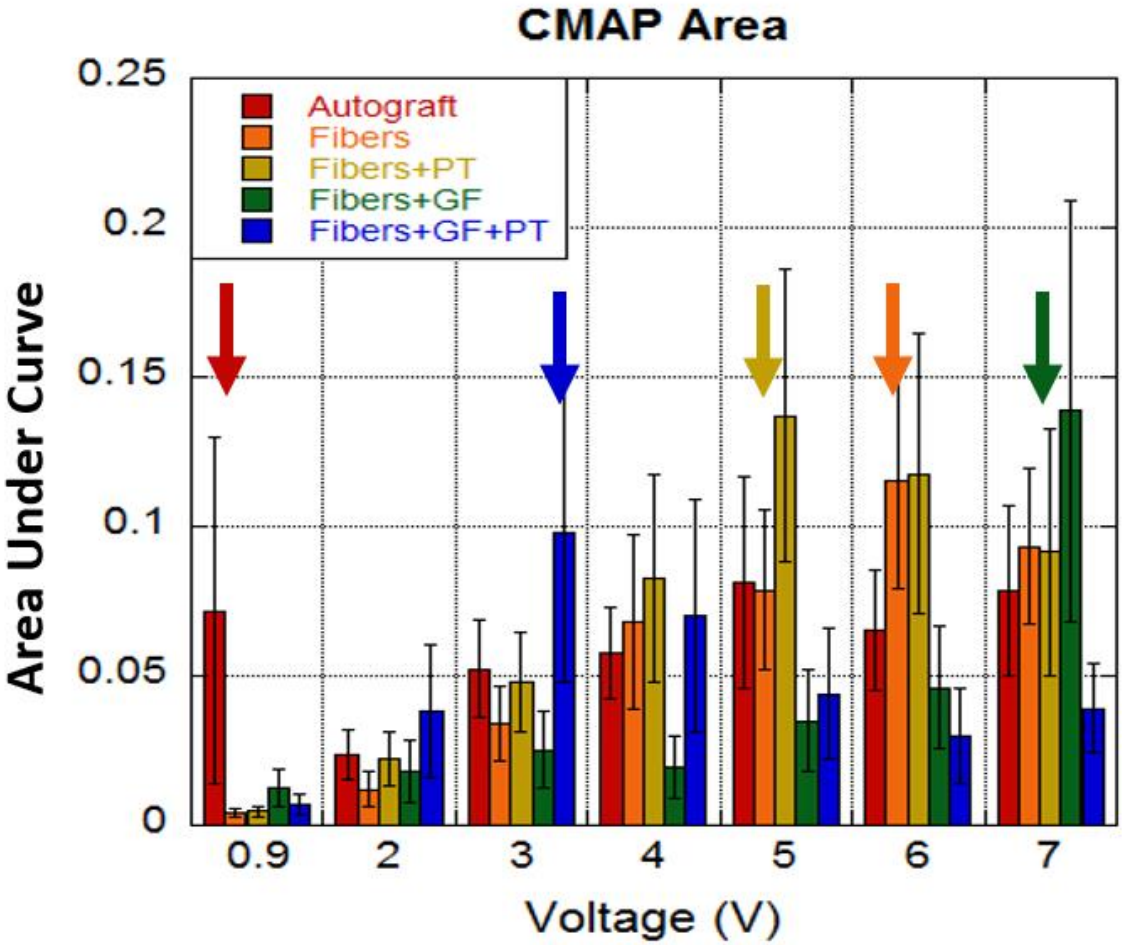

Figure 3-13: Area of Compound Muscle Action Potential. The CMAP signal increases as more muscle fibers fire simultaneously. Arrows indicate where groups show a peak in area. The Fibers + GF + PT group shows the strongest response first at stimulation of 3V, while other experimental groups require more stimulation to reach the same area.

Area under the CMAP curve can indicate the number of fibers stimulated, while the amplitude provides information about how coordinated the signals are. For CMAP area at a stimulation of 5 V the Fibers + PT group is significantly higher than the Fibers + GF group. The stimulation voltage which has the peak response for each group is also important. In this case Fibers + GF + PT shows a peak at a lower stimulation voltage than all other experimental groups.

CMAP Amplitude can indicate when the motor units are working together best. Again, the Fibers + GF + PT group reaches a peak before others in the class. At 0.9 and 4 V the autograft group is significantly higher than all other groups.

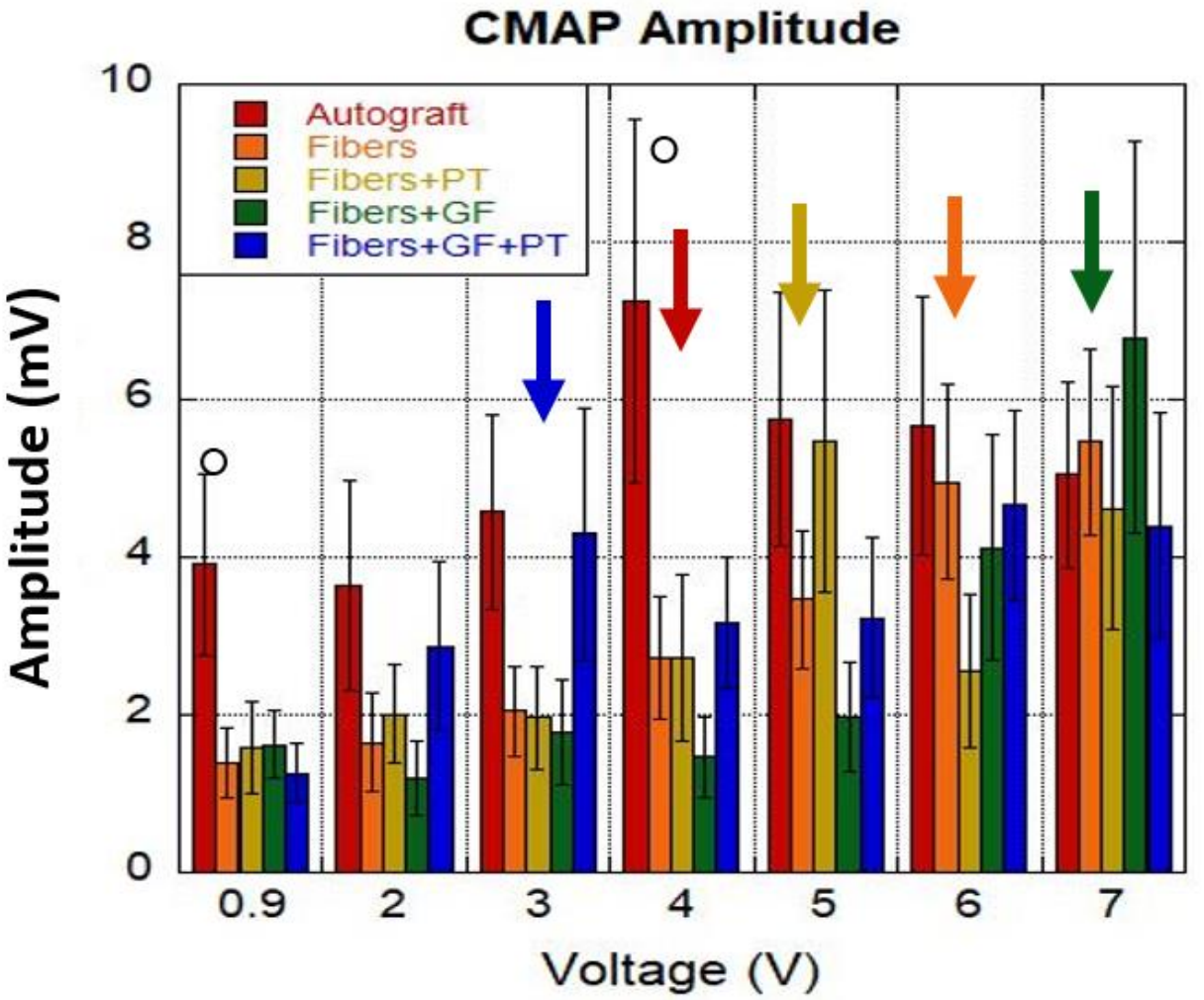

Figure 3-14: Amplitude of Compound Muscle Action Potential. The CMAP signal increases as more muscle fibers fire simultaneously. The Fibers + GF + PT group shows increasing amplitude at lower stimulation voltages than the other experimental groups. Arrows indicate were that group shows a peak in amplitude. Statistical significance ($p < 0.05$): ○ Autograft different from all other groups

Another value that can be calculated for CMAP is the latency of the signal. Due to the short distance and corresponding short time to CMAP initiation, latency here is calculated from stimulation to the peak of the action potential. At stimulation voltages of 4 and 5 V the Fibers + GF group has a significantly shorter latency than the Fibers + PT group.

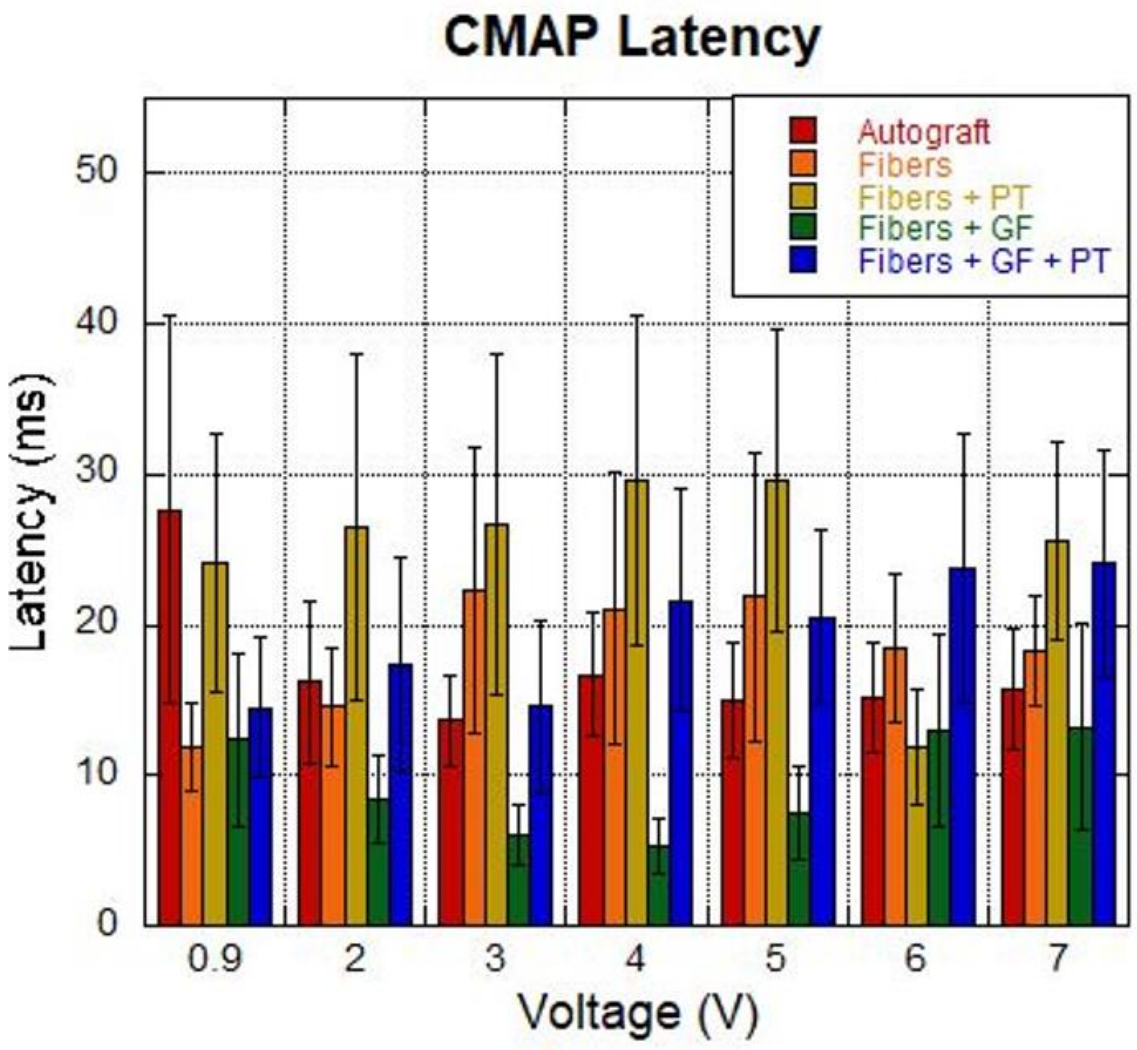

Figure 3-15: Latency of Compound Muscle Action Potential. Latency is a measure of the time it takes for the signal to take effect. Shorter times indicate improved signal transmission.

The amount of time the action potential is occurring, or duration, can also be calculated. Multiple factors can contribute to the duration. A strong action potential can lead to a longer recovery and thus a longer duration. This is likely what occurred with the autograft group. Alternatively, poor signaling leading to motor units firing out of sync could also lead to increased duration. This could be what occurred with the groups which didn't receive growth factors. There were no significant differences in the duration data.

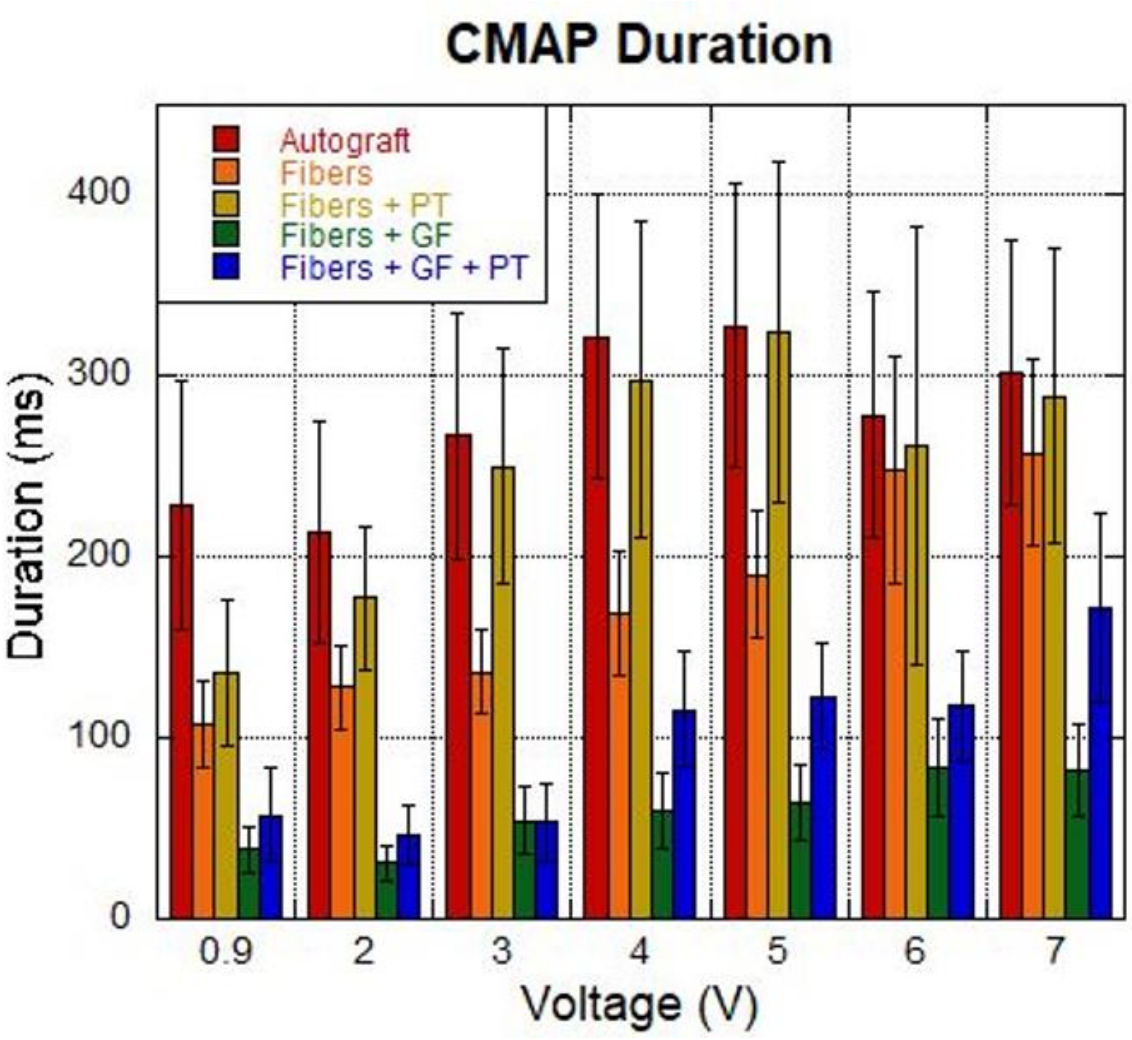

Figure 3-16: Duration of Compound Muscle Action Potential. Duration is calculated from the onset of action potential until the signal stabilizes again. Duration can be increased by the strength of the action potential or by motor units firing out of sync.

Histology and Immunohistochemistry

H&E staining can provide a glimpse into the health of tissue. Cell cytoplasm is stained pink and nuclei are stained purple. Sample images of are provided in Figure 3-17.

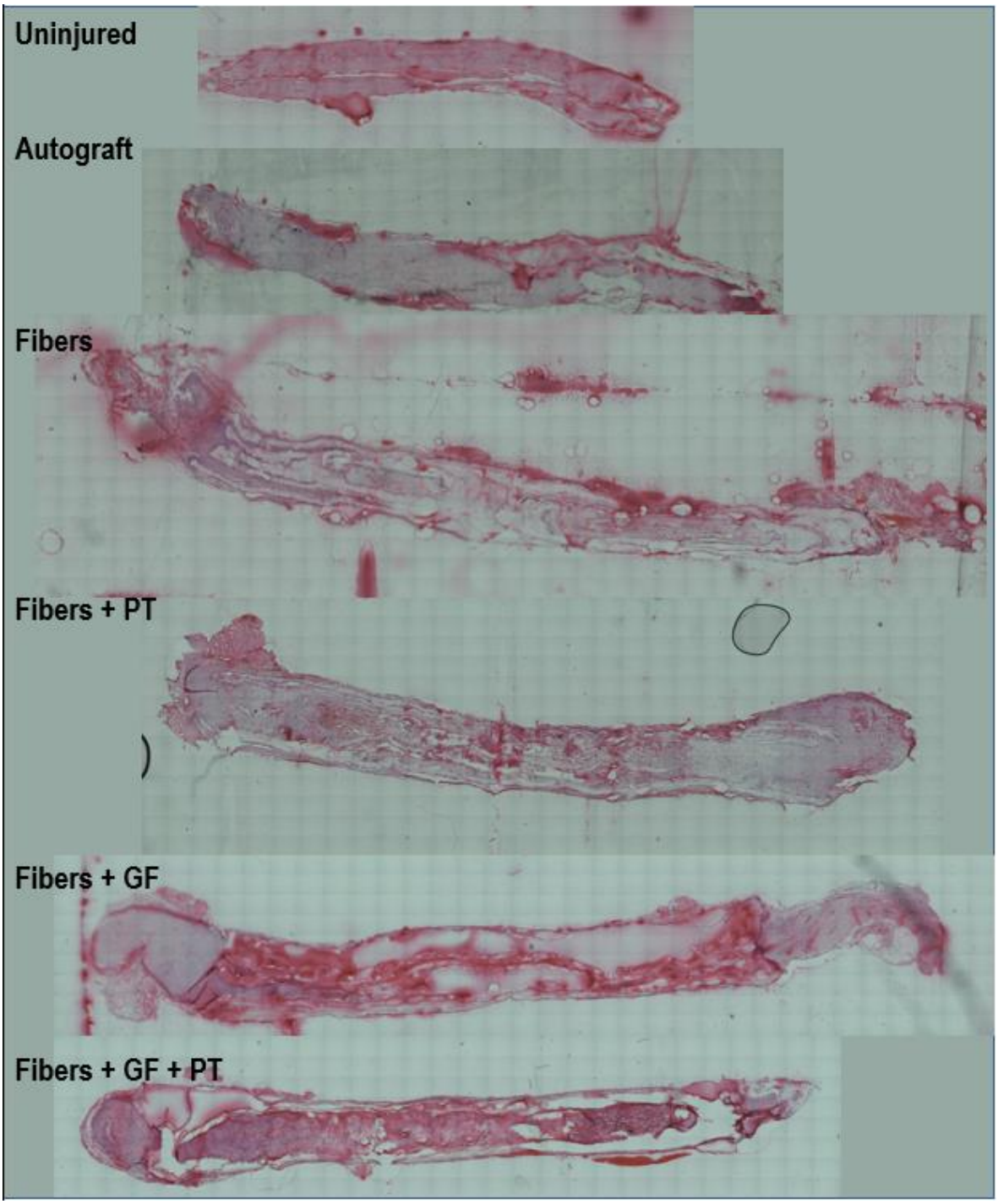

Figure 3-17: H&E Stained Longitudinal Slices. Sample slices for each treatment group and uninjured control. Cell nuclei can be seen throughout most tissue slices.

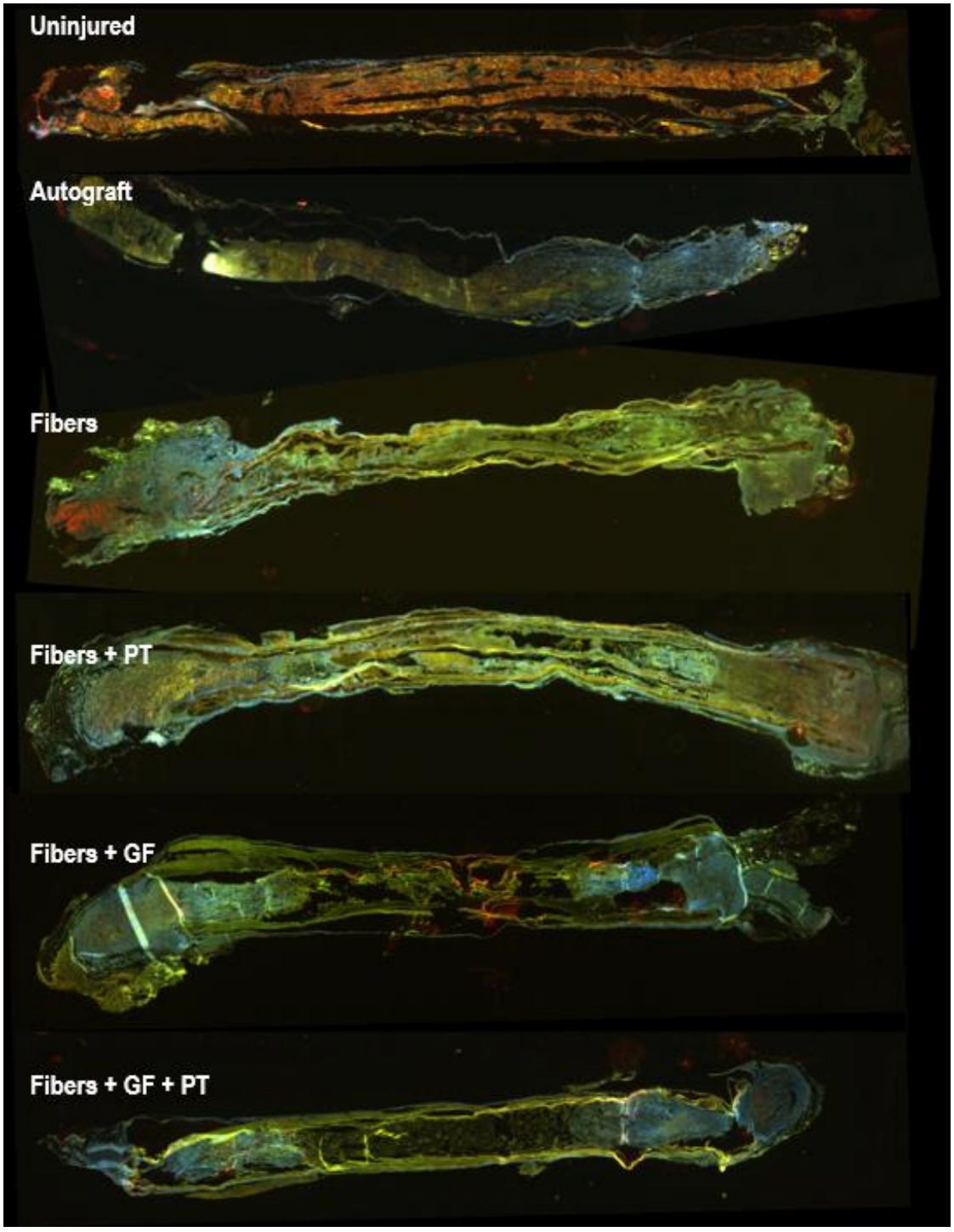

Figure 3-18: Immunohistochemistry. Nerve slices stained for Neurofilament (green), S100 (red), and DAPI (blue). Proximal end is on the left. S100 is seen most prominently in the uninjured control.

Immunohistochemistry can give more detailed information about the types cells present in a tissue sample. The cell types of interest are in nerve axon regeneration and the proliferation of support cells in the

conduit. Neurofilament is a protein most commonly found in nerve cells, which can be used to identify neurons. Similarly, S100 is a protein that is readily expressed in many support cells such as Schwann cells. Prevalence of S100 near neurons indicates potentially myelinating cells being present in the system. (Figure 3-18)

Discussion

This study created a unique nerve growth conduit providing multiple cell growth signals and combined it with physical therapy in the form of treadmill running to improve functional recovery following peripheral nerve injury. The conduit consisted of an outer shell of PCL to provide structural integrity to prevent conduit collapse, which would restrict regeneration. Researchers have used many natural and synthetic materials to create conduits for nerve regeneration studies [77, 78]. PCL was selected because it is an FDA approved implantable material which degrades over more than 6 months by hydrolysis under normal physiological conditions; this allows the conduit to remain intact for the duration of nerve regeneration, while precluding the need for an additional surgery to remove it [180]. The aligned fibers are electrospun flat and then rolled to be oriented around the nerve. The rolling creates an outward pressure in the conduit to resist crushing, which is a primary design factor for nerve conduits.

PCL provides the structural support for the conduit, but nerves have been shown to prefer a substrate of lower mechanical stiffness, so it is not a mechanically ideal growth substrate for nerve tissue. HA was selected for the inner structure to provide that growth signal. The mechanical stiffness of HA can be modified through the precise addition of methacrylate sites, which are then used to crosslink the polymer. The HA of the inner structure was electrospun into aligned nanofibers to provide a topographical cue. Regenerating neurites have been shown to grow along aligned fibers and to prefer nano size fibers over larger fibers [93].

Growth factors can also help to enhance nerve regeneration after injury; studies have shown that extended release of growth factors creates longer neurites. To allow for extended delivery, growth factor was encapsulated into PLGA microspheres. As proof of concept, only one growth factor was selected,

however, this model can easily be modified to include multiple growth factors in future studies. This study used a rat sciatic nerve injury model for testing and was focused on functional recovery. The sciatic nerve is a mixed nerve, containing both sensory and motor neurons. GDNF was selected as the growth factor because it has been shown to support both motor and sensory neurons specifically in the peripheral nervous system [78]. Based on the literature, Other growth factors that were considered included nerve growth factor (NGF), brain-derived neurotrophic factor (BDNF), and ciliary neurotrophic factor (CNTF), however GDNF appears to have the broadest benefit in the PNS for a mixed nerve [18, 181]. The production process and properties of the scaffold used for the internal structure of the conduit are similar to those reported by our group in a previous study [5, 170].

Two different conduits were produced for this study: one in which the internal structure was only nanofibers (Fibers) and a second that contained nanofibers and growth factor releasing microspheres (Fibers + GF). The second conduit can be seen in Figure 3-7. The PCL and HA layers are clearly visible as are the embedded microspheres. Conduits were implanted into a rat sciatic nerve model and the two different conduit groups were further divided into two groups that received physical therapy (Fibers + PT, Fibers + GF + PT) and two that did not (Fibers, Fibers + GF). For a control group a 10 mm segment of the nerve was removed and reversed to simulate an autograft (Autograft).

Throughout the two-month study animals were tested weekly to monitor motor and sensory function. First, gross motor skills were tested by having the animal walk across a ladder while the number of times they missed a rung was recorded. From the results shown in Figure 3-8, the Fibers + GF + PT group outperformed the Autograft group in the first two weeks, after which they were nearly consistent with the Autograft. The Fibers + GF group also performed close to Autograft in the first several weeks, while the groups without growth factors lagged behind. Additionally, at most timepoints the group receiving PT performed better than the corresponding group that did not. By week 5 the Fibers + PT group was similar to the control and GF groups. This result is consistent with previous studies which showed that rats receiving treadmill physical therapy and balance testing for 4 weeks performed at the same rate as controls, while those that did not receive training continued to miss rungs on the ladder [182]. These results indicate that

both growth factors and physical therapy support gross motor recovery, however they do not show an additive benefit to GF + PT. The Fibers + GF + PT only slightly outperformed the Fibers + PT and Fibers + GF groups at week 2 and 5.

Sensory response to mechanical stimulus was tested using the von Frey fibers. The fibers provide a known amount of force which can be used to indicate pain recognition. As seen in Figure 3-9 the Autograft and both GF groups began showing hypersensitivity at 3 weeks, which is indicative of new neurite growth. All groups show this hypersensitivity at 4 weeks. Tests were done on the center of the paw; the sural nerve has been shown to extend to the center of the foot to compensate for the loss of the sciatic nerve by 4 weeks. T get a better understanding of the reinnervation from the sciatic nerve, the fifth toe needs to be tested [177]. Fifth toe data was collected for all groups at week 8 (not shown), however without baseline data for comparison it was inconclusive. Future studies will be done on the fifth toe throughout.

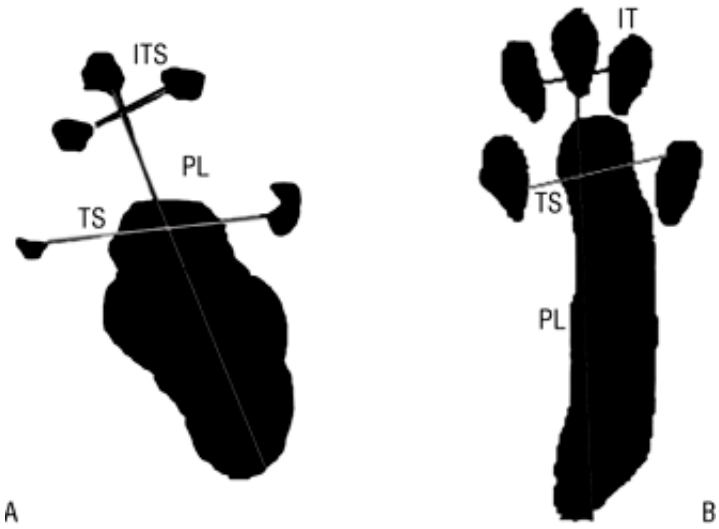

Figure 3-19: Sciatic Index Measurements. Three measurements are taken of the paw: inner toe spread (ITS) from the second to fourth toe; toe spread (TS) from the first to the fifth toe; and print length (PL) from the tip of the third toe to the heal. The values differ from a normal paw (A) to a paw with a sciatic nerve injury (B). The values are then used to calculate sciatic functional index (SFI) or static sciatic index (SSI). This figure has been reproduced freely under a Creative Commons Attribution license. © 2008 Reis et al. Originally published by Brazilian Journal of Physical Therapy. [15]

One of the functions of the sciatic nerve in rats is control of the muscles which govern their ability to spread their feet. This lead to the use of the Sciatic Function Index (SFI) to quantify the return of function after sciatic nerve injury in rats. To calculate the SFI, foot prints are measured for 3 parameters (Figure 3-

19): Print Length (PL), which is the length from the top of the middle toe to the heel; Toe Spread (TS), which is the distance from the tip of the first toe to the tip of the fifth toe; and Intermediate Toe Spread (ITS), which is the distance from the tip of the second toe to the tip of the fourth toe. A percentage difference between the experimental and contralateral sides is then calculated. The individual factors are then entered into an equation published by Bain in 1989 [183]. The resulting SFI has a range of 0, representing a fully functional sciatic nerve, to -100 representing complete impairment. Originally, this was done by dipping the rat's feet in ink and allowing them to walk across a paper. However, this could be flawed by over or under application of the ink and smearing from the animal dragging feet. As technology advanced, researchers began using glass bottom tracks and mirrors to record the animal walking on video [184]. This method improved the ability to get clean prints, however it required high-speed and high-resolution cameras, which can be cost prohibitive. With both methods the experimental data collection was very time-consuming as it required the animals to walk in a set path. Even with proper training in advance, animals could refuse to participate. More recently, researchers discovered that measurements taken from the animal while standing correlated closely to results received from the walking measurements, leading to the development of the Static Sciatic Index (SSI) [185]. This method allows images to be record of the animal while stationary in a glass bottom cage. Only a few seconds of video are required after the animal is allowed to acclimate to the recording cage. Also, the camera can be positioned much closer and it does not need to be as high quality. For these reasons, this is the method used in this study.

The SSI measurements recorded for the autograft group in this study, Figure 3-10, show the same upward trend from injury that is seen in most studies of sciatic nerve injury in the literature [138, 186-188]. Though the experimental groups showed little change over the duration of the study, there are some interesting points to note: first, in weeks 2 and 3 both PT groups show slight improvements from their week 1 values and are above those for their corresponding no PT group. Following those weeks, the values drop to become similar to the no PT groups. The week 2 and 3 recordings fall into the 4 weeks when the PT groups are doing daily treadmill walking. This could indicate that the PT has some ability to delay the most sever impartment that results from sciatic injury. Another point to note is that in week 7 and 8 the Fiber +

PT and Fiber + GF group reach their highest value. This could be the beginning of an upward trend indicating that these groups are starting to achieve reinnervation. This would indicate that a longer end point, or multiple end points, perhaps 8 and 16 weeks, would be preferred for future studies to more clearly see the differences between treatment groups. Another recent study looking at a 20 mm nerve gap also did not show improvement in treatment group SSI until after 4 weeks, however, that study saw the treatment group, which consisted of a collagen based conduit with Schwann Cells, catch up to the autograph by 8 weeks[186].

The sensory and motor function tests recorded weekly throughout the study indicate that the addition of GFs or PT to the basic topographical and mechanical cue of the nanofibers speeds repair. However, there is no clear indication that the combination of both GFs and PT have any additional benefit. Additional analysis is required to support the functional testing and provide more insight into the amount of regeneration that is occurring.

In this study we conducted electrophysiological recordings to determine if the regenerating nerves were able to produce and transmit action potentials that had a meaningful effect on the target muscles. Additionally, the gastrocnemius muscle and sciatic nerve were harvested for analysis. Looking first at the muscle weight, we can see that all of the treatment groups lost a large amount of muscle mass. The Autograft group has significantly higher experimental side muscle mass. However, the Fibers + PT is also significantly ($p=0.05$) heavier than the Fibers + GF + PT group. This would indicate that the muscle had less atrophy, which could lead to better muscle control in the foot, which supports what was seen in the SSI testing where the Fiber + PT group was beginning to recover at the final time points.

Beyond just muscle size, the contraction force of the muscle following nerve stimulation can be examined. The Fibers only group had significantly lower experimental side contraction force, but little difference is seen between the other experimental groups. This parallels what was seen in the functional testing. CMAP recording can provide deeper understanding of what is happening within the muscle.

This study used a range of stimulation voltages to give a full picture of the amount of stimulation that was required to produce functional action potentials. Considering the area under the CMAP curve,

Fibers + GF + PT has a peak of response around 3V, while other experimental groups peak later. This indicates that a lower stimulation is required to produce a peak in that group, which could indicate more myelinated nerve fibers.

Higher amplitude of CMAP peaks can indicate the involvement of additional muscle fibers. The Fibers + GF + PT group shows a stronger response sooner than other groups, but is not significantly different. Analysis of neuromuscular junctions and muscle fiber size will be used to confirm the involvement of additional muscle fibers later.

Exact nerve conduction velocity cannot be calculated from CMAP due to the varied depth and path of propagation in the muscle fiber. However, latency, which is the amount of time between the stimulation and the resulting action potential recording can give an estimate of the nerve conduction. Mature myelinated fibers will conduct more quickly. The recording in this study show a significant difference between Fibers + GF and Fibers + PT at 4 and 5 weeks. Additionally, though not significant, the latency for PT groups is longer than those for the corresponding non-PT group in all but 1 case. This increased latency might indicate that the motor neurons in the sciatic nerve are not maturing as quickly. Alternatively, the physical therapy could have helped encourage other nerves in the area to attempt to compensate. Thus, the increase in latency could result from the action potential propagating through another nerve to the gastrocnemius. Finally, considering duration of the CMAP waves, the PT groups have consistently longer durations than the non-PT groups. The duration here measures from the beginning of the CMAP wave until it stabilizes again. The increased duration could be due to signals arriving at different times via varying nerve pathways.

Some of the conflicting results received could be cleared with additional end point CMAP recordings. Stimulating the nerve both proximal and distal to the conduit repair shows the health of both the sensory and motor neurons. Multiple muscles could also be recorded to reduce the contamination of signals with stimulus from other nerves.

Finally, immunohistochemistry and histology were performed on longitudinal slices of the nerve. H&E staining, which shows cell structure and nuclei, shows cells throughout all of the conditions. Looking closely at some of the slices, specifically from the examples in Figure 3-17 Fibers and Fibers + PT, voids

are seen in the cell staining; this is where the PCL conduit was. In the experimental groups we can also see that the tissue is not completely continuous throughout the conduit area. This study ended early in the nerve regeneration process, so complete nerve fibers aren't expected to be seen throughout the slices. To clearly see where nerve cells were present fluorescent immunohistochemistry was also done. Neurofilament 200 antibody with a green tag was used to highlight nerve fibers. S100 antibody with a red tag was used to identify Schwann Cells, and DAPI was used for nuclei. Colocations of Schwann Cells and nerves will appear orange. PCL autofluoresces also appearing green in the images. All conditions had DAPI throughout the conduit, indicating the presence of cells. Nerve tissue was present in all conditions, but the level of infiltration varied. Additional stains are needed to differentiate the conduit from the nerve fibers. Sample images in Figure 3-18 show the most neurofilament in the Fibers and Fibers + PT group. Very little S100 was seen in the center of the conduits in the experimental groups. This is surprising as Schwann Cells assist in building paths for regenerating nerves to follow.

Conclusion

This study compared several different elements that can affect peripheral nerve regeneration. First, the study indicated benefits of GDNF releasing microspheres. The footfall test showed that GDNF growth factor groups recovered gross motor function faster than their corresponding non-GDNF groups (Figure 3-8). Additionally, the GDNF groups recovered sensory pain sensation faster (Figure 3-9). The contractile force also peaked at a lower stimulation indicating less voltage required to initiate coordinated muscle contraction (Figure 3-12).

Next, the study indicated benefits of physical therapy in the form of treadmill running. Groups receiving physical therapy performed slightly better on the footfall test than the corresponding group that did not receive physical therapy (Figure 3-8). At the beginning of the study, while the animals were still undergoing the daily treadmill running, the physical therapy groups had higher SSI scores than the corresponding non-physical therapy group (Figure 3-10). At the end of the study, the Fibers +PT group showed less muscle atrophy than other experimental groups (Figure 3-11). Both of the physical therapy

groups required lower stimulation voltage then their corresponding non-physical therapy group to reach peak muscle contraction force (Figure 3-12).

Finally, a couple of interesting points appear when looking at the combination of GDNF and physical therapy. In the footfall test the Fibers + GF + PT group had fewer misses than the other experimental groups at week 2 and 5, however the difference was not significant (Figure 3-8). Additionally, that group had the lowest stimulation voltage required of experiment groups to reach its peak in both CMAP area under the curve (Figure 3-13) and CMAP amplitude (Figure 3-14).

Functional testing in this study indicated faster recovery for groups that received GDNF or PT. However, a strong indication that the combination of the two creates a synergistic effect was not found. Additional information about the number and types of cells present in the conduit could provide more insight into the regeneration that occurred. This will be calculated from cross-sectional slices of the nerves at the proximal, center, and distal end of the conduits. Muscle tissue analysis will provide information about the number and quality of neural muscular junctions, which is an indicator of reinnervation. To allow for a clearer distinction between experimental groups a longer study will need to be conducted. The study should include multiple CMAP recordings. The results from this study further support the body of research that shows topographical, mechanical, and chemical cues can enhance nerve regeneration after peripheral nerve injury, and suggest further study is warranted to determine if there is a long term additive effect to the combination.

CHAPTER 4: FUTURE WORK: TAKING ELECTROSPUN SCAFFOLDS WITH GROWTH FACTOR RELEASING MICROSPHERES BEYOND PERIPHERAL NERVE INJURY

Introduction

This thesis provided a foundation for combing multiple cell signaling cues in an injury environment for improved recovery. While it specifically focused on peripheral nerve injury, there are many other injury environments that could benefit from similar systems. In its current form, the scaffold and microsphere (MS) system previously described has the potential to work with other growth factors (GFs) and have its mechanical properties tuned to be better suited to other tissue types. By improving the GF release profile of this model, combining it with other promising therapies – such as stem cells – or using different materials, this novel system can be further developed in several ways. This chapter will discuss a few of the possible directions in which this work could proceed.

Spatiotemporal Growth Factor Release

The next step for this system is to produce more consistent MS, which would allow for more precise control of GF delivery. Many researchers have used microfluidics to produce MS in a very narrow size range [25, 189-191]. One device of particular interest, developed by Kong et al., provides the ability to predictably control the thickness of the MS shell simply by adjusting flow rates and osmolality of the three solutions in the device [25]. Figure 4-1 shows examples of the different droplets the system produced and the predicted and actual inner and outer diameters. Adjusting the thickness of the Poly-lactic-co-glycolic (PLGA) shell of the MS has a direct relationship to the breakdown of the microsphere and thus growth factor release [156]. Having the ability to precisely adjust the MS size and shell thickness leads to consistent breakdown and more tunable release profiles. We hypothesize that when these MSs are used in the electrospinning system described in earlier chapters, the distribution of microspheres in the scaffold will also be more uniform. This will result in a homogeneous growth factor profile throughout the scaffold and thus the conduit.

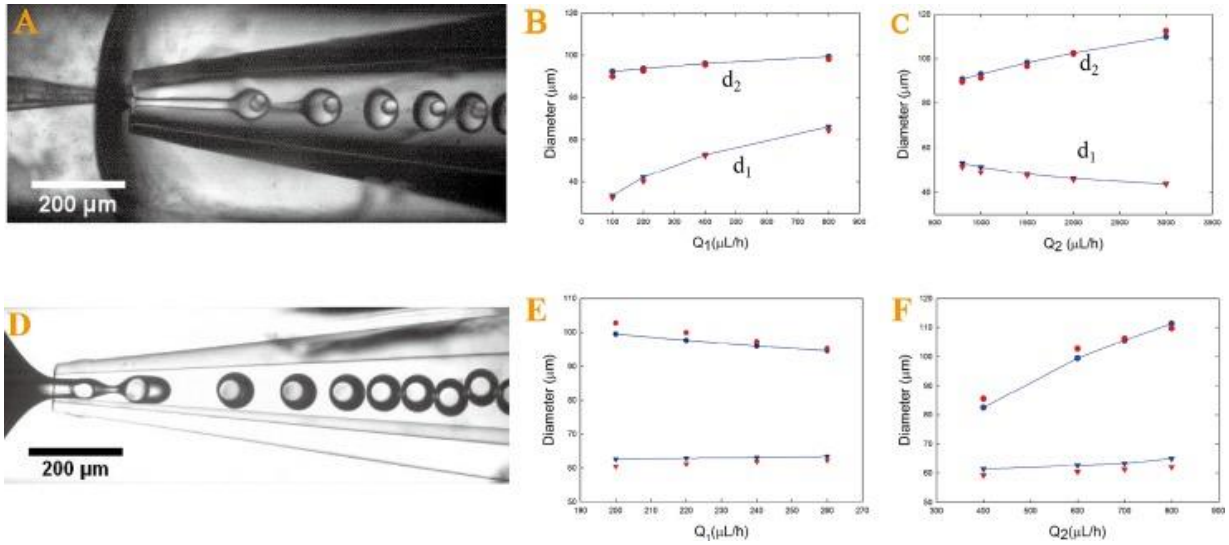

Figure 4-1: Microfluidic Microsphere Production. Optical microscopic images of (A) microfluidic generation of W/O/W double emulsions; predicted inner droplet size d_1 and the whole droplet size (blue symbols) and compared with size measured through image analysis (red symbols) for changing inner phase flow rate (Q_1) (B) and middle phase flow rate (Q_2) (C) while keeping other flow rates constant. Optical microscopic images of (D) microfluidic generation of monodisperse O/W/O double emulsion droplets in a modified geometry; predicted inner droplet size d_1 and the whole droplet size d_2 (blue symbols) and compared with sizes measured by image analysis (red symbols) for changing inner phase flow rate (Q_1) (E) and middle phase flow rate (Q_2) (F) while keeping other flow rates constant. Reprinted from Kong, T., et al., Microfluidic fabrication of polymeric core-shell microspheres for controlled release applications. Acta Biomaterialia, 2013, with the permission of AIP Publishing. [25]

Homogeneous growth factor delivery is not necessarily the ideal model, which leads to the next advancement for this line of study: spatiotemporal release of multiple growth factors. The natural environment for nerve growth and regeneration has a very complex profile of growth factors. As an example, Fibroblast Growth Factor-2 (FGF2) is known to enhance nerve regeneration [8, 9, 24], but FGF2 is only upregulated from day 0 to day 18 after PNI with a peak at day 7 [192, 193]. FGF2 is known to suppress myelination of axons and support axonal growth; though this may be ideal at the beginning of the nerve injury, having prolonged FGF2 exposure can lead to thinner myelin sheaths and a lack of resting Schwann cells [192, 193]. Brain Derived Neurotrophic Factor (BDNF) which is also known for enhancing nerve regeneration [8, 9], has an opposing effect to FGF2. BDNF promotes Schwann cell differentiation to the myelination state[192], and is expressed from day 3 after PNI until approximately day 42 with a peak at day 28 [192, 194]. This example demonstrates the complexities of the release timing and interaction of just two growth factors that exist in the nerve growth environment. When we begin to consider that there are more than a dozen growth factors commonly associated with nerve regeneration all interacting with one

another in the microenvironment, the need for precise growth factor release control becomes clear (Table 4-1).

Table 4-1: Growth Factors used for Nerve Regeneration

Growth Factor	Abbreviation	Reference
Neural Growth Factor*	NGF	[1-7]
Brain Derived Neurotrophic Factor*	BDNF	[8, 9]
Epidermal Growth Factor	EGF	[10, 11]
Neurotrophic Factor 3*	NT-3	[8, 9, 12]
Neurotrophic Factor 4/5*	NT-4/5	[8]
Ciliary Neurotrophic Factor*	CNTF	[8, 20]
Glial Cell Line-derived Growth Factor*	GDNF	[1, 22]
Fibroblast Growth Factor-1*	FGF-1	[8, 9, 23]
Fibroblast Growth Factor-2*	FGF-2	[8, 9, 24]
Platelet Derived Growth Factor*	PDGF	[8]
Glial Growth Factor*	GGF	[8, 26, 27]
Vascular Endothelial Growth Factor*	VEGF	[8, 9]
Leukemia Inhibitory Factor*	LIF	[8]
Insulin-like Growth Factor*	IGF-1	[8, 9]
Transforming Growth Factor - β	TGF-β	[28]
Tumor Necrosis Factor*	TNF-α	[8]

*Growth factor was also in a table in a review [8], see original table for more sources.

The system tested in this thesis can be modified to encapsulate any hydrophilic growth factor. Encapsulating multiple growth factors into MS with varying shell thicknesses and including them in a scaffold in different proportions is a step toward the precise spatiotemporal release needed to completely model the nerve growth environment. However, additional tools may be needed due to the complexity of the environment and the need to keep growth factors within the target area. One method is to sequester GFs in the scaffold fibers. GF sequestration is a naturally occurring phenomenon where heparin binding sites in the extracellular matrix bind free floating GFs. This is useful because it prevents the GF from being degraded while still being available to bind and signal cells. Heparin binding has been used in cardiac tissue [195] and nerve tissue[6, 109, 196] as a way to prolong GF delivery duration. By adding heparin to the methacrylated hyaluronic acid (MeHA) used as the scaffold fiber material, GF loss from the delivery site will be naturally slowed.

Beyond the temporal aspect of GF release, this model could also have improved spatial delivery of GFs. While one important aspect described above is keeping the GF in the injury location, studies have also

shown that gradients of GFs can also help direct growth [197-201]. By electrospinning fibers from multiple sources onto the same mandrel we can produce gradients of MS within the scaffold material. Figure 4-2 shows the electrospinning setup to achieve this gradient creation. Combining specifically tuned microspheres containing different GFs, delivered in a gradient, with sequestration via heparin binding creates a peripheral nerve regeneration scaffold system that is a close mimic to the natural environment.

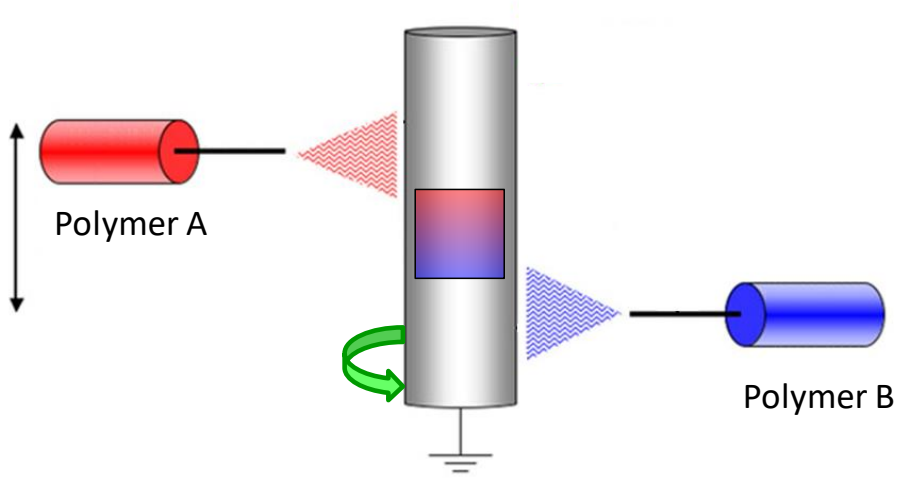

Figure 4-2: Gradient Electrospinning Setup. Gradient electrospinning is achieved by using multiple syringe pumps simultaneously, each containing a different solution. By placing MS is in one solution, but not the other, a gradient of MS is created within the length of the scaffold. Image adapted from Ifkovits et. al. [17]

Artificial Spinal Cord Implant

This work can also move beyond peripheral nerve regeneration to other tissues. Staying within the nervous system we can use aspects of this work to help address spinal cord injury (SCI). An estimated 2.5 million people live with SCI, with over 100,000 new cases each year [202]. The results of these injuries vary by the location of the injury, but all result in catastrophic changes to patient's functionality and can have a drastically negative affect on their quality of life. There are several similarities between peripheral nervous system regeneration and central nervous system regeneration, however, the central nervous system presents additional challenges: in the central nervous system, within hours of injury and continuing for several days, there is cell death of neurons and glial cells through both necrotic and apoptotic pathways [203-195]. This leads to the formation of a central fluid-filled cavity. Another challenge particular to SCI is the inhibitory scar that forms after injury and blocks regrowth of axons remaining near the injury site

[206, 207]. Ascending sensory and descending motor axonal pathways still retain the capacity for growth but will slowly recede from the injury site [208]. These problems are most difficult to overcome when the spinal cord is completely severed, leaving no residual connections to the lower limbs. Studies have shown that providing scaffolding and stem cells to the gap can increase axonal growth, resulting in new neuronal relay-circuits, and/or improving cell survival [209-214]. However, there are no therapies that lead to substantial recovery and there has been little clinical success. In collaboration with Dr. Jean Peduzzi-Nelson a hydrogel implant for spinal cord injury was produced that incorporated this scaffold and MS model.

The construct, referred to as an "artificial spinal cord" (ASC), consisted of three layers methacrylated hyaluronic acid (MeHA) fibers with stem cells inside of an MeHA hydrogel formed by photo cross-linking. Two layers of fibers contained opposing gradients of glial-derived neurotrophic factor (GDNF) and brain-derived neurotrophic factor (BDNF) releasing microsphere and had olfactory ensheathing cells grown on them. The remaining layer had fibers only with olfactory progenitor cells grown on them. The MeHA hydrogel solution also contained Chondroitinase ABC, which several preclinical studies have shown to help reduce scar formation and promote recovery by degrading chondroitin sulfate [206, 207].

The ASC was tested in a rat model of spinal cord segment removal. The study included four treatment groups: 1) sham surgery - laminectomy only; 2) spinal cord segment removal, no graft; 3) hydrogel only after spinal cord segment removal; 4) ASC after spinal cord segment removal. The animals were tested weekly for 15 weeks using the Basso, Beattie and Bresnahan (BBB) locomotor rating scale, modified Hargreaves device, beam test, and inclined plane test. Additionally, in week 14 and 15 animals were tested using a ladder walk. For the ladder walk the placement of the foot was evaluated on a 0-7 scale, 0 is when the rung is completely missed while 7 is correct placement. By the end of the 15 weeks, the ASC group BBB score had improved from complete impairment nearly to what is considered only 'mild injury' (Figure 4-3). The other functional tests also showed the ASC group significantly outperforming the other injury groups at most time points, indicating that both motor and sensory neurons were benefitting from the ASC (Figure 4-4).

This example goes beyond simply signaling nerve cells, but also attempts to help direct the action of support cells and direct differentiation of stem cells in the injury microenvironment. The results indicate that fibrous scaffolds with extended growth factor release from microspheres can be beneficial to not only support peripheral nerves, but the central nervous system as well. By further modifying the fiber and microsphere model, we can create a biomaterial scaffold that provides multiple signals to other tissue types as well.

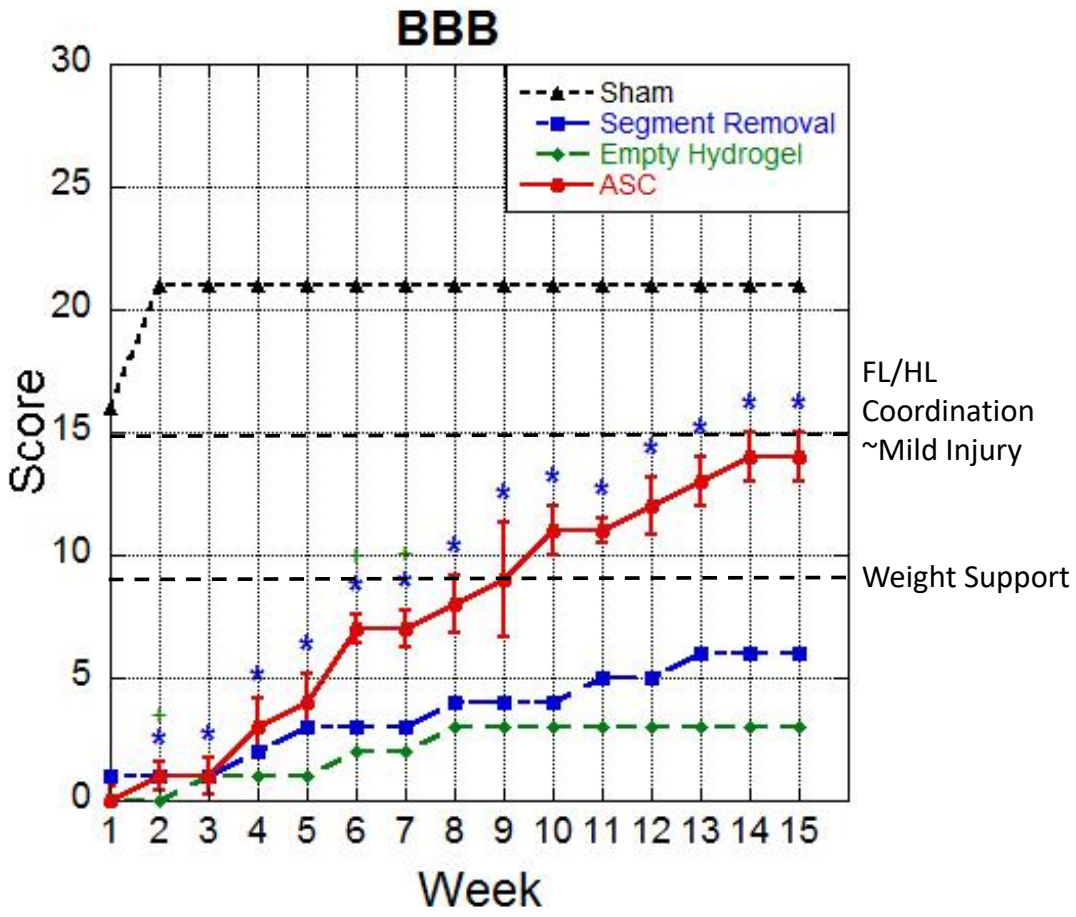

Figure 4-3: BBB Locomotor Test. Animals are rated on a scale of 0, complete impairment, to 21, normal function. The animals receiving the ASC greatly outperformed the hydrogel only and segment removal groups. * indicated ASC is significantly different then segment removal condition ($p<0.05$). +indicates ASC is significantly different then empty hydrogel condition ($p<0.05$).

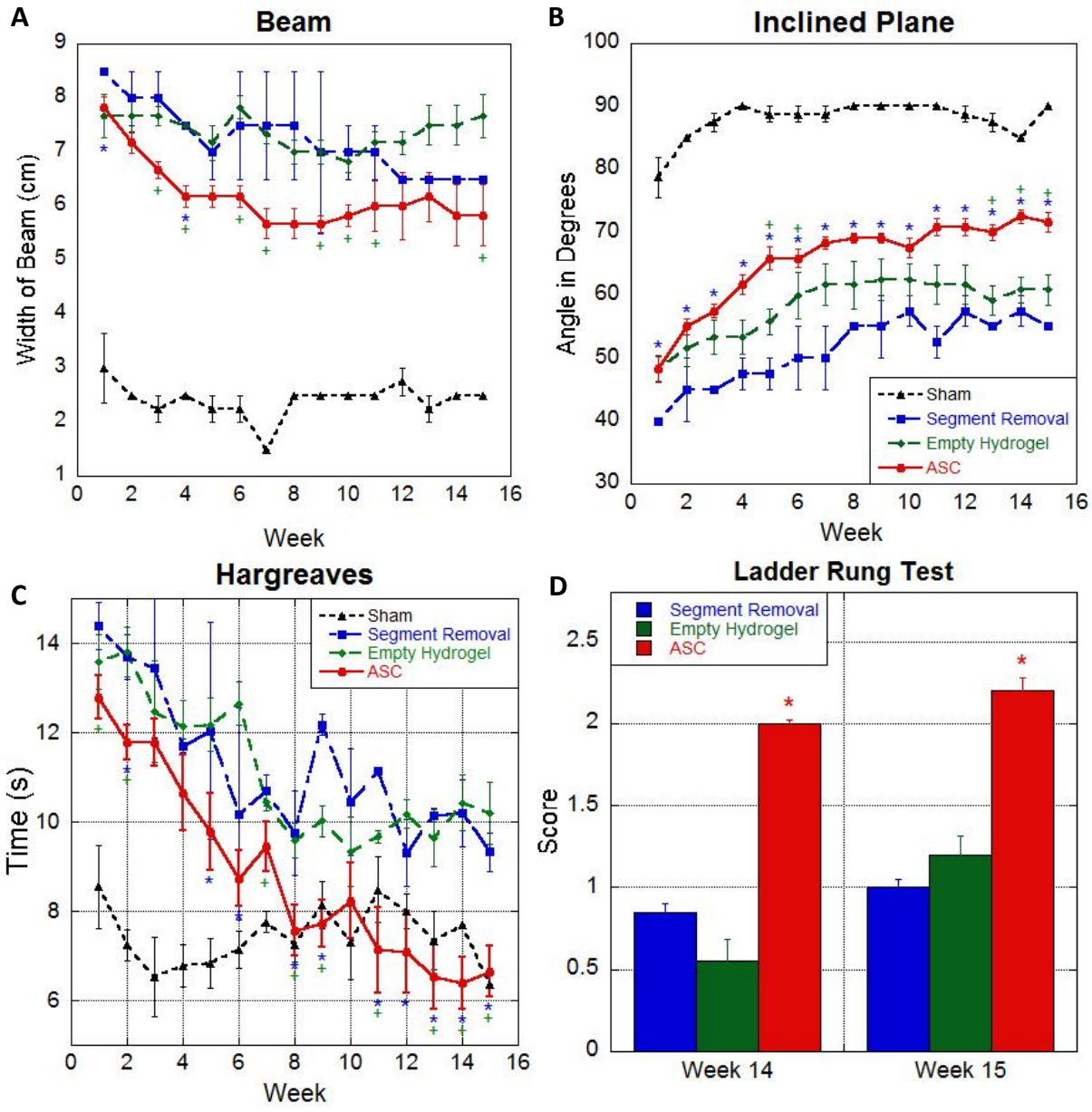

Figure 4-4: Functional Test Results. A. Beam walking test, smaller beam indicates less fear and better balance, B. Inclined plane, higher angle indicates higher grip in rear limbs, C. Hargreaves, shorter times indicate higher heat sensitivity, D. Ladder rung test, higher number indicates more normal foot placement. * indicated ASC is significantly different then segment removal condition ($p<0.05$). +indicates ASC is significantly different then empty hydrogel condition ($p<0.05$). In ladder rung test, ASC was significantly different then both other conditions.

Non-Nervous System Tissue

Biomaterial scaffolds are used to support cell growth in many injury environments. HA has been used in wound healing applications for decades due to its anti-inflammatory properties [215-218]. Both fibers and gels of HA are popular and used clinically, especially for particularly difficult wounds

[219]. Additionally, direct delivery of several GFs has also been shown to speed healing. Some of the growth factors involved with wound healing include vascular endothelial growth factor (VEGF), platelet-derived growth factor (PDGF), basic fibroblast growth factor (bFGF), transforming growth factor-β (TGF-β), insulin-like growth factor (IGF), and endothelial growth factor (EGF) [220-222]. A recent review looking over the various methods used to deliver GFs to the wound environment, noted that some of the most recent work has been in combining scaffolds and GF release to further improve results [221]. With some optimizations, including the spatiotemporal improvements mentioned earlier, our system could be used to precisely deliver GFs to the injury site with the added benefit of the HA's anti-inflammatory characteristics. Similar work is already underway elsewhere; one example created an electrospun scaffold with GF releasing nanoparticles in the core of the nanofibers [223]. Another study used a spray production technique to create a fibrous scaffold that also incorporated GF releasing nanoparticles [222]. Both showed shortened wound healing time.

Another possible target for an HA scaffold system is cartilage. Multiple studies have used HA based scaffolds or hydrogels as a delivery and support system for stem cells in cartilage repair [137, 224-226]. One reason is that the substrate can be mechanically tuned to help direct stem cell differentiation [225]. The mechanical properties of our electrospun fibrous scaffolds can be tuned by adjusting the number of methacrylate sites which are then crosslinked. We can also add additional support for cartilage repair by incorporating appropriate growth factors into microspheres in the scaffold [227]. Some examples of GF used in cartilage repair are TGF-β, IGF, FGF, and bone morphogenetic protein-2 (BMP-2) [228-231]. As with the scaffolds for other injury environments the precise combination of spatiotemporal release of growth factors and other cell signaling modalities will need to be carefully balanced to achieve optimal tissue repair.

Other soft tissue repair studies have also utilized HA substrates. Some examples include heart valve repair, which benefited from valvular interstitial cells being cultured on HA hydrogels [232], vascular tissue, when combined with collagen [233], and even cornea repair [234]. These could also potentially benefit from the HA scaffold with microspheres model. In addition, this system has increased flexibility in

expanding beyond HA to other polymer materials as the electrospun fibrous substrate. Several natural and synthetic polymers have been used in electrospinning applications [235]. Moving further from the original design will require substantial reoptimization, but incorporating other polymers can extend the potential mechanical and adhesive properties of the system.

Conclusion

This thesis has presented a novel system to deliver multiple regenerative signals to peripheral nerves *in vitro* and *in vivo*. Specifically, we looked at mechanical cues, using crosslinked MeHA that's mechanical properties can be adjusted by changing the amount of methacrylate sights which are added to the polymer. For nerves, a pliable substrate was selected. Topographical cues were created by electrospinning the MeHA into aligned nanofibers. Chemical cues were added by incorporating GF releasing microspheres into the scaffold. For *in vivo* study, exercise was included to provide the added benefit of physical therapy, which helps combat side effects of peripheral nerve injury and encourages the creation of new synapses. Improving the spatiotemporal control of the GF delivery could advance this work; we can further enhance its benefit by incorporating stem cells specific to the injury environment in which the system is being used. The topographical, mechanical, and chemical signals can be changed to make the system suitable for other tissue types, leading to potential treatment models for a number of injuries.

REFERENCES

1. Kemp, S.W., S.K. Walsh, and R. Midha, *Growth factor and stem cell enhanced conduits in peripheral nerve regeneration and repair.* Neurological research, 2008. **30**(10): p. 1030-1038.
2. Camarata, P.J., et al., *Sustained Release of Nerve Growth Factor from Biodegradable Polymer Microspheres.* Neurosurgery, 1992. **30**(3).
3. Chang, C.J., *The effect of pulse-released nerve growth factor from genipin-crosslinked gelatin in schwann cell-seeded polycaprolactone conduits on large-gap peripheral nerve regeneration.* Tissue Eng Part A, 2009. **15**(3): p. 547-57.
4. Dodla, M.C. and R.V. Bellamkonda, *Differences between the effect of anisotropic and isotropic laminin and nerve growth factor presenting scaffolds on nerve regeneration across long peripheral nerve gaps.* Biomaterials, 2008. **29**(1): p. 33-46.
5. Whitehead, T.J. and H.G. Sundararaghavan, *Electrospinning Growth Factor Releasing Microspheres into Fibrous Scaffolds.* Jove-Journal of Visualized Experiments, 2014(90).
6. Sakiyama-Elbert, S.E. and J.A. Hubbell, *Controlled release of nerve growth factor from a heparin-containing fibrin-based cell ingrowth matrix.* Journal of Controlled Release, 2000. **69**(1): p. 149-158.
7. Lee, A.C., et al., *Controlled release of nerve growth factor enhances sciatic nerve regeneration.* Experimental neurology, 2003. **184**(1): p. 295-303.
8. Kemp, S.W., S.K. Walsh, and R. Midha, *Growth factor and stem cell enhanced conduits in peripheral nerve regeneration and repair.* Neurol Res, 2008. **30**(10): p. 1030-8.
9. Lohmeyer, J., et al., *Basics and Current Approaches to Tissue Engineering in Peripheral Nerve Reconstruction.* Neurosurgery quarterly. **19**(2): p. 101-109.
10. Grulova, I., et al., *Delivery of Alginate Scaffold Releasing Two Trophic Factors for Spinal Cord Injury Repair.* Sci Rep, 2015. **5**: p. 13702.

11. Goraltchouk, A., et al., *Incorporation of protein-eluting microspheres into biodegradable nerve guidance channels for controlled release.* J Control Release, 2006. **110**(2): p. 400-7.

12. Xu, X.M., et al., *A combination of BDNF and NT-3 promotes supraspinal axonal regeneration into Schwann cell grafts in adult rat thoracic spinal cord.* Exp Neurol, 1995. **134**(2): p. 261-72.

13. Menorca, R.M.G., T.S. Fussell, and J.C. Elfar, *Peripheral Nerve Trauma: mechanisms of injury and recovery.* Hand clinics. **29**(3): p. 317-330.

14. Brattain, K., *Analysis of the Peripheral Nerve Repair Market in the United States.* Magellan Medical Technology Consultants, Inc, 2014.

15. Reis, F.A., et al., *Effect of gallium-aluminum-arsenide laser therapy (660Nm) on recovery of the sciatic nerve in rats following neurotmesis lesion and epineural anastomosis: functional analysis.* Brazilian Journal of Physical Therapy, 2008. **12**(3): p. 215-221.

16. Burnett, M.G. and E.L. Zager, *Pathophysiology of peripheral nerve injury: a brief review.* Neurosurgical Focus, 2004. **16**(5): p. 1-7.

17. Ifkovits, J.L., H.G. Sundararaghavan, and J.A. Burdick, *Electrospinning fibrous polymer scaffolds for tissue engineering and cell culture.* Journal of visualized experiments: JoVE, 2009(32).

18. Schmidt, C.E. and J.B. Leach, *Neural tissue engineering: strategies for repair and regeneration.* Annual Review of Biomedical Engineering, 2003. **5**: p. 293-347.

19. Arslantunali, D., et al., *Peripheral nerve conduits: technology update.* Medical Devices (Auckland, N.Z.), 2014. **7**: p. 405-424.

20. Barbon, S., et al., *In vitro assessment of TAT - Ciliary Neurotrophic Factor therapeutic potential for peripheral nerve regeneration.* Toxicol Appl Pharmacol, 2016.

21. Siemionow, M. and G. Brzezicki, *Chapter 8: Current techniques and concepts in peripheral nerve repair.* International Review of Neurobiology, 2009. **87**: p. 141-172.

22. Roam, J.L., et al., *A modular, plasmin-sensitive, clickable poly(ethylene glycol)-heparin-laminin microsphere system for establishing growth factor gradients in nerve guidance conduits.* Biomaterials, 2015. **72**: p. 112-124.

23. Ni, H.C., et al., *Fabrication of bioactive conduits containing the fibroblast growth factor 1 and neural stem cells for peripheral nerve regeneration across a 15 mm critical gap.* Biofabrication, 2013. **5**(3): p. 035010.

24. Matsumine, H., et al., *Facial nerve regeneration using basic fibroblast growth factor-impregnated gelatin microspheres in a rat model.* J Tissue Eng Regen Med, 2014.

25. Kong, T., et al., *Microfluidic fabrication of polymeric core-shell microspheres for controlled release applications.* Acta Biomaterialia, 2013.

26. Bryan, D.J., et al., *Influence of glial growth factor and Schwann cells in a bioresorbable guidance channel on peripheral nerve regeneration.* Tissue Eng, 2000. **6**(2): p. 129-38.

27. Kuihua, Z., et al., *Aligned SF/P(LLA-CL)-blended nanofibers encapsulating nerve growth factor for peripheral nerve regeneration.* J Biomed Mater Res A, 2014. **102**(8): p. 2680-91.

28. Nie, X., et al., *Axonal regeneration and remyelination evaluation of chitosan/gelatin-based nerve guide combined with transforming growth factor-beta1 and Schwann cells.* Cell Biochem Biophys, 2014. **68**(1): p. 163-72.

29. Quigley AF , e.a., *Engineering a multimodal nerve conduit for repair of injured peripheral nerve. - PubMed - NCBI.* 2017.

30. Daly, W., et al., *A biomaterials approach to peripheral nerve regeneration: bridging the peripheral nerve gap and enhancing functional recovery.* Journal of the Royal Society, Interface / the Royal Society, 2012. **9**(67): p. 202-221.

31. Kehoe, S., X.F. Zhang, and D. Boyd, *FDA approved guidance conduits and wraps for peripheral nerve injury: A review of materials and efficacy.* Injury-International Journal of the Care of the Injured, 2012. **43**(5): p. 553-572.

32. Siemionow, M. and E. Sonmez, *Nerve Allograft Transplantation: A Review*. Journal of Reconstructive Microsurgery, 2008. **23**: p. 511-520.

33. Mackinnon, S.E., et al., *Clinical outcome following nerve allograft transplantation.* Plast Reconstr Surg, 2001. **107**(6): p. 1419-29.

34. Nectow, A.R., K.G. Marra, and D.L. Kaplan, *Biomaterials for the development of peripheral nerve guidance conduits.* Tissue engineering. Part B, Reviews, 2012. **18**(1): p. 40-50.

35. Xu, X., et al., *Peripheral nerve regeneration with sustained release of poly(phosphoester) microencapsulated nerve growth factor within nerve guide conduits.* Biomaterials, 2003. **24**(13): p. 2405-2412.

36. Zander, N.E., et al., *Coaxial electrospun poly(methyl methacrylate)-polyacrylonitrile nanofibers: atomic force microscopy and compositional characterization.* The journal of physical chemistry. B, 2011. **115**(43): p. 12441-12447.

37. Yao, L., et al., *Orienting neurite growth in electrospun fibrous neural conduits.* Journal of biomedical materials research. Part B, Applied biomaterials, 2009. **90**(2): p. 483-491.

38. Wrobel, M.R. and H.G. Sundararaghavan, *Directed Migration in Neural Tissue Engineering.* Tissue Engineering Part B-Reviews, 2014. **20**(2): p. 93-105.

39. Ratner, B.D., et al., *Biomaterials Science: An Introduction to Materials in Medicine*. 2012: Academic Press. 1597.

40. Geuna, S., et al., *Chapter 3: Histology of the peripheral nerve and changes occurring during nerve regeneration.* International Review of Neurobiology, 2009. **87**: p. 27-46.

41. Kerns, J.M., *The microstructure of peripheral nerves.* Techniques in Regional Anesthesia and Pain Management, 2008. **12**(3): p. 127-133.

42. Kaplan, S., et al., *Chapter 2 Development of the Peripheral Nerve*, in *International Review of Neurobiology*, S.G. Battiston, T. Pierluigi, and Bruno, Editors. 2009, Academic Press. p. 9-26.

43. Battiston, B., et al., *Chapter 1 Peripheral Nerve Repair and Regeneration Research: A Historical Note*, in *International Review of Neurobiology*, S.G. Battiston, T. Pierluigi, and Bruno, Editors. 2009, Academic Press. p. 1-7.

44. Battiston, B., et al., *Chapter 11 Tissue Engineering of Peripheral Nerves*, in *International Review of Neurobiology*, S.G. Battiston, T. Pierluigi, and Bruno, Editors. 2009, Academic Press. p. 227-249.

45. Battiston, B., et al., *Nerve repair by means of tubulization: literature review and personal clinical experience comparing biological and synthetic conduits for sensory nerve repair.* Microsurgery, 2005. **25**(4): p. 258-267.

46. Hudson, T.W., G.R. Evans, and C.E. Schmidt, *Engineering strategies for peripheral nerve repair.* The Orthopedic clinics of North America, 2000. **31**(3): p. 485-498.

47. Hudson, T.W., G.R. Evans, and C.E. Schmidt, *Engineering strategies for peripheral nerve repair.* Clinics in plastic surgery, 1999. **26**(4): p. 617-628, ix.

48. Ross, M. and W. Pawlina, *Nerve Tissue*, in *Histology: A Text and Atlas with Correlated Cell and Molecular Biology, 7e*. 2016, Wulters Kluwer Health.

49. Young, B., P. Woodford, and G. O'Dowd, *Wheater's Functional Histology E-Book*. 2017.

50. Buchthal, F. and H. Schmalbruch, *Motor unit of mammalian muscle.* Physiological reviews, 1980. **60**(1): p. 90-142.

51. Geuna, S., P. Tos, and B. Battiston, *Essays on Peripheral Nerve Repair and Regeneration*. 2009: Academic Press. 603.

52. Gaudet, A.D., P.G. Popovich, and M.S. Ramer, *Wallerian degeneration: gaining perspective on inflammatory events after peripheral nerve injury.* Journal of Neuroinflammation, 2011. **8**: p. 110.

53. Geuna, S., et al., *Tissue engineering and peripheral nerve reconstruction: an overview.* International Review of Neurobiology, 2013. **108**: p. 35-57.

54. Swett, J.E., et al., *Motoneurons of the rat sciatic nerve.* Experimental Neurology, 1986. **93**(1): p. 227-252.

55. Swett, J.E., et al., *Sensory neurons of the rat sciatic nerve.* Experimental Neurology, 1991. **114**(1): p. 82-103.

56. Noble, J., et al., *Analysis of upper and lower extremity peripheral nerve injuries in a population of patients with multiple injuries.* The Journal of Trauma, 1998. **45**(1): p. 116-122.

57. English, A.W., J.C. Wilhelm, and P.J. Ward, *Exercise, Neurotrophins, and Axon Regeneration in the PNS.* Physiology, 2014. **29**(6): p. 437-445.

58. Razaq, S., et al., *The pattern of peripheral nerve injuries among Pakistani soldiers in the war against terror.* J Coll Physicians Surg Pak, 2015. **25**(5): p. 363-6.

59. Fu, S.Y. and T. Gordon, *The cellular and molecular basis of peripheral nerve regeneration.* Molecular Neurobiology, 1997. **14**(1-2): p. 67-116.

60. Müller, H.W. and G. Stoll, *Nerve injury and regeneration: basic insights and therapeutic interventions.* Current Opinion in Neurology, 1998. **11**(5): p. 557-562.

61. Grinsell, D. and C.P. Keating, *Peripheral Nerve Reconstruction after Injury: A Review of Clinical and Experimental Therapies.* BioMed Research International, 2014. **2014**.

62. Gravvanis, A.I., et al., *The beneficial effect of genetically engineered Schwann cells with enhanced motility in peripheral nerve regeneration: review.* Acta neurochirurgica. Supplement, 2007. **100**: p. 51-56.

63. Tos, P., et al., *Chapter 4 Methods and Protocols in Peripheral Nerve Regeneration Experimental Research: Part I—Experimental Models*, in *International Review of Neurobiology*, S.G. Battiston, T. Pierluigi, and Bruno, Editors. 2009, Academic Press. p. 47-79.

64. Tos, P., et al., *Future perspectives in nerve repair and regeneration.* International Review of Neurobiology, 2013. **109**: p. 165-192.

65. Seddon, H.J., *A Classification of Nerve Injuries.* British Medical Journal, 1942. **2**(4260): p. 237-239.

66. Sunderland, S., *A Classification of Peripheral Nerve Injuries Producing Loss of Function.* Brain, 1951. **74**(4): p. 491-516.

67. Casha, S., V.W. Yong, and R. Midha, *Minocycline for axonal regeneration after nerve injury: a double-edged sword.* Experimental Neurology, 2008. **213**(2): p. 245-248.

68. Höke, A., *Mechanisms of Disease: what factors limit the success of peripheral nerve regeneration in humans?* Nature clinical practice. Neurology, 2006. **2**(8): p. 448-454.

69. Cinteza, D., et al., *Peripheral Nerve Regeneration - an Appraisal of the Current Treatment Options.* Maedica (Buchar), 2015. **10**(1): p. 65-8.

70. Glasby, M.A., et al., *The dependence of nerve regeneration through muscle grafts in the rat on the availability and orientation of basement membrane.* Journal of Neurocytology, 1986. **15**(4): p. 497-510.

71. Angius, D., et al., *A systematic review of animal models used to study nerve regeneration in tissue-engineered scaffolds.* Biomaterials, 2012. **33**(32): p. 8034-8039.

72. Weber, R.A., et al., *A randomized prospective study of polyglycolic acid conduits for digital nerve reconstruction in humans.* Plastic and Reconstructive Surgery, 2000. **106**(5): p. 1036-1045; discussion 1046-1048.

73. de Ruiter, G.C.W., et al., *Designing ideal conduits for peripheral nerve repair.* Neurosurgical focus, 2009. **26**(2): p. E5.

74. Griffin, J., et al., *Design and evaluation of novel polyanhydride blends as nerve guidance conduits.* Acta Biomaterialia, 2010. **6**(6): p. 1917-1924.

75. Shoffstall, A.J., D.M. Taylor, and E.B. Lavik, *Engineering therapies in the CNS: What works and what can be translated.* Neuroscience Letters, 2012. **519**(2): p. 147-154.

76. Muheremu, A. and Q. Ao, *Past, Present, and Future of Nerve Conduits in the Treatment of Peripheral Nerve Injury.* Biomed Res Int, 2015. **2015**: p. 237507.

77. Safa, B. and G. Buncke, *Autograft Substitutes: Conduits and Processed Nerve Allografts.* Hand Clin, 2016. **32**(2): p. 127-40.

78. Gaudin, R., et al., *Approaches to Peripheral Nerve Repair: Generations of Biomaterial Conduits Yielding to Replacing Autologous Nerve Grafts in Craniomaxillofacial Surgery.* Biomed Res Int, 2016. **2016**: p. 3856262.

79. Rbia, N. and A.Y. Shin, *The Role of Nerve Graft Substitutes in Motor and Mixed Motor/Sensory Peripheral Nerve Injuries.* J Hand Surg Am, 2017. **42**(5): p. 367-377.

80. Rydevik, B.L., et al., *An in vitro mechanical and histological study of acute stretching on rabbit tibial nerve.* Journal of Orthopaedic Research: Official Publication of the Orthopaedic Research Society, 1990. **8**(5): p. 694-701.

81. Sundararaghavan, H.G., et al., *Neurite growth in 3D collagen gels with gradients of mechanical properties.* Biotechnology and bioengineering, 2009. **102**(2): p. 632-643.

82. Sundararaghavan, H.G., R.B. Metter, and J.A. Burdick, *Electrospun fibrous scaffolds with multiscale and photopatterned porosity.* Macromolecular bioscience, 2010. **10**(3): p. 265-270.

83. Seidlits, S.K., J.Y. Lee, and C.E. Schmidt, *Nanostructured scaffolds for neural applications.* Nanomedicine (London, England), 2008. **3**(2): p. 183-189.

84. Curtis, A. and C. Wilkinson, *Topographical control of cells.* Biomaterials, 1997. **18**(24): p. 1573-1583.

85. Fan, Y.W., et al., *Culture of neural cells on silicon wafers with nano-scale surface topograph.* Journal of Neuroscience Methods, 2002. **120**(1): p. 17-23.

86. Abrams, G.A., et al., *Nanoscale topography of the basement membrane underlying the corneal epithelium of the rhesus macaque.* Cell and Tissue Research, 2000. **299**(1): p. 39-46.

87. Cecchi, C., et al., *Neuronal differentiation of human mesenchymal stromal cells increases their resistance to Aβ(42) aggregate toxicity.* Journal of Alzheimer's Disease: JAD, 2011. **27**(3): p. 651-664.

88. Wang, B. and Z. Shao, *[Application of self-assembling peptide nanofiber scaffold in nerve tissue engineering].* Zhongguo xiu fu chong jian wai ke za zhi = Zhongguo xiufu chongjian waike zazhi = Chinese journal of reparative and reconstructive surgery, 2009. **23**(7): p. 861-863.

89. Johansson, F., et al., *Axonal outgrowth on nano-imprinted patterns.* Biomaterials, 2006. **27**(8): p. 1251-1258.

90. Norman, J.J. and T.A. Desai, *Methods for fabrication of nanoscale topography for tissue engineering scaffolds.* Annals of Biomedical Engineering, 2006. **34**(1): p. 89-101.

91. Yang, F., et al., *Electrospinning of nano/micro scale poly(L-lactic acid) aligned fibers and their potential in neural tissue engineering.* Biomaterials, 2005. **26**(15): p. 2603-2610.

92. Kim, Y.-t., et al., *The role of aligned polymer fiber-based constructs in the bridging of long peripheral nerve gaps.* Biomaterials, 2008. **29**(21): p. 3117-3127.

93. Jiang, X., et al., *Nanofibrous nerve conduit-enhanced peripheral nerve regeneration.* Journal of Tissue Engineering and Regenerative Medicine, 2014. **8**(5): p. 377-385.

94. Bamber, N.I., et al., *Neurotrophins BDNF and NT-3 promote axonal re-entry into the distal host spinal cord through Schwann cell-seeded mini-channels.* The European journal of neuroscience, 2001. **13**(2): p. 257-268.

95. Blesch, A. and M.H. Tuszynski, *Neurotrophic Factor Therapy: NGF, BDNF and NT-3*, in *Encyclopedia of Neuroscience*, R.S. Larry, Editor. 2009, Academic Press: Oxford. p. 1093-1100.

96. Burdick, J.A., et al., *Stimulation of neurite outgrowth by neurotrophins delivered from degradable hydrogels.* Biomaterials, 2006. **27**(3): p. 452-459.

97. Gordon, T., *The role of neurotrophic factors in nerve regeneration.* Neurosurgical focus, 2009. **26**(2): p. E3.

98. Madduri, S., et al., *Effect of controlled co-delivery of synergistic neurotrophic factors on early nerve regeneration in rats.* Biomaterials, 2010. **31**(32): p. 8402-8409.

99. Madduri, S., et al., *Collagen nerve conduits releasing the neurotrophic factors GDNF and NGF.* Journal of controlled release: official journal of the Controlled Release Society, 2010. **143**(2): p. 168-174.

100. Martinotti, G., et al., *Nerve growth factor and brain-derived neurotrophic factor concentrations in schizophrenia: a review.* Journal of biological regulators and homeostatic agents, 2012. **26**(3): p. 347-356.

101. Labroo, P., et al., *Novel drug delivering conduit for peripheral nerve regeneration.* J Neural Eng, 2017.

102. Tan, Q., et al., *Controlled release of chitosan/heparin nanoparticle-delivered VEGF enhances regeneration of decellularized tissue-engineered scaffolds.* International journal of nanomedicine, 2011. **6**: p. 929-942.

103. Takagi, T., et al., *Sustained bFGF-release tubes for peripheral nerve regeneration: comparison with autograft.* Plastic and reconstructive surgery, 2012. **130**(4): p. 866-876.

104. Lang, E.M., et al., *Single-dose application of CNTF and BDNF improves remyelination of regenerating nerve fibers after C7 ventral root avulsion and replantation.* Journal of neurotrauma, 2008. **25**(4): p. 384-400.

105. Chen, J., et al., *Synergistic effects of NGF, CNTF and GDNF on functional recovery following sciatic nerve injury in rats.* Advances in Medical Sciences, 2010. **55**(1): p. 32-42.

106. Mohtaram, N.K., A. Montgomery, and S.M. Willerth, *Biomaterial-based drug delivery systems for the controlled release of neurotrophic factors.* Biomedical materials (Bristol, England), 2013. **8**(2): p. 022001.

107. Willerth, S.M., et al., *Rationally designed peptides for controlled release of nerve growth factor from fibrin matrices.* Journal of biomedical materials research. Part A, 2007. **80**(1): p. 13-23.

108. Martino, M.M., et al., *Heparin-binding domain of fibrin(ogen) binds growth factors and promotes tissue repair when incorporated within a synthetic matrix.* Proceedings of the National Academy of Sciences of the United States of America, 2013. **110**(12): p. 4563-4568.

109. Wood, M.D., et al., *Heparin-binding-affinity-based delivery systems releasing nerve growth factor enhance sciatic nerve regeneration.* Journal of biomaterials science. Polymer edition, 2010. **21**(6): p. 771-787.

110. Wang, Z., et al., *Improved peripheral nerve regeneration with sustained release nerve growth factor microspheres in small gap tubulization.* American Journal of Translational Research, 2014. **6**(4): p. 413-421.

111. Wang, W., et al., *Effects of Schwann cell alignment along the oriented electrospun chitosan nanofibers on nerve regeneration.* Journal of biomedical materials research. Part A, 2009. **91**(4): p. 994-1005.

112. Yan, H., et al., *Chapter 10 Conduit Luminal Additives for Peripheral Nerve Repair*, in *International Review of Neurobiology*, S.G. Battiston, T. Pierluigi, and Bruno, Editors. 2009, Academic Press. p. 199-225.

113. Prabhakaran, M.P., J.R. Venugopal, and S. Ramakrishna, *Mesenchymal stem cell differentiation to neuronal cells on electrospun nanofibrous substrates for nerve tissue engineering.* Biomaterials, 2009. **30**(28): p. 4996-5003.

114. Kemp, S.W.P., et al., *Collagen Nerve Conduits Promote Enhanced Axonal Regeneration, Schwann Cell Association, and Neovascularization Compared to Silicone Conduits.* Tissue Engineering Part A, 2009. **15**(8): p. 1975-1988.

115. Udina, E., A. Puigdemasa, and X. Navarro, *Passive and active exercise improve regeneration and muscle reinnervation after peripheral nerve injury in the rat.* Muscle & Nerve, 2011. **43**(4): p. 500-509.

116. Udina, E., et al., *Effects of activity-dependent strategies on regeneration and plasticity after peripheral nerve injuries.* Annals of Anatomy = Anatomischer Anzeiger: Official Organ of the Anatomische Gesellschaft, 2011. **193**(4): p. 347-353.

117. Molteni, R., et al., *Voluntary exercise increases axonal regeneration from sensory neurons.* Proceedings of the National Academy of Sciences of the United States of America, 2004. **101**(22): p. 8473-8478.

118. Hutchinson, K.J., et al., *Three exercise paradigms differentially improve sensory recovery after spinal cord contusion in rats.* Brain: A Journal of Neurology, 2004. **127**(Pt 6): p. 1403-1414.

119. Seo, T.B., et al., *ERK1/2-mediated Schwann cell proliferation in the regenerating sciatic nerve by treadmill training.* Journal of Neurotrauma, 2009. **26**(10): p. 1733-1744.

120. Sabatier, M.J., et al., *Treadmill training promotes axon regeneration in injured peripheral nerves.* Experimental Neurology, 2008. **211**(2): p. 489-493.

121. Thompson, N.J., D.R. Sengelaub, and A.W. English, *Enhancement of peripheral nerve regeneration due to treadmill training and electrical stimulation is dependent on androgen receptor signaling.* Developmental Neurobiology, 2014. **74**(5): p. 531-540.

122. Sabatier, M.J., et al., *Slope walking causes short-term changes in soleus H-reflex excitability.* Physiological Reports, 2015. **3**(3).

123. Asensio-Pinilla, E., et al., *Electrical stimulation combined with exercise increase axonal regeneration after peripheral nerve injury.* Experimental Neurology, 2009. **219**(1): p. 258-265.

124. Armada-da-Silva, P.A.S., et al., *Role of physical exercise for improving posttraumatic nerve regeneration.* International Review of Neurobiology, 2013. **109**: p. 125-149.

125. Savastano, L.E., et al., *Sciatic nerve injury: a simple and subtle model for investigating many aspects of nervous system damage and recovery.* Journal of Neuroscience Methods, 2014. **227**: p. 166-180.

126. Wood, M.D., et al., *Outcome measures of peripheral nerve regeneration.* Annals of Anatomy = Anatomischer Anzeiger: Official Organ of the Anatomische Gesellschaft, 2011. **193**(4): p. 321-333.

127. Dahlin, L., et al., *Chapter 28 Future Perspective in Peripheral Nerve Reconstruction*, in *International Review of Neurobiology*, S.G. Battiston, T. Pierluigi, and Bruno, Editors. 2009, Academic Press. p. 507-530.

128. Jiang, X., et al., *Current applications and future perspectives of artificial nerve conduits.* Experimental Neurology, 2010. **223**(1): p. 86-101.

129. Salgado, A.J., et al., *Tissue engineering and regenerative medicine: past, present, and future.* International Review of Neurobiology, 2013. **108**: p. 1-33.

130. Madduri, S. and B. Gander, *Growth factor delivery systems and repair strategies for damaged peripheral nerves.* Journal of controlled release: official journal of the Controlled Release Society, 2012. **161**(2): p. 274-282.

131. Goulart, C.O., et al., *A combination of Schwann-cell grafts and aerobic exercise enhances sciatic nerve regeneration.* PloS One, 2014. **9**(10): p. e110090.

132. Wang, J., et al., *No synergistic effect of mesenchymal stem cells and exercise on functional recovery following sciatic nerve transection.* Functional Neurology, 2010. **25**(1): p. 33-43.

133. *Peripheral Neuropathy Fact Sheet | National Institute of Neurological Disorders and Stroke*. 2017; Available from: https://www.ncbi.nlm.nih.gov/pubmed/.

134. Jenkins, P.M., et al., *A nerve guidance conduit with topographical and biochemical cues: potential application using human neural stem cells.* Nanoscale Res Lett, 2015. **10**(1): p. 972.

135. Zander, N.E., et al., *Surface-modified nanofibrous biomaterial bridge for the enhancement and control of neurite outgrowth.* Biointerphases, 2010. **5**(4): p. 149-58.

136. Yan, Q., Y. Yin, and B. Li, *Use new PLGL-RGD-NGF nerve conduits for promoting peripheral nerve regeneration.* Biomedical engineering online, 2012. **11**: p. 36.

137. Burdick, J.A., et al., *Controlled degradation and mechanical behavior of photopolymerized hyaluronic acid networks.* Biomacromolecules, 2005. **6**(1): p. 386-391.

138. Niu, Y., et al., *Scaffolds from block polyurethanes based on poly(ε-caprolactone) (PCL) and poly(ethylene glycol) (PEG) for peripheral nerve regeneration.* Biomaterials, 2014. **35**(14): p. 4266-4277.

139. Niu, X., et al., *Porous nano-HA/collagen/PLLA scaffold containing chitosan microspheres for controlled delivery of synthetic peptide derived from BMP-2.* Journal of Controlled Release: Official Journal of the Controlled Release Society, 2009. **134**(2): p. 111-117.

140. de Boer, R., et al., *In vitro and in vivo release of nerve growth factor from biodegradable poly-lactic-co-glycolic-acid microspheres.* Journal of biomedical materials research. Part A, 2010. **95**(4): p. 1067-1073.

141. Péan, J.-M., et al., *NGF release from poly(d,l-lactide-co-glycolide) microspheres. Effect of some formulation parameters on encapsulated NGF stability.* Journal of Controlled Release, 1998. **56**(1–3): p. 175-187.

142. Santos, D., et al., *Focal release of neurotrophic factors by biodegradable microspheres enhance motor and sensory axonal regeneration in vitro and in vivo.* Brain research, 2016. **1636**: p. 93-106.

143. Szentivanyi, A., et al., *Electrospun cellular microenvironments: Understanding controlled release and scaffold structure.* Advanced drug delivery reviews, 2011. **63**(4-5): p. 209-220.

144. Nakai, J. and D.o.A. Tissue Culture Laboratory, The University of Texas, Medical Branch, Galveston, *Dissociated dorsal root ganglia in tissue culture.* Developmental Dynamics, 2017. **99**(1): p. 81-129.

145. Derby, M.A., *Analysis of glycosaminoglycans within the extracellular environments encountered by migrating neural crest cells.* Developmental Biology, 1978. **66**(2): p. 321-336.

146. Leach, J.B., et al., *Development of photocrosslinkable hyaluronic acid-polyethylene glycol-peptide composite hydrogels for soft tissue engineering.* J Biomed Mater Res A, 2004. **70**(1): p. 74-82.

147. Jin, J., et al., *Peripheral Nerve Repair in Rats Using Composite Hydrogel-Filled Aligned Nanofiber Conduits with Incorporated Nerve Growth Factor.* Tissue Engineering Part A, 2013. **19**(19-20): p. 2138-2146.

148. Suri, S., et al., *Solid freeform fabrication of designer scaffolds of hyaluronic acid for nerve tissue engineering.* Biomedical Microdevices, 2011. **13**(6): p. 983-993.

149. Yu, H., et al., *Local delivery of controlled released nerve growth factor promotes sciatic nerve regeneration after crush injury.* Neuroscience letters, 2014. **566**: p. 177-181.

150. Davies, A.M., *Neurotrophins: neurotrophic modulation of neurite growth.* Curr Biol, 2000. **10**(5): p. R198-200.

151. Madduri, S., M. Papaloizos, and B. Gander, *Synergistic effect of GDNF and NGF on axonal branching and elongation in vitro.* Neurosci Res, 2009. **65**(1): p. 88-97.

152. Wright, D.E. and W.D. Snider, *Neurotrophin receptor mRNA expression defines distinct populations of neurons in rat dorsal root ganglia.* J Comp Neurol, 1995. **351**(3): p. 329-38.

153. Dahlin, R.L., F.K. Kasper, and A.G. Mikos, *Polymeric nanofibers in tissue engineering.* Tissue Eng Part B Rev, 2011. **17**(5): p. 349-64.

154. Agarwal, S. and A. Greiner, *On the way to clean and safe electrospinning—green electrospinning: emulsion and suspension electrospinning.* Polymers for Advanced Technologies, 2011. **22**(3): p. 372-378.

155. Zamani, M., M.P. Prabhakaran, and S. Ramakrishna, *Advances in drug delivery via electrospun and electrosprayed nanomaterials.* Int J Nanomedicine, 2013. **8**: p. 2997-3017.

156. Makadia, H.K. and S.J. Siegel, *Poly Lactic-co-Glycolic Acid (PLGA) as Biodegradable Controlled Drug Delivery Carrier.* Polymers, 2011. **3**(3): p. 1377-1397.

157. Sahay, G., D.Y. Alakhova, and A.V. Kabanov, *Endocytosis of nanomedicines.* J Control Release, 2010. **145**(3): p. 182-95.

158. Kokai, L.E., A.M. Ghaznavi, and K.G. Marra, *Incorporation of double-walled microspheres into polymer nerve guides for the sustained delivery of glial cell line-derived neurotrophic factor.* Biomaterials, 2010. **31**(8): p. 2313-2322.

159. Shive, M.S. and J.M. Anderson, *Biodegradation and biocompatibility of PLA and PLGA microspheres.* Adv Drug Deliv Rev, 1997. **28**(1): p. 5-24.

160. Pfister, L.A., et al., *Nerve conduits and growth factor delivery in peripheral nerve repair.* Journal of the peripheral nervous system: JPNS, 2007. **12**(2): p. 65-82.

161. Oh, S.H., et al., *Effect of surface pore structure of nerve guide conduit on peripheral nerve regeneration.* Tissue engineering. Part C, Methods, 2013. **19**(3): p. 233-243.

162. Liao, C., et al., *Multi-channel chitosan-polycaprolactone conduits embedded with microspheres for controlled release of nerve growth factor.* Reactive & Functional Polymers, 2013. **73**(1): p. 149-159.

163. Zhang, Y.Z., et al., *Biomimetic and bioactive nanofibrous scaffolds from electrospun composite nanofibers.* International journal of nanomedicine, 2007. **2**(4): p. 623-638.

164. Kim, J.I., et al., *A controlled design of aligned and random nanofibers for 3D Bi-functionalized nerve conduits fabricated via a novel electrospinning set-up.* Scientific reports, 2016. **6**: p. 23761.

165. Bhutto, M.A., et al., *Development of poly (L-lactide-co-caprolactone) multichannel nerve conduit with aligned electrospun nanofibers for Schwann cell proliferation.* International Journal of Polymeric Materials and Polymeric Biomaterials, 2016. **65**(7): p. 323-329.

166. Zhang, X.F., et al., *Laminin-modified and aligned poly (3-hydroxybutyrate-co-3-hydroxyvalerate)/polyethylene oxide nanofibrous nerve conduits promote peripheral nerve regeneration.* Journal of tissue engineering and regenerative medicine, 2017.

167. Panagopoulos, G.N., P.D. Megaloikonomos, and A.F. Mavrogenis, *The Present and Future for Peripheral Nerve Regeneration.* Orthopedics, 2017. **40**(1): p. e141-e156.

168. Park, J.-S. and A. Höke, *Treadmill exercise induced functional recovery after peripheral nerve repair is associated with increased levels of neurotrophic factors.* PloS one, 2014. **9**(3): p. e90245.

169. Xu, H., et al., *Conductive PPY/PDLLA conduit for peripheral nerve regeneration.* Biomaterials, 2014. **35**(1): p. 225-235.

170. Whitehead, T.J., C.O.C. Avila, and H.G. Sundararaghavan, *Combining Growth Factor Releasing Microspheres within Aligned Nanofibers Enhances Neurite Outgrowth.* Journal of Biomedical Materials Research Part A, 2017.

171. Zhang, Y.P., et al., *A topical mixture for preventing, abolishing, and treating autophagia and self-mutilation in laboratory rats.* Contemporary Topics in Laboratory Animal Science / American Association for Laboratory Animal Science, 2001. **40**(2): p. 35-36.

172. Smit, X., et al., *Static footprint analysis: a time-saving functional evaluation of nerve repair in rats.* Scandinavian Journal of Plastic and Reconstructive Surgery and Hand Surgery / Nordisk Plastikkirurgisk Forening [and] Nordisk Klubb for Handkirurgi, 2004. **38**(6): p. 321-325.

173. Bervar, M., *Video analysis of standing—an alternative footprint analysis to assess functional loss following injury to the rat sciatic nerve.* Journal of neuroscience methods, 2000. **102**(2): p. 109-116.

174. Bolton, D.A.E., et al., *Task specific adaptations in rat locomotion: Runway versus horizontal ladder.* Behavioural Brain Research, 2006. **168**(2): p. 272-279.

175. Schaeffer, V., et al., *Sciatic nerve injury induces apoptosis of dorsal root ganglion satellite glial cells and selectively modifies neurosteroidogenesis in sensory neurons.* Glia, 2010. **58(**2): p. 169-180.

176. Scipio, F.D., et al., *A simple protocol for paraffin-embedded myelin sheath staining with osmium tetroxide for light microscope observation.* Microscopy research and technique, 2008. **71**(7): p. 497-502.

177. Cobianchi, S., J. de Cruz, and X. Navarro, *Assessment of sensory thresholds and nociceptive fiber growth after sciatic nerve injury reveals the differential contribution of collateral reinnervation and nerve regeneration to neuropathic pain.* Experimental neurology, 2014. **255**: p. 1-11.

178. Kanda, K. and K. Hashizume, *Factors causing difference in force output among motor units in the rat medial gastrocnemius muscle.* The Journal of physiology, 1992. **448**(1): p. 677-695.

179. Navarro, X. and E. Udina, *Chapter 6 Methods and Protocols in Peripheral Nerve Regeneration Experimental Research: Part III—Electrophysiological Evaluation*, in *International Review of Neurobiology*, S.G. Battiston, T. Pierluigi, and Bruno, Editors. 2009, Academic Press. p. 105-126.

180. Lam, C.X., et al., *Evaluation of polycaprolactone scaffold degradation for 6 months in vitro and in vivo.* Journal of biomedical materials research Part A, 2009. **90**(3): p. 906-919.

181. Lackington, W.A., A.J. Ryan, and F.J. O'Brien, *Advances in nerve guidance conduit-based therapeutics for peripheral nerve repair.* ACS Biomaterials Science & Engineering, 2017. **3**(7): p. 1221-1235.

182. Bonetti, L.V., et al., *Balance and coordination training after sciatic nerve injury.* Muscle & Nerve, 2011. **44**(1): p. 55-62.

183. Bain, J.R., S.E. Mackinnon, and D.A. Hunter, *Functional evaluation of complete sciatic, peroneal, and posterior tibial nerve lesions in the rat.* Plastic and Reconstructive Surgery, 1989. **83**(1): p. 129-138.

184. Varejão, A.S.P., et al., *Functional evaluation of peripheral nerve regeneration in the rat: walking track analysis.* Journal of Neuroscience Methods, 2001. **108**(1): p. 1-9.

185. Bervar, M., *An alternative video footprint analysis to assess functional loss following injury to the rat sciatic nerve.* Acta chirurgiae plasticae, 2001. **44**(3): p. 86-89.

186. Bozkurt, A., et al., *Efficient bridging of 20 mm rat sciatic nerve lesions with a longitudinally micro-structured collagen scaffold.* Biomaterials, 2016. **75**: p. 112-122.

187. Wang, C.-Y., et al., *The effect of aligned core-shell nanofibres delivering NGF on the promotion of sciatic nerve regeneration.* Journal of biomaterials science. Polymer edition, 2012. **23**(1-4): p. 167-184.

188. Karimi, M., et al., *Rat sciatic nerve reconstruction across a 30 mm defect bridged by an oriented porous PHBV tube with Schwann cell as artificial nerve graft.* ASAIO journal (American Society for Artificial Internal Organs: 1992), 2014. **60**(2): p. 224-233.

189. Duncanson, W., *Microfluidic synthesis of monodisperse porous microspheres with size-tunable pores.* 2012.

190. Hung, L.-H., et al., *PLGA micro/nanosphere synthesis by droplet microfluidic solvent evaporation and extraction approaches.* 2010.

191. Xu, Q., et al., *Preparation of Monodisperse Biodegradable Polymer Microparticles Using a Microfluidic Flow-focusing Device for Controlled Drug Delivery.* Small, 2009. **5**(13): p. 1575-81.

192. Chen, Z.L., W.M. Yu, and S. Strickland, *Peripheral regeneration.* Annu Rev Neurosci, 2007. **30**: p. 209-33.

193. Grothe, C., et al., *Expression of fibroblast growth factor-2 and fibroblast growth factor receptor 1 messenger RNAs in spinal ganglia and sciatic nerve: regulation after peripheral nerve lesion.* Neuroscience, 1997. **76**(1): p. 123-35.

194. Marquardt, L.M., et al., *Finely Tuned Temporal and Spatial Delivery of GDNF Promotes Enhanced Nerve Regeneration in a Long Nerve Defect Model.* Tissue Eng Part A, 2015. **21**(23-24): p. 2852-64.

195. Chu, H., et al., *The effect of a heparin-based coacervate of fibroblast growth factor-2 on scarring in the infarcted myocardium.* Biomaterials, 2013. **34**(6): p. 1747-56.

196. Purcell, B.P., et al., *Incorporation of Sulfated Hyaluronic Acid Macromers into Degradable Hydrogel Scaffolds for Sustained Molecule Delivery.* Biomater Sci, 2014. **2**: p. 693-702.

197. Cao, X. and M. Shoichet, *Defining the concentration gradient of nerve growth factor for guided neurite outgrowth.* Neuroscience, 2001. **103**(3): p. 831-840.

198. Dinis, T.M., et al., *Method to form a fiber/growth factor dual-gradient along electrospun silk for nerve regeneration.* ACS applied materials & interfaces, 2014. **6**(19): p. 16817-16826.

199. Katz, J.S. and J.A. Burdick, *Hydrogel mediated delivery of trophic factors for neural repair.* Wiley Interdisciplinary Reviews-Nanomedicine and Nanobiotechnology, 2009. **1**(1): p. 128-139.

200. Oh, S.H., et al., *Enhanced peripheral nerve regeneration through asymmetrically porous nerve guide conduit with nerve growth factor gradient.* Journal of Biomedical Materials Research Part A, 2017.

201. Roam, J.L., P.K. Nguyen, and D.L. Elbert, *Controlled release and gradient formation of human glial-cell derived neurotrophic factor from heparinated poly(ethylene glycol) microsphere-based scaffolds.* Biomaterials, 2014. **35**(24): p. 6473-6481.

202. *Wings for Life - Spinal Cord Research Foundation*. 2017; Available from: http://www.wingsforlife.com/us/.

203. Balentine, J.D., *Pathology of experimental spinal cord trauma. II. Ultrastructure of axons and myelin.* Lab Invest, 1978. **39**(3): p. 254-66.

204. Crowe, M.J., et al., *Apoptosis and delayed degeneration after spinal cord injury in rats and monkeys.* Nat Med, 1997. **3**(1): p. 73-6.

205. Liu, X.Z., et al., *Neuronal and glial apoptosis after traumatic spinal cord injury.* J Neurosci, 1997. **17**(14): p. 5395-406.

206. Carter, L.M., S.B. McMahon, and E.J. Bradbury, *Delayed treatment with chondroitinase ABC reverses chronic atrophy of rubrospinal neurons following spinal cord injury.* Exp Neurol, 2011. **228**(1): p. 149-56.

207. Cheng, C.H., et al., *Local Delivery of High-Dose Chondroitinase ABC in the Sub-Acute Stage Promotes Axonal Outgrowth and Functional Recovery after Complete Spinal Cord Transection.* PLoS One, 2015. **10**(9): p. e0138705.

208. Kwon, B.K., T.R. Oxland, and W. Tetzlaff, *Animal models used in spinal cord regeneration research.* Spine (Phila Pa 1976), 2002. **27**(14): p. 1504-10.

209. Zahir, T., et al., *Bioengineering neural stem/progenitor cell-coated tubes for spinal cord injury repair.* Cell Transplant, 2008. **17**(3): p. 245-54.

210. Lai, B.Q., et al., *Transplantation of tissue engineering neural network and formation of neuronal relay into the transected rat spinal cord.* Biomaterials, 2016. **109**: p. 40-54.

211. Olson, H.E., et al., *Neural stem cell- and Schwann cell-loaded biodegradable polymer scaffolds support axonal regeneration in the transected spinal cord.* Tissue Eng Part A, 2009. **15**(7): p. 1797-805.

212. Zeng, X., et al., *Autocrine fibronectin from differentiating mesenchymal stem cells induces the neurite elongation in vitro and promotes nerve fiber regeneration in transected spinal cord injury.* J Biomed Mater Res A, 2016. **104**(8): p. 1902-11.

213. Madigan, N.N., et al., *Comparison of cellular architecture, axonal growth, and blood vessel formation through cell-loaded polymer scaffolds in the transected rat spinal cord.* Tissue Eng Part A, 2014. **20**(21-22): p. 2985-97.

214. Cholas, R., H.P. Hsu, and M. Spector, *Collagen scaffolds incorporating select therapeutic agents to facilitate a reparative response in a standardized hemiresection defect in the rat spinal cord.* Tissue Eng Part A, 2012. **18**(19-20): p. 2158-72.

215. King, S., W. Hickerson, and K. Proctor, *Beneficial actions of exogenous hyaluronic acid on wound healing.* Surgery, 1991. **109**(1): p. 76-84.

216. Koehn, R., et al., *Cross-linked hyaluronic acid based gel and wound healing.* Veterinary surgery: VS, 2014. **43**(2): p. 227.

217. Manuskiatti, W. and H.I. Maibach, *Hyaluronic acid and skin: wound healing and aging.* International journal of dermatology, 1996. **35**(8): p. 539-544.

218. Neuman, M.G., et al., *Hyaluronic Acid and Wound Healing.* Journal of Pharmacy & Pharmaveutical Sciences, 2015. **18**(1): p. 53-60.

219. Collins, M.N. and C. Birkinshaw, *Hyaluronic acid based scaffolds for tissue engineering—A review.* Carbohydrate polymers, 2013. **92**(2): p. 1262-1279.

220. Barrientos, S., et al., *Clinical application of growth factors and cytokines in wound healing.* Wound Repair and Regeneration, 2014. **22**(5): p. 569-578.

221. Gainza, G., et al., *Advances in drug delivery systems (DDSs) to release growth factors for wound healing and skin regeneration.* Nanomedicine: Nanotechnology, Biology and Medicine, 2015. **11**(6): p. 1551-1573.

222. Losi, P., et al., *Fibrin-based scaffold incorporating VEGF-and bFGF-loaded nanoparticles stimulates wound healing in diabetic mice.* Acta biomaterialia, 2013. **9**(8): p. 7814-7821.

223. Xie, Z., et al., *Dual growth factor releasing multi-functional nanofibers for wound healing.* Acta biomaterialia, 2013. **9**(12): p. 9351-9359.

224. Gobbi, A. and G.P. Whyte, *One-stage cartilage repair using a hyaluronic acid–based scaffold with activated bone marrow–derived mesenchymal stem cells compared with microfracture: five-year follow-up.* The American journal of sports medicine, 2016. **44**(11): p. 2846-2854.

225. Kim, I.L., et al., *Fibrous hyaluronic acid hydrogels that direct MSC chondrogenesis through mechanical and adhesive cues.* Biomaterials, 2013. **34**(22): p. 5571-5580.

226. Mintz, B.R. and J.A. Cooper, *Hybrid hyaluronic acid hydrogel/poly(ε-caprolactone) scaffold provides mechanically favorable platform for cartilage tissue engineering studies.* Journal of Biomedical Materials Research Part A, 2014. **102**(9): p. 2918-2926.

227. Fortier, L.A., et al., *The role of growth factors in cartilage repair.* Clinical Orthopaedics and Related Research®, 2011. **469**(10): p. 2706-2715.

228. Reyes, R., et al., *Cartilage repair by local delivery of transforming growth factor-β1 or bone morphogenetic protein-2 from a novel, segmented polyurethane/polylactic-co-glycolic bilayered scaffold.* Journal of biomedical materials research Part A, 2014. **102**(4): p. 1110-1120.

229. Cuevas, P., J. Burgos, and A. Baird, *Basic fibroblast growth factor (FGF) promotes cartilage repair in vivo.* Biochemical and biophysical research communications, 1988. **156**(2): p. 611-618.

230. Luo, Z., et al., *Mechano growth factor (MGF) and transforming growth factor (TGF)-β3 functionalized silk scaffolds enhance articular hyaline cartilage regeneration in rabbit model.* Biomaterials, 2015. **52**: p. 463-475.

231. Nixon, A.J., et al., *Insulinlike growth factor-I gene therapy applications for cartilage repair.* Clinical orthopaedics and related research, 2000. **379**: p. S201-S213.

232. Burdick, J.A. and G.D. Prestwich, *Hyaluronic acid hydrogels for biomedical applications.* Advanced materials, 2011. **23**(12).

233. Perng, C.-K., et al., *In vivo angiogenesis effect of porous collagen scaffold with hyaluronic acid oligosaccharides.* Journal of Surgical Research, 2011. **168**(1): p. 9-15.

234. Espandar, L., et al., *Adipose-Derived Stem Cells on Hyaluronic Acid–Derived Scaffold: A New Horizon in Bioengineered Cornea.* Archives of ophthalmology, 2012. **130**(2): p. 202-208.

235. Sill, T.J. and H.A. von Recum, *Electrospinning: applications in drug delivery and tissue engineering.* Biomaterials, 2008. **29**(13): p. 1989-2006.

ABSTRACT

AN ENHANCED NERVE CONDUIT COMBINED WITH EXERCISE TO IMPROVE FUNCTIONAL RECOVERY AFTER PERIPHERAL NERVE INJURY

by

TONYA JO WHITEHEAD

December 2017

Advisor: Dr. Harini G Sundararaghavan

Major: Biomedical Engineering

Degree: Doctor of Philosophy

Peripheral nerve injuries affect millions of people each year around the world. Current treatments include an autograft, the gold standard, and commercially available nerve growth conduits (NGC). Autografts have several drawbacks including donor site morbidity and nerve size mismatch, which leads to incomplete recovery. Commercial NGCs can help with recovery but do not contain any specific cues to guide nerve regeneration. This thesis first evaluated mechanical, topographical and chemical cues that can be included in a NGC to promote and direct nerve regeneration. To incorporate all of the cues, a compliant substrate methacrylated hyaluronic acid (MeHA, mechanical cue) is electrospun into aligned fibers (topographical cue), with poly-lactic-co-glycolic acid (PLGA) microspheres to deliver growth factors (GF, chemical cue).

The properties of the scaffold were evaluated under physiological conditions using environmental scanning electron microscopy and mechanical testing in a physiological environment. The resulting scaffolds have hydrated porosities of 35-55% and young's modulus from 0.43-2.86MPa. Nerve growth factor (NGF) was used as the GF for *in vitro* testing. The bioactivity of the encapsulated NGF was tested both during the short and long term. Results showed that NGF remains bioactive through the encapsulation and electrospinning process. ELISA showed that NGF is released from the microspheres for up to 4 weeks. Dorsal root ganglia (DRG) neurons were used to evaluate NGF bioactivity and testing showed that the released NGF was bioactive and could increase neurite outgrowth for up to 4

weeks. DRG testing on the scaffolds also showed that the combination of NGF released from the microspheres and the aligned nanofibers significantly directed and enhanced neurite outgrowth.

The study continued with in vivo testing by creating an NGC that included the scaffold as an inner support mechanism. An additional cue was then added in the form of treadmill running, to simulate physical therapy (PT). Circumferentially aligned nanofibers of Polycaprolactone (PCL) were layered with longitudinally aligned electrospun methacrylated Hyaluronic Acid (MeHA) fibers, with or without microspheres containing glial cell line-derived neurotrophic factor (GDNF), and rolled into conduits with an inner diameter of 1.25mm and length of 14mm. The conduits were implanted into an 8mm sciatic nerve gap in female Lewis rats. The animals were divided into five groups: fibers, fibers + PT, fibers + GF, fibers + GF + PT, and autograft control. All animals received the following behavior and functional testing prior to surgery and weekly post-surgery: Static Sciatic Index, Von Frey Filament Mechanical Sensory Test, and Ladder Walking Test. At the end of the study Compound Muscle Action Potentials (CMAP) and contractile force of the gastrocnemius muscle was measured. Sciatic nerves were harvested bilaterally for histological analysis. Weekly testing showed that fibers with GFs enhanced or sped functional recovery. Footfall measures the number of times an animal misses a rung when traversing a ladder, indicating gross muscle control. By 4 weeks both the GF groups were performing similarly to the autograft. Von Frey fibers were used to test the sensory perception. All groups showed hypersensitivity similar to the autograft by week 4, however the GF groups showed a response pattern similar to the autograft at all time points. Sciatic Index testing showed some improvement over the 8 weeks of testing. The groups receiving GDNF had greater improvement than those that did not. CMAP showed similar results.

Future work includes improvements to the microsphere production technique and additions of support cells to the system.

AUTOBIOGRAPHICAL STATEMENT

Tonya Whitehead

EDUCATION

2017	**PhD – Biomedical Engineering** Wayne State University, Detroit, MI
2012	**MS – Biomedical Engineering** Wayne State University, Detroit, MI
2004	**MS – Manufacturing and Engineering Management** Eli Broad College of Business, Michigan State University, East Lansing, MI
2002	**BS – Computer Engineering** Michigan State University, East Lansing, MI

SELECTED PUBLICATIONS

Peer Reviewed Journals

Whitehead TJ, Avila COC, Sundararaghavan HG, "Combining Growth Factor Releasing Microspheres within Aligned Nanofibers Enhances Neurite Outgrowth"; *Journal of Biomedical Materials Research: Part A* 2017 Sep 23

Whitehead TJ, Sundararaghavan HG, "Electrospinning Growth Factor Releasing Microspheres into Fibrous Scaffolds"; *Journal of Visualized Experiments* 2014 Aug 16:(90).

Conference Proceedings

Whitehead TJ, Mays EA, Peduzzi J, Mazhari A, Chen C, Cavanaugh JM, Sundararaghavan HG, "Improving Nerve Growth Conduits with Aligned Nanofibers, Growth Factors, and Physical Therapy"; Biomedical Engineering Society Annual Fall Meeting, October 2017, *Podium*

Whitehead TJ, Potoff JJ, "Work in Progress: Self Directed Projects to Increase Engagement and Satisfaction in Basic Programming Course"; First Year Engineering Experience Conference, August 2017, *Podium*

Whitehead TJ, Peduzzi J, Mazhari A, Chen C, Cavanaugh JM, Sundararaghavan HG, "Physical Therapy Combined with a PCL/HA Nanofiber Conduit for Enhanced Peripheral Nerve Repair"; Biomedical Engineering Society Annual Fall Meeting, October 2016, *Podium*

AWARDS AND HONORS

2017	Garrett T. Heberlein Excellence in Teaching Award
2016	College of Engineering Three Minute Thesis (3MT) Winner
2016	College of Engineering 3MT People's Choice Winner
2013-1915	King Chavez Parks Future Faculty Fellowship
2014	Laureate, Tau Beta Pi, National Engineering Honor Society
2012-2013	Thomas C Rumble University Graduate Fellowship